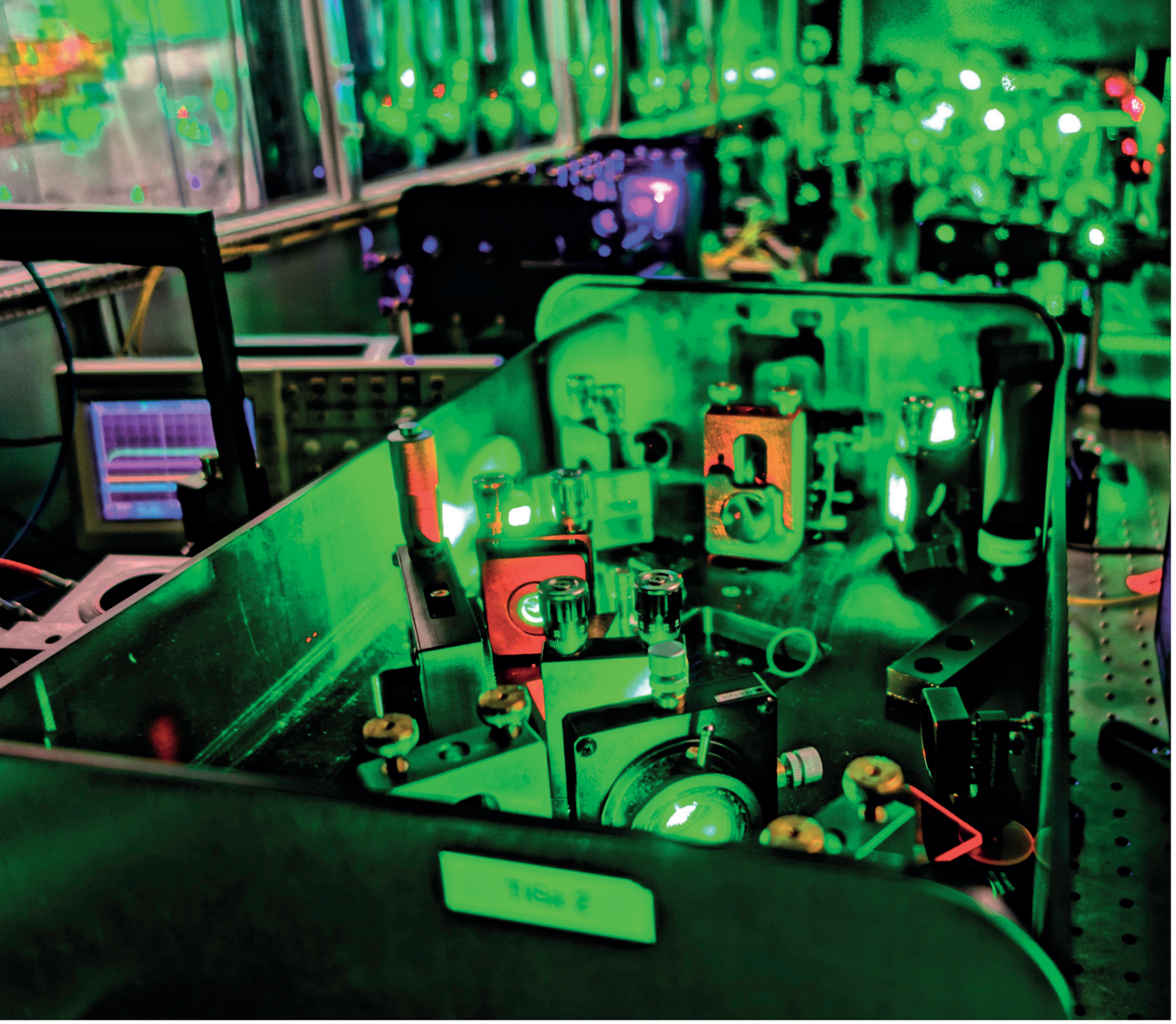

2.1 Precision Nuclear Ground-State Properties

Photo of the resonance ionisation laser ion source (RILIS) installed at ISOLDE-CERN to produce exotic ion beams for, e.g. laser spectroscopy and mass spectrometry (Photo: Bruce March, CERN).

Introduction

Similar to an individual which can be described by its size, weight, and shape etc. we can describe a nucleus. Every atomic nuclide of a different element is unique by its mass and radius, like a fingerprint. These quantities provide valuable information about the internal structure of the nucleus and the forces which form it. Over the past years we have developed and improved novel atomic physics techniques that allowed probing these nuclear physics quantities with unprecedented precision, namely high-precision Penning-trap mass spectrometry and high-resolution collinear laser spectroscopy. The results have numerous applications in nuclear structure physics, nuclear astrophysics, neutrino physics and many more in order to answer fundamental questions like “How many nuclides exist?”, “How were heavy elements formed and why do they exist at all?”, “What is the mass of the neutrino?”.

If the mass of a particular nuclide is to be determined with very high precision, Penning-trap mass spectrometry is just the method of choice. This technique is superior in achievable sensitivity, accuracy and resolving power over all other mass-measurement methods due to the very idea which forms the basis of a Penning trap. One confines a single particle with mass m and electrical charge q to a tiny volume with the help of a superposition of an extremely stable and homogeneous magnetic field B and a weak static quadrupole electric potential. In such a field configuration a charged particle performs a quite complex periodic motion, which is considered to be a product of three harmonic motions with very stable eigenfrequencies. A certain combination of these eigenfrequencies yields the so-called free cyclotron frequency $\omega_c = q \cdot B/m$ – the frequency of the charged particle motion in a pure magnetic field B. A determination of the mass of a charged particle via a measurement of its free cyclotron frequency – the most precisely measurable quantity in physics – is a remarkable trick, which makes the Penning-trap method unbeatable by any other mass-measurement technique.

All high-precision Penning-trap mass spectrometers naturally fall into two groups: (1) on-line facilities for mass measurements on very short-lived exotic nuclides and (2) off-line setups for experiments with long-lived and stable species. These two classes of devices employ substantially different methods for measuring the free cyclotron frequency. On-line facilities are based on the relatively simple ToF-ICR technique, which allows for very fast mass measurements on singly charged ions with a down to a few hundred eV/c^2 uncertainty. The price one has to pay for the fastness and simplicity is a relatively large number of subsequently trapped ions – at least a few hundred – required in order to reach a low uncertainty in mass determination. Off-line setups employ the FT-ICR technique, which enables one to perform mass measurements on a single highly-charged ion with an unprecedentedly low relative uncertainty of 10^{-11}. One pays for such an extraordinary performance with a high complexity of the setup.

Collinear laser spectroscopy of radioactive atomic beams was introduced at ISOLDE-CERN more than three decades ago. In recent years numerous advances in radioactive beam production have promoted experimental inquiries in some of the exotic corners of the nuclear chart. To a large extent the latter is a result from important developments elevating the experimental sensitivity of collinear laser spectroscopy by multiple orders of magnitude.

The basic principle of measuring nuclear properties using collinear laser spectroscopy relies on the hyperfine interaction between the nucleus and the surrounding atomic electrons, which results in a small shift and splitting in the atomic energy levels. In the general scheme presented in Fig. 1, this atomic hyperfine structure is recorded via the Doppler shift resulting from induced variations in the ion-beam energy. The atomic excitations are then identified through the beam fluorescence. This method has produced outstanding results in the past. A number of developments have been devised throughout the years in order to increase the sensitivity and to obtain access to exotic nuclides otherwise unreachable by fluorescence detection. Generally, those approaches have replaced the detection of photons by detection of charged particles. This led to the implementation of laser-induced nuclear orientation, state-selective charge exchange, collisional ionisation, and collinear laser ionisation. The alternative approach to this charged-particle detection is to increase the sensitivity of the fluorescence spectroscopy by vastly reducing the background originating mostly from laser scattering. This meant implementing photon-ion coincidence. In practice though, photon-ion coincidence are rarely applicable at Isotope Separation On-Line facilities due to a considerable isobaric contamination. A universal scheme for working in photon-ion coincidence mode is to accumulate the ion beam periodically in an ion trap and then to release it as a short bunch in order to record photons in the corresponding time window. In recent years bunched-beam laser spectroscopy was successfully introduced at ISOLDE-CERN and employed at the collinear laser spectroscopy setup COLLAPS. In the following, highlights of recent results from the precise determination of nuclear ground and partly isomeric-state properties are presented.

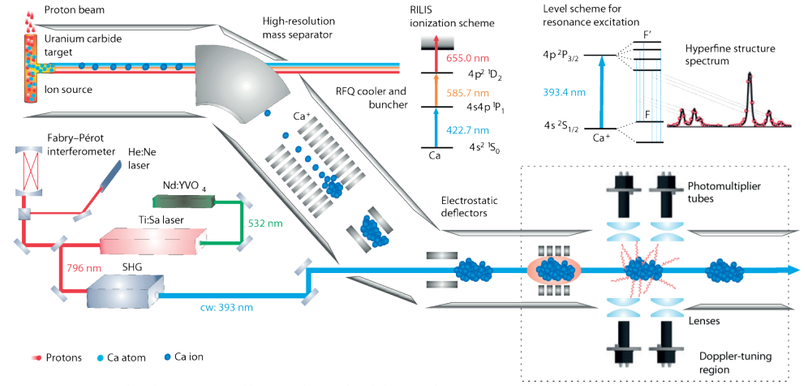

Fig. 1: General scheme of collinear bunched-beam laser spectroscopy at COLLAPS (ISOLDE-CERN). Details, such as the wavelengths are specific to the measurements described in [1].

Probing nuclear structure from radii and moments

The properties of nuclei are determined by how the protons (Z) and neutrons (*N*) are organised within the nucleus. For around 70 years now, the nuclear shell model can account for many of these properties by assuming the protons and neutrons occupy well-defined energy orbitals grouped into "shells". Notably, this model can reproduce the observation of unusually stable nuclei at certain numbers of protons and neutrons, the so-called magic numbers (2, 8, 20, 28, 50 etc.) which correspond to completely filled shells. Still today, magic numbers provide benchmarks for the exploration of nuclear structure and a large part of the physics programme at the collinear laser spectroscopy setup COLLAPS has been focussed on regions at and around these numbers. In particular, it was investigated how the nuclear shell structure changes when going to isotopes with a large neutron excess, trying to identify the drivers of this structural evolution with the ultimate goal of improving our understanding of the strong nuclear interaction.

The collinear laser spectroscopy technique is a powerful tool for these studies as it gives simultaneous access to the nuclear spin, magnetic dipole moment, electric quadrupole moment and mean-square charge radius. These observables provide complementary information: on the one hand, they are sensitive to the configuration of the nucleons in the shell-model orbitals, and on the other hand, they probe the collective interplay between the nucleons, reflecting for example the size and shape of the nucleus. As such, they provide excellent tests for state-of-the-art nuclear models.

With a magic proton number (Z = 20) and two stable isotopes with magic neutron numbers (*N* = 20, 28), the calcium isotopes played an important role in the development of nuclear theory from the very beginning. Recent COLLAPS measurements of the unexpectedly large mean-square charge radius of the exotic ^{52}Ca with respect to the trend defined by lighter isotopes in Fig. 2 continues to challenge the available models [1]. To assess the impact of core breaking effects, which are generally important for the description of electromagnetic moments in this region, one studied the proton occupancies of natural orbitals above the Z = 20 shell. *Ab initio* calculations showed a weak, but gradual erosion of the proton core as neutrons are added. Although this defies the simple pattern of a rigid proton core expected for the magic calcium isotopes, the estimated magnitude of core breaking effects, including coupling to the neutrons, is not sufficient to explain the large charge radius of ^{52}Ca. These results open intriguing questions on the evolution of charge radii away from stability and constitute a major challenge in the search of a unified description of the atomic nucleus.

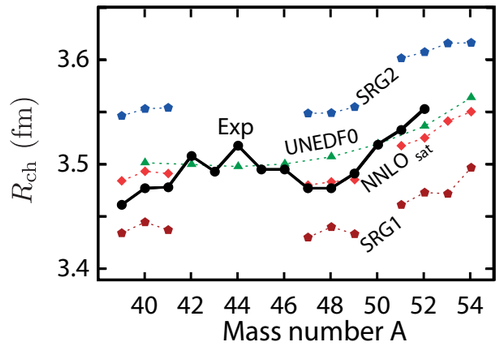

Fig. 2: Experimentally determined charge radii (black dots) of calcium isotopes compared to different theoretical predictions.

Shape coexistence is the remarkable phenomenon where in one nucleus, two nuclear states with a similar energy are found to have very different shapes. This is the consequence of the subtle balance between several competing effects within the nucleus and hence the theoretical reproduction depends critically on the correct parametrisation of the used models. In a recent experiment at COLLAPS, the existence of a long-lived isomer in ^{79}Zn (Z = 30) has been confirmed and its properties have been found to diverge as compared to those of the ground state [2]. The intruder nature of this isomer was determined from its *g* factor which in terms of the spherical shell model was accounted for in a much larger model space with respect to the one of the ground state. Moreover, the large isomer shift is consistent with a large difference in deformation, thus providing evidence for shape coexistence. This challenges the robustness of the doubly-closed shell nucleus ^{78}Ni (Z = 28, *N* = 50).

As one of the leading radioactive isotope production facilities ISOLDE provides superb yields of neutron-rich cadmium (Z = 48) isotopes, just below the Z = 50 magic number. The systematic laser spectroscopic investigation of over 20 different cadmium isotopes magnificently illustrated that surprisingly simple structures can emerge from the complex interaction of over 100 nucleons in the nucleus [3]. Atomic isomer shifts [4] and the corresponding mean square charge-radii changes were studied and found to follow a distinct parabolic dependence as a function of the atomic mass. The isomers have been previously associated with simplicity due to the linear increase of their quadrupole moments. The regularity of the isomer shifts suggests a higher order of symmetry affecting the ground states in addition. No such effect had ever been observed or discussed before.

Klaus Blaum, Hanne Heylen, Deyan Yordanov

Masses of neutron-rich nuclei for neutron star and nucleosynthesis studies

Atomic masses constitute primary experimental information for the modelling of astrophysical environments and processes. These include the candidate scenarios for the nucleosynthesis of elements heavier than iron, such as type-II supernova explosions or neutron-star mergers, as well as the cooling of neutron stars in binary systems. The processes by which heavy elements are created in the Universe constitute one of the great questions of physics today. More than 50% of the elements heavier than iron are thought to be created by the so-called rapid neutron-capture process (r-process), which is a series of neutron captures in competition with photodisintegration, beta decay and possibly fission. The simulation of the candidate scenarios aimed at reproducing the observed abundance of heavy elements in the Solar System are an intertwine between the description of the astrophysical environments themselves and the properties of the nuclei that are involved in the process. The latter is bearing great importance, because the main peaks in the observed mass distribution of heavy elements correspond to doubly-magic, neutron–rich nuclei. One prominent example is the peak around mass *A* = 130, which is thought to be related to the properties of nuclei in the region of the doubly-magic ^{132}Sn. Experimentally determining these properties increases the sensitivity of astrophysical simulations to the description of the r-process itself.

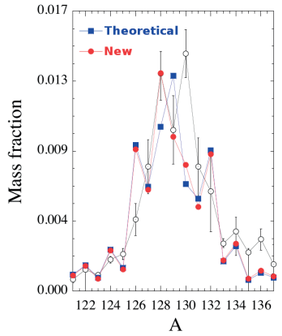

Fig. 3: Change in the predicted fraction of A≈130 elements when theoretical masses are replaced by the newly-measured $^{129\text{-}131}$Cd values [5]. The r-process solar abundance distribution is shown by open circles.

In the context of the world-wide effort of measuring the properties of neutron-rich nuclei around ^{54}Ca and ^{132}Sn, the ISOLTRAP mass spectrometer at ISOLDE/CERN recently determined the masses of the neutron-rich potassium ^{52,53}K [5] and cadmium isotopes $^{129\text{-}131}$Cd [6]. The experiment employed a combination of state-of-the-art experimental techniques for ion-beam preparation, purification and mass measurement using ion traps. The multi-reflection, time-of-flight mass spectrometer (MR-TOF MS), now an integral part of ISOLTRAP, allowed identifying both ions of interest and contaminants, as well as optimizing on-line the production parameters of the potassium and cadmium isotopes. For ^{129,130}Cd the well-established Penning-trap mass measurement technique was used, while the measurement of ^{52,53}K and ^{131}Cd was performed directly with the MR-TOF MS. The use of the MR-TOF MS has significantly increased the sensitivity of ISOLTRAP to weaker produced and shorter-lived isotopes than previously accessible, at a rate of below 10 ions/s ^{131}Cd being one of the rarest nuclides ever studied with ISOLTRAP. A very large deviation was found to the literature mass of ^{130}Cd, previously determined indirectly based on beta-decay Q-value measurements. By consequence, similarly large deviations were found to the extrapolated masses of ^{129,131}Cd, which were determined experimentally for the first time. The new masses were included in realistic simulations of the r-process and confirmed their sensitivity to the masses of neutron-rich cadmium isotopes, despite the large number of nuclides globally involved (see Fig. 3).

Accreting neutron stars are among the most studied objects in space. They host a large variety of observable phenomena ideally suited to test theoretical models and their underlying physics. The most prominent features of accreting neutron stars are type-I and type-II X-ray bursts, X-ray superbursts, magnetar giant flares, neutron star oscillations, and quiescent neutron stars. Material accreted from the accompanying star is buried on the neutron star surface, sinks into the crust, and is transformed by a sequence of electron captures into more and more neutron-rich nuclei towards the dripline. Neutron capture and emission together with pycnonuclear fusion further transforms the composition of the neutron star. Along with these nuclear processes energy deposition and energy emission alter the thermal profile of the outer layers of neutron stars. Here, the newly postulated Urca neutrino cooling process taking place in the outer neutron star crust is to mention. Its potential cooling power can be constrained by mass measurements of neutron-rich nuclei present in the particular depth of the neutron star crust. The mass measurement of ^{56}Sc [7] contributed significantly to the question about the role of Urca cooling. It is a key nucleus in the $A = 56$ mass number chain, predicted to be dominantly abundant in the neutron star crust. The new mass of ^{56}Sc reveals a much weaker Urca cooling contribution to in $A = 56$-dominated accreted neutron star crusts than previously expected, but in agreement with most recent observations of the transiently accreting system MAXI J0556-332.

Dinko Atanasov, Sebastian George, Vladimir Manea

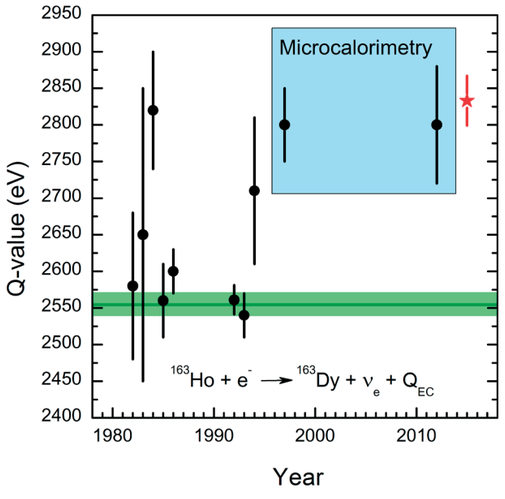

Fig. 4: The Q-value of the electron capture in ^{163}Ho as a function of the publication year obtained in several experiments from the analysis of the electron-capture spectrum and microcalorimetry. The accepted literature value and its uncertainty prior our measurement (red star, [10]) is indicated with the green line and band.

Mass and nature of neutrinos

The neutrino mass is one of the stupendous challenges of modern science. So far, only upper limits on the effective masses of this tiny mysterious particle are known: ca. 2 eV/c² for the antineutrino and 225 eV/c² for the neutrino. In the near future several sophisticated experiments aim to push down both limits to a level well below 2 eV/c² (95% CL) Experiments on a determination of the neutrino mass measure an atomic de-excitation spectrum, which occurs after the atomic orbital electron capture (EC), by means of cryogenic microcalorimetry (CMC). An analytical description of this spectrum allows for a determination of the neutrino mass on a sub-eV level provided the decay energy Q_{EC}, i. e. the mass difference between the mother and the daughter state, is independently and directly measured with an uncertainty of a few eV or better.

The most relevant nuclide for such experiments is ^{163}Ho, which disintegrates only via electron capture. It is remarkable that there are no α-, β-, and γ-radiation associated with the decay of its ground state. In addition, a very attractive feature of this unique

nuclide is the smallest EC-decay energy ever measured. However, the Q_{EC}-value determined by CMC is considerably different from the evaluated one in the literature (Fig. 4, green line and error band). To solve this long-standing puzzle, direct precise measurements of the atomic masses of ^{163}Ho and ^{163}Dy, and thus the Q_{EC}-value, with Penning-Trap Mass Spectrometry (PTMS) has been reliably performed. To prepare a suitable ^{163}Ho-sample for measurements, a sophisticated procedure has been undertaken to first irradiate ^{162}Er with thermal neutrons at the ILL-reactor (in Grenoble), then to chemically separate with subsequent mass-separation the produced ^{163}Ho from the overwhelming amount of other nuclides in the sample (in Mainz), and to finally perform a preliminary investigation of the Ho-sample by means of PTMS [8] (Fig. 5).

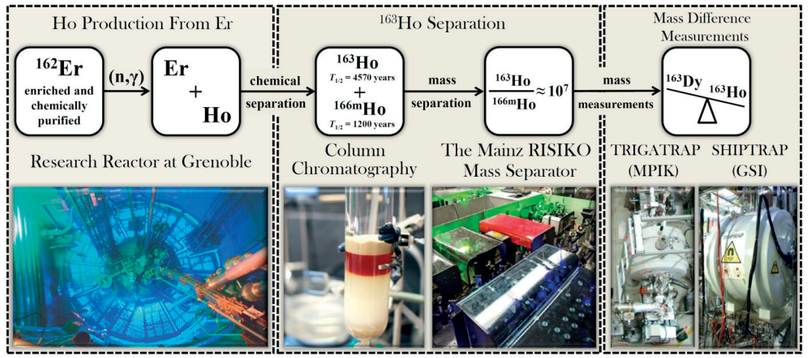

Fig. 5: Steps to take for a high-precision Q-value measurement of ^{163}Ho-^{163}Dy starting from the source preparation (left) and purification of the sample (centre) to the actual Penning-trap measurement (right).

Careful and precision measurements of the mass difference with the use of the new method of phase-imaging detection of resonance frequency developed at the SHIPTRAP-facility [9] have demonstrated that the CMC Q_{EC} value is correct. PTMS has yielded the Q_{EC}-value of 2833(34) eV [10] (see red star in Fig. 4), which differs from the evaluated value (in green) by about 7 standard deviations. This result means a significant step in the campaign of the neutrino mass measurement, because it opens the door for the possibility to use CMC for the neutrino mass determination with ^{163}Ho on a sub-eV/c² level. It shows that there are no systematic effects inherent in microcalorimetry, which would have a severe impact on the uncertainty of the planned experiments to determine the neutrino mass with this technique. In the future a more precise Q_{EC} value should be measured by the new generation PENTATRAP-facility at MPIK within the ECHo-collaboration, in order to reach a sensitivity of better than 1 eV/c² (95% CL) for the neutrino mass.

Klaus Blaum, Sergey Eliseev, Szilard Nagy, Yuri Novikov

References:

[1] R.F. Garcia Ruiz, M.L. Bissell, K. Blaum, A. Ekström et al., Nature Physics 12, 594 (2016)
[2] X.F. Yang, C. Wraith, L. Xie, C. Babcock et al., Phys. Rev. Lett. 116, 182502 (2016)
[3] D.T. Yordanov, D.L. Balabanski, J. Bieron, M.L. Bissell et al., Phys. Rev. Lett. 110, 192501 (2013)
[4] D.T. Yordanov, D.L. Balabanski, M.L. Bissell, K. Blaum et al., Phys. Rev. Lett. 116, 032501 (2016)
[5] M. Rosenbusch, P. Ascher, D. Atanasov, C. Barbieri et al., Phys. Rev. Lett. 114, 202501 (2015)
[6] D. Atanasov, P. Ascher, K. Blaum, R.B. Cakirli et al., Phys. Rev. Lett. 115, 232501 (2015)
[7] Z. Meisel, S. George, S. Ahn, D. Bazin et al., Phys. Rev. Lett. 115, 162501 (2015)
[8] F. Schneider, T. Beyer, K. Blaum, M. Block et al., Eur. Phys. J. A 51, 89 (2015)
[9] S. Eliseev, K. Blaum, M. Block, A. Dörr et al., Appl. Phys. B 114, 107 (2014)
[10] S. Eliseev, K. Blaum, M. Block, S. Chenmarev et al., Phys. Rev. Lett. 115, 062501 (2015)

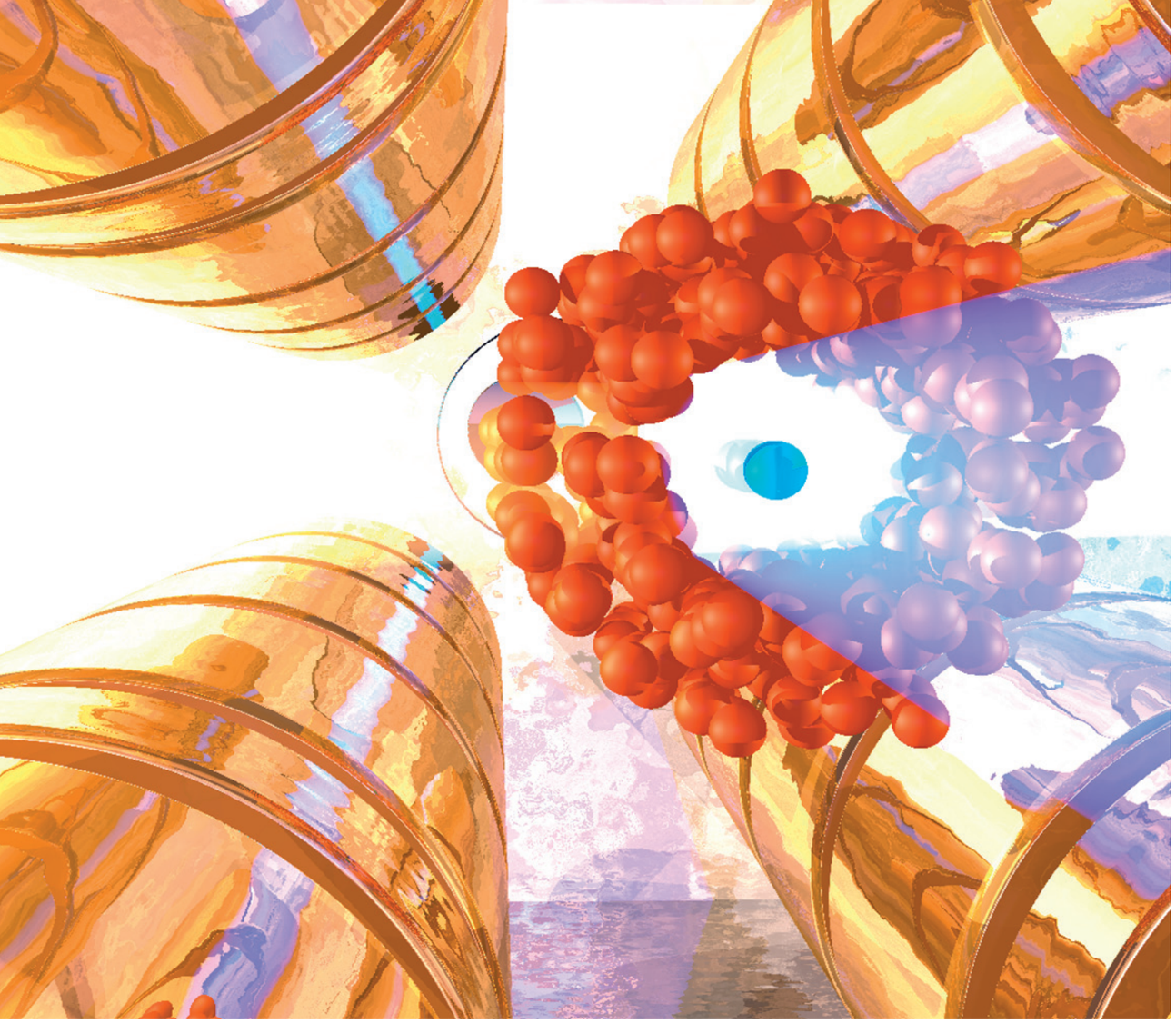

Highly charged ions (HCI) are injected into the central axis of a Coulomb crystal of laser-cooled Be^+ ions, and due to strong Coulomb repulsion push those out and heat up the crystal. Continued laser cooling then brings the new ensemble to crystallise again, with the HCI occupying fixed positions in space. The ions can be individually imaged and monitored for future optical clock studies.

2.2 Fundamental Tests with Trapped Ions

Introduction

Since many years MPIK has maintained a leading position in research with trapped cooled ions. We continue expanding our capabilities for the study of fundamental interactions and their symmetries with novel and challenging techniques. As an example, high-precision measurements of bound-electron *g*-factors in highly charged ions (HCI) accompanied by advanced theoretical work have recently yielded the most accurate value of the electron mass. In addition, an effective way to determine the fine-structure constant α from *g*-factors of HCI was put forward in a theoretical study. In the near future, the new high-precision Penning trap ALPHATRAP will extend those measurements to much heavier HCI, such as hydrogen-like lead Pb^{81+} supplied from an electron beam ion trap (EBIT). In this regime, further decisive gains in accuracy are expected.

Several EBITs developed at MPIK have also been used to study in free-electron lasers and synchrotron radiation facilities resonant interactions of HCI with X rays for QED tests. Moreover, cooling HCI by means of laser-cooled Coulomb crystal has also been made possible with CryPTEx, a cryogenic radio-frequency trap which for the first time allows to performing high resolution laser spectroscopy with such ions. Future experiments will apply this method for the development of optical atomic clocks capable of testing possible time variations of fundamental constants, and in particular of α.

Installed at CERN, the AEGIS antimatter gravity experiment is making use of MPIK's expertise in advanced ion trapping and manipulation techniques for the production of ultracold antihydrogen. Recently, several milestones towards a measurement of the gravitational interaction of antimatter have been realised.

Determination of the Atomic Mass of the Electron

In the last years, the fundamental theory of atomic structure, bound-state quantum electrodynamics, has been tested with unrivalled precision. A culmination of this development was the test of the *g*-factor of a single electron bound to a silicon nucleus ($^{28}Si^{13+}$) which has been measured on the sub-ppb level: $g_{exp}(^{28}Si^{13+}) = 1.99534895910(7)_{stat}(7)_{syst}(80)_{el.\,mass}$, with the last error due to the uncertainty of the electron mass dominating the experimental error budget. The theoretically predicted value was $g_{theo}(^{28}Si^{13+}) = 1.9953489580(17)$.

Motivated by this ultra-precise agreement between experiment and theory in strong fields, we exploited the strong scaling of the theoretical uncertainty with the atomic number to determine the mass of the electron by studying the bound-electron *g*-factor in the weaker field of hydrogenlike carbon $^{12}C^{5+}$. We performed a new measurement, improving the accuracy as compared to earlier experiments with this ion by more than an order of magnitude [1,2]. Additionally, we have reduced the relative theoretical uncertainty of $g(^{12}C^{5+})$ to 2.3×10^{-12}. To this end, we have also included estimates of so far uncalculated higher-order two-loop radiative corrections which were determined by rescaling these terms extracted from the experimental *g*-factor value for $^{28}Si^{13+}$.

Besides the very precise knowledge of the mass of the $^{12}C^{5+}$ ion with $\delta m/m = 1.5 \times 10^{-13}$, the measurement approach requires the precise determination of the frequency ratio of the spin precession frequency (Larmor frequency) ν_L of the bound electron and the cyclotron

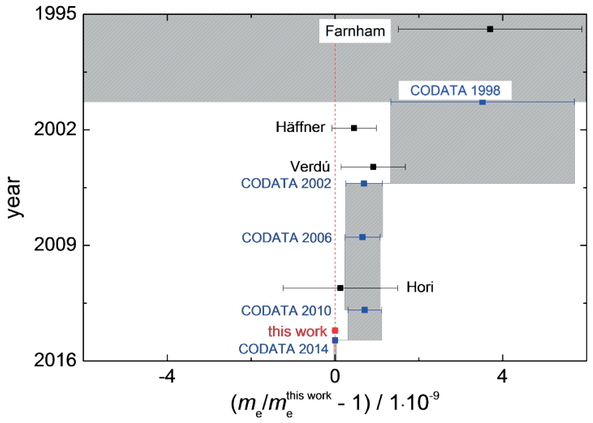

Fig. 1: Historical Review: Relative uncertainties of the atomic mass of the electron in the last 20 years.

frequency ν_c of the ion itself. This frequency ratio $\Gamma \equiv \nu_L/\nu_c$ was measured on a single $^{12}C^{5+}$ ion confined in a Penning trap setup. An extremely high vacuum of less than 10^{-16} mbar and therefore a closed setup and an *in situ* ion creation via a miniature electron beam ion trap (mEBIT) enabled measurement campaigns lasting for months. The cyclotron frequency was measured in a cylindrical five-electrode Penning trap (radius = 3.5 mm) by a recently developed and very fast phase sensitive measurement technique, PnA. During the 5 s phase evolution time at very low temperatures, the Larmor frequency was probed simultaneously. The spin state of the bound electron was determined via the continuous Stern-Gerlach effect in an adjacent trap. Here, the ring electrode made out of nickel generates a large quadratic inhomogeneity $dB = 10100\ \mathrm{T/m^2 \cdot z^2}$, shifting the axial frequency of the ion slightly in dependence of the spin state.

Combining our new high-precision frequency ratio measurement ($\delta\Gamma/\Gamma = 2.8 \times 10^{-11}$), the improved theoretical prediction of the *g*-factor, and the value of the ion's mass, the atomic mass of the electron has been improved by a factor of 13 with respect to the CODATA 2010 value (see Fig. 1). Our result was included in the CODATA 2014 evaluation. Presently, the measurement is limited by the uncertainty of the dominant systematic shift, the image charge shift, where the induced image charges on the trap electrodes decelerate the cyclotron motion. With $\delta m_e/m_e = 2.8 \times 10^{-11}$ we ensure also for the next years that the electron mass will not limit the determination of the fine structure constant α via recoil measurements on e. g. rubidium atoms.

Sven Sturm, Zoltán Harman, Christoph H. Keitel, Klaus Blaum

Test of Isotope Shifts and Access to the Fine-Structure Constant via *g*-Factors of Highly Charged Ions

Aiming for an explicit test of the impact of nuclear properties on bound electrons, the *g*-factors of two different highly charged isotopes have been measured for the first time [3]. The comparison of the *g*-factors of two isotopes enables a cancellation of most quantum electrodynamic contributions, which are partly even not known, and thus provide a highly sensitive probe of nuclear effects. Featuring on the one hand a 20% mass difference and on the other hand almost identical nuclear charge radii, the calcium isotopes ^{40}Ca and ^{48}Ca provide a unique system across the entire nuclear chart to test the relativistic nuclear recoil shift in presence of a magnetic field (see Fig. 2). In combination with an improved measurement of the mass of ^{48}Ca by the offline configuration of the Penning-trap mass spectrometer SHIPTRAP, $\delta m/m = 4.0 \times 10^{-10}$, the *g*-factors of the valence electrons of both lithiumlike ions $^{40}Ca^{17+}$ and $^{48}Ca^{17+}$ have been measured with relative uncertainties of a few 10^{-10}, constituting a so-far unrivalled level of precision for lithiumlike ions. The corresponding and successfully tested theoretical prediction is based on bound-state quantum electrodynamics but goes beyond the standard formalism, the so-called Furry picture, where the nucleus is considered as a classical, static source of the Coulomb field.

Such and similar nuclear effects and the uncertainties associated with them are however detrimental when the comparison of experiment and theory is to be used to determine fundamental constants, such as the fine-structure constant α, to high precision. An independent value of α may be extracted from the measurement of the *g*-factor of an electron bound in a hydrogenlike ion. This can be accomplished by identifying the leading relativistic (Dirac) contribution $g_D = 2/3(1 + 2(1 - (Z\alpha)^2)^{1/2})$, with Z being the atomic number, after subtracting corrections induced by quantum electrodynamics and nuclear effects from the measured value. We have, however, limited knowledge on nuclear charge distributions and nuclear polarizabilities, which restricts the number of *g*-factor digits theory can reliably calculate. In order to circumvent this problem, we devised a scheme employing a weighted difference of the *g*-factors of two types of ions, namely, that of a hydrogen- and lithium-like ion with the same atomic number. In both ions, the ground-state valence electron is in an s state and thus their wave function behaves similarly in the overlap region with the nucleus. Therefore, a weighting factor can be calculated to high accuracy to effectively cancel nuclear effects in the specific difference [4].

In an earlier study from 2006, a specific weighted difference of the *g*-factors of heavy hydrogen- and boronlike ions with the same Z was put forward. It was demonstrated that the theoretical uncertainty of the nuclear size effect in this difference can be reduced to 4×10^{-10} for heavy ions around Pb, which was several times smaller than the uncertainty due to α at that time. Since then, however, the uncertainty of α was brought down by an order of magnitude by other methods, making it more difficult to further improve the accuracy of α by means of bound-electron *g*-factor experiments. In case of the scheme we put forward, low-Z ions are considered, for which a much stronger cancellation of nuclear effects can be achieved. This independent scheme may be used to extract α from a comparison of experiment and theory with accuracy competitive with or better than the current value. Motivated by these prospects, lately, extensive theoretical efforts on bound-electron *g*-factors of light and medium-light hydrogen- and lithiumlike ions have been started, which will enable a significant improvement of $g_{\text{theo}}(^{28}Si^{11+})$. Measurements on $^{28}Si^{11+}$ have been recently finished with at least one order of magnitude improvement.

In the next years bound-electron *g*-factor measurements are organised within the HITRAP initiative. Referring to this, a new experiment, the ALPHATRAP experiment, is currently being built at MPIK. Highly charged ions will be injected from the Heidelberg EBIT. In that way, ALPHATRAP will be specialised in bound-electron *g*-factors of heavy highly charged ions up to hydrogenlike lead (Z = 82, $E_{\text{ionisation}} \approx 100$ keV). The determination of the Larmor frequency will be based also on the continuous Stern-Gerlach effect. In order to reduce various energy-dependent systematic shifts, the ion of interest will be sympathetically cooled by laser-cooled beryllium ions to extremely low temperatures. In addition to high-precision tests of QED in ultra-strong fields, the *g*-factors of heavy or light elements accessible with ALPHATRAP will also provide a new approach to measure the fine structure constant.

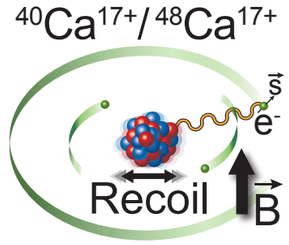

Fig. 2: Illustration of the nuclear recoil effect which has been tested by measuring and calculating the bound electron g-factor difference of the lithiumlike calcium isotopes $^{40}Ca^{17+}$ and $^{48}Ca^{17+}$.

Florian Köhler-Langes, Sven Sturm, Vladimir A. Yerokhin, Zoltán Harman

Cold Highly Charged Ions for Tests of the Time Variation of Fundamental Constants

Fundamental constants parametrise all physical laws, and thus our understanding of Nature; yet, neither their values can be calculated, nor their hierarchy predicted. Since they govern as coupling strengths both the structure and dynamics of physical systems at all scales, we can experimentally measure them. Our assumption of their constancy is, strictly speaking, purely based on observation. However, various extensions of the Standard Model of physics allow or even call for possible variations of their numerical values in time and space. Testing those hypotheses in the laboratory by means of atomic clocks over short time and space scales has become an active field of research, complementing cosmological investigations that are based on astronomical observations of much older and far-located systems.

In order to test present claims of a cosmological-scale variation of the fine-structure constant α, we have started a research program aiming at the development of ultra-precise frequency standards based on forbidden transitions in sympathetically cooled highly charged ions (HCI) as frequency references. In the optical range, standard ultra-stable lasers will be our tool for their study; for the vacuum-ultraviolet range, a high-harmonic-based frequency comb is currently being built. Such experiments are potentially capable of setting upper limits to the time variation of a more stringent than current ones elsewhere, and also of performing benchmark experiments for benchmarking QED and testing physics beyond the standard model. Optical frequency comparisons using lasers nowadays yield, without any doubt, the highest numerical relative accuracies (currently already at the tune of one part in 10^{18}) of any scientific measurements. Relying on the natural frequency stability of electronic transitions in ions and atoms, frequency ratios became much better experimentally accessible since the inception of frequency combs. For overcoming their current limitations, several paths are worldwide explored. Further reducing the systematic uncertainties in measuring in single-ion as well as optical-lattice clocks is the major one. Another focuses on ^{229}Th, a unique isotope with a long-lived, low energy (6 to 19 eV) nuclear

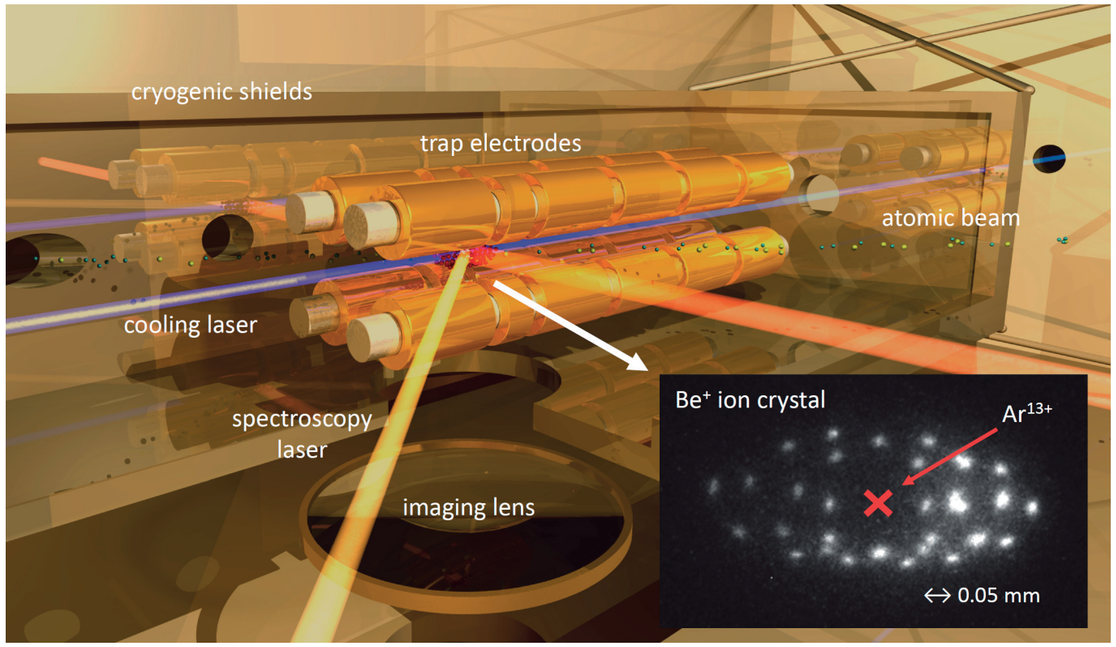

Fig. 3: Schematic representation of the cryogenic Paul trap CryPTEx. The radio-frequency electrodes trap a Coulomb crystal consisting of laser-cooled Be^+ ions. In the center of the depicted image of a real crystal, an Ar^{13+} ion has been implanted and repels the bright Be^+ ions that surround and sympathetically cool it.

isomeric state that could be addressed with lasers. The third one is the use of HCI, which combines several advantages. First, a wealth of accessible optical transitions exist, with a low sensitivity to external perturbations but a high one to a variation of the fine-structure constant α. Second, a systematic understanding is afforded by both experimental and theoretical studies of the transitions along isoelectronic sequences.

While atomic structure theory seems a mature field, its methods, driven by extraordinary experimental accuracies, are still undergoing continuous improvements. The mutual advances enable one to probe not only effects which are part of the Standard Model, such as QED, nuclear size effects and parity violation in the neutral sector, but in principle also the aforementioned time variation of fundamental constants, the possible existence of certain types of dark matter particles or upper bounds for non-Newtonian gravitation. All this relies on the exquisite sensitivity of universally reproducible electronic wave functions to smallest perturbations, and the ability of laser methods to interrogate the binding energy, symmetry and mutual couplings of the electronic system. Classic laser spectroscopic targets, such as alkali atoms and earth-alkali singly charged ions have yielded an enormous scientific harvest in those fields. Introducing HCI as targets would drastically broaden the possibilities in terms of accessible photon energies, variety of ions, and ground-state electronic configurations.

A first step to achieve those goals is the preparation of cold HCI, a task pursued since the early 1990's by several groups. With the construction of the Cryogenic Paul Trap Experiment (CryPTEx) at MPIK, HCI could be brought down to sub-kelvin temperatures for the first time. [5]. Meanwhile, we reach HCI temperatures lower than 30 mK. We have also developed an upgraded design which is now being set up both at the Physikalisch-Technische Bundesanstalt (PTB) and in our institute. The principle is sketched in Fig. 3. Since direct laser cooling of HCI is not possible, we employ the method of sympathetic cooling. A cloud of singly charged beryllium ions is prepared by photoionisation of an atomic beam inside of a cryogenic radio-frequency trap. The Be^+ ions are then laser cooled by driving their strong optical transition at 313 nm with a stabilised laser. At temperatures around 10 mK, the trapped ions arrange themselves in a stable structure, a so-called Coulomb crystal. We then implant HCI produced with one of our electron beam ion traps into this crystal by strongly decelerating the HCI and letting them lose nearly all their kinetic and thermal energy through repeated interactions with the continuously laser-cooled crystal. Finally, after thermalisation with the other ions, one or a few HCI occupy a central position

in the crystal and can be used for laser spectroscopic studies at much higher resolution than hitherto possible. HCI storage times of 20 minutes are achieved, since the background pressure in the trap region is below 10^{-14} mbar.

Since the electronic structures of HCI proposed by several theoretical groups for investigations with extremely high sensitivity to changes in the fine-structure constant are only very coarsely known, we have carried out experiments aiming at the systematic spectral analysis of those ionic species predicted to be most advantageous for this pursue. At a value of the atomic number Z = 77, the electronic structure of neodymium-like ions (i. e., with 60 bound electrons) passes through a remarkable level crossing (Fig. 4). The near-degeneracy of three electronic configurations including the ground state in Ir^{17+} ion supports several highly forbidden transitions which have been predicted to have the strongest dependence of their frequency on a possible variation of the fine structure constant among all ions, and therefore ideal conditions for such studies [7]. Here, we have had strong support from the theory division (Keitel).

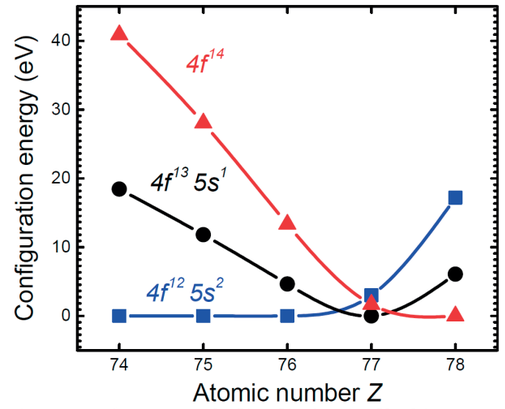

Fig. 4: Level crossing of $4f^{14}$, $4f^{13}\,5s^1$ and $4f^{12}\,5s^2$ Z = 77 in Nd-like ions [7].

Further work on fundamental physics was dedicated to precision tests of bound-state QED. Our results contradicted a hypothetical deviation that had been based on less accurate archival data. These experiments were performed using synchrotron radiation for both photoionisation and inner-shell photoexcitation of HCI in the highest charge states and photon energies ever reported in the field. By reaching the energy of the Mößbauer transition in the ^{57}Fe isotope at 14.4 keV, we achieved directly linking the hitherto most accurate X-ray metrological standard to the less well known electronic transitions in the X-ray domain, enabling the worldwide most precise analysis of HCI spectra. In collaborations with Jena University and PetraIII (DESY) we also aim at developing novel and ultra-stable X-ray energy standards using HCI. For this, a miniaturised EBIT with an off-axis gun that gives the unique advantage of transmitting X-ray beams along the trap axis has been built and tested.

For our collaboration with TRIUMF we are building a new cryogenic EBIT dedicated to experiments with rare isotope beams, and in particular to investigations of nuclei far from stability needed to model nucleosynthesis in supernovae, white dwarfs and neutron stars. The properties of HCI produced ("charge breeding") with the new CANREB-EBIS will significantly expand the experimental capabilities of the TRIUMF facility.

José R. Crespo López-Urrutia

Towards an Antimatter Gravity Measurement with Antihydrogen

The Antiproton Decelerator (AD) at CERN is currently the only facility worldwide for experiments with low-energy antiprotons ($\bar{p}$). Since 2002 it routinely synthesises antihydrogen ($\bar{H}$), the simplest atomic system consisting entirely of antiparticles, and also an ideal system for testing CPT (the symmetry between matter and antimatter) and antimatter gravity. While other existing CPT tests compare fundamental properties of particle–antiparticle pairs, the gravitational interaction of antimatter has never been studied experimentally. Since 2010, the AEGIS Collaboration (Antimatter Experiment: Gravity, Interferometry, Spectroscopy) prepares the first such experiment: The gravitational force acting on a slow beam of antihydrogen atoms will be determined by measuring its vertical deflection as it passes through a set of fine gratings called a deflectometer [8].

Gravity is the only fundamental interaction not currently formulated as a quantum field theory. Various quantum gravity theories aim at unifying gravity and the Standard Model of particle physics. In quantum gravity, additional exchange bosons beyond the ordinary 'Newtonian' tensor graviton are conceivable. Depending on their properties, they could induce striking deviations in the gravitational force between matter and antimatter which would not be detectable in existing high-precision gravity tests with ordinary matter. Any deviation from Newtonian gravity would violate the Weak Equivalence Principle (WEP) of General Relativity, which states that the trajectory of a test body in a gravitational field is independent of its structure and composition. All limits on a WEP violation for antimatter

based on experiments using ordinary matter are indirect and model-dependent: hence, the antimatter gravity must be studied in a dedicated, direct experiment, such as AEGIS. As of 2016, most of its major components have been completed and installed: The e^+ source, the e^+ accumulator, two superconducting magnets and all ion traps have been commissioned. Antiproton pulses from the AD have already been captured, stacked and stored for 10 minutes. A scintillating tracker monitors $\bar{H}$ production. The laser for excitation of positronium (Ps*), as needed for the reaction $Ps^* + \bar{p} \rightarrow \bar{H}^* + e^-$ yielding $\bar{H}^*$ is in place.

As for the deflectometer, two significant advances have been achieved. The principle of the method was demonstrated with an intense $\bar{p}$ beam [9]. In a photographic emulsion used as annihilation detector, antiprotons produced the same star-shaped signature as $\bar{H}$. A miniaturised deflectometer with two gratings was placed in a $\bar{p}$ beam (100 keV kinetic energy), as shown in Fig. 5a. The reference position (without deflection) was recorded by the shadow of grating in direct contact with the detector partly exposed to the $\bar{p}$ beam. Both the deflectometer and the contact grating were then illuminated with diffuse light passing through the grating in the interferometric regime. Photons reach the detector undeflected, and the pattern they imprint is aligned with another one taken with antiprotons, as shown in the left pane of Fig. 5b. Antiprotons flying through the deflectometer appear displaced in the positive y direction (right pane). The graph in Fig. 5c shows the vertical positions of $\bar{p}$ annihilations modulo the grating period (blue bins and black line) compared to the light signal (red line). A vertical deflection of $\delta y = 9.8 \pm 0.9\,(\text{stat}) \pm 6.4\,(\text{syst})$ μm corresponding to an upward force of $530 \pm 50\,(\text{stat}) \pm 350\,(\text{syst})$ aN is most likely due to the Lorentz force from a magnetic fringe fields of about 8 G. While the gravity force on $\bar{H}$ atoms is many orders of magnitude smaller, their expected deflection is comparable due to the significantly lower velocity and longer flight distance in the full-scale experiment.

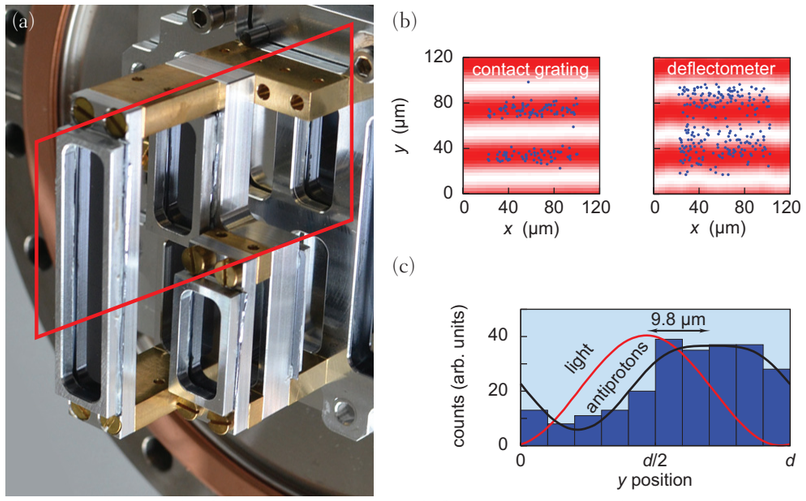

Fig. 5: (a) Photograph of the miniaturised moiré deflectometer setup used in the proof-of-principle measurement with a $\bar{p}$ beam. (b) Positions of recorded $\bar{p}$ annihilation events (blue dots) and light pattern (red) behind the contact grating (left) and the deflectometer setup (right). (c) Antiproton annihilation events summed up modulo the grating period (blue bins and black line), compared to the intensity of the light pattern (red line).

For the direct excitation of Ps to a Rydberg state we pursue a two-step excitation using an ultraviolet laser ($\lambda_{UV} = 204\ldots206$ nm) for the $n = 1 \rightarrow 3$ transition and an infrared laser ($\lambda_{IR} = 1064$ nm) from $n = 3$ to higher levels. As a test of the novel scheme, we perform single-shot positronium annihilation lifetime spectroscopy (SSPALS) [10] exploiting the Ps lifetime dependence on its internal quantum state. As shown in Fig. 6a, Ps was produced by a beam of e^+ hitting a converter target also illuminated by both the UV laser and the IR laser. Ps annihilations were recorded with a lead tungstate scintillator located above the converter. First, the IR laser was tuned to a transition from $n = 3$ to the continuum, dissociating the Ps. The free positrons were drawn away from the detector, resulting in a decrease of the annihilation rate shown by the grey line in the left pane of Fig. 6b. This rate was the recorded as a function of the UV laser wavelength scanned around the $n = 1 \rightarrow 3$ transition, displaying a resonance (right pane) at 205.05(2) nm.

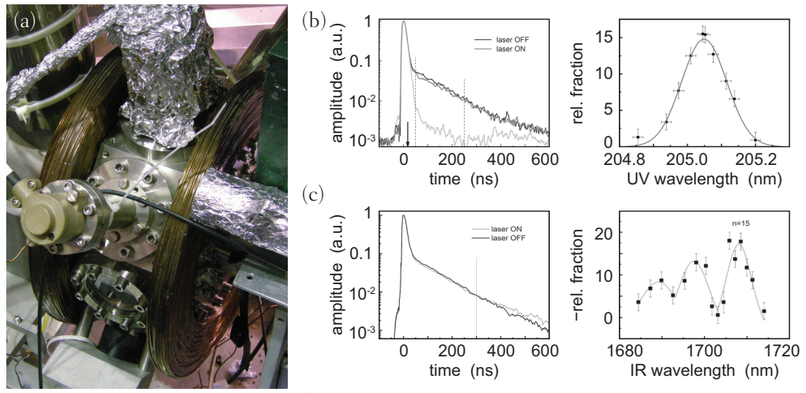

Fig. 6: (a) Vacuum chamber which houses the positron annihilation lifetime spectroscopy setup. Positrons enter from the right and impinge on a central target. Lasers enter from the front; an annihilation detector is placed 40 mm above the target. (b) SSPALS data for the IR laser tuned to a transition from n = 3 to the continuum (left) and the resulting resonance of the $n = 1 \rightarrow 3$ transition (right). (c) SSPALS data for the IR laser tuned to $n = 3 \rightarrow$ Rydberg (left) and observed resonances for $n = 3 \rightarrow 15$ (right) (from [10]).

In a second measurement, the IR laser was tuned to the transition from $n = 3$ to Rydberg states while the UV laser wavelength was kept constant on the $n = 3$ resonance. Rydberg states have longer lifetimes since the overlap of the e^+ and e^- wavefunctions is reduced. The annihilation rate thus drops 300 ns after Ps production, followed by an excess at 300…600 ns, when Ps particles finally hit the chamber wall, as illustrated in the left and right panes of Fig. 6c respectively. Resonances of $n = 15\ldots17$ are clearly visible and in good agreement with earlier surveys. These measurements, thus, demonstrate laser excitation scheme of Ps needed for the production of antihydrogen.

Alban Kellerbauer

References

[1] S. Sturm, F. Köhler, J. Zatorski, A. Wagner, Z. Harman, G. Werth, W. Quint, C.H. Keitel and K. Blaum, Nature 506, 467 (2014)

[2] F. Köhler, S. Sturm, A. Kracke, G. Werth, W. Quint and K Blaum, J. Phys. B 48, 144032 (2015)

[3] F. Köhler, K. Blaum, M. Block, S. Chenmarev, S. Eliseev, D.A. Glazov, M. Goncharov, J. Hou, A. Kracke, D.A. Nesterenko, Y.N. Novikov, W. Quint, E. M. Ramirez, V.M. Shabaev, S. Sturm, A.V. Volotka and Günter Werth, Nature Commun. 7, 10246 (2016)

[4] V.A. Yerokhin, E. Berseneva, Z. Harman, I.I. Tupitsyn and C.H. Keitel, Phys. Rev. Lett. 116, 100801 (2016); Phys. Rev. A 94, 022502 (2016)

[5] L. Schmöger, O.O. Versolato, M. Schwarz, M. Kohnen, A. Windberger, B. Piest, S. Feuchtenbeiner, J. Pedregosa-Gutierrez, T. Leopold, P. Micke1, A.K. Hansen, T.M. Baumann, M. Drewsen, J. Ullrich, P.O. Schmidt and J.R. Crespo López-Urrutia, Science 347, 1233 (2015)

[6] A.K. Hansen, O.O. Versolato, Ł. Kłosowski, S.B. Kristensen, A. Gingell, M. Schwarz, A. Windberger, J. Ullrich, J. R. Crespo López-Urrutia and M. Drewsen, Nature 508, 76 (2014)

[7] A. Windberger, J.R. Crespo López-Urrutia, H. Bekker, N.S. Oreshkina, J.C. Berengut, V. Bock, A. Borschevsky, V.A. Dzuba, E. Eliav, Z. Harman, U. Kaldor, S. Kaul, U.I. Safronova, V.V. Flambaum, C.H. Keitel, P.O. Schmidt, J. Ullrich and O.O. Versolato et al., Phys. Rev. Lett. 114, 150801 (2015)

[8] A. Knecht et al. (AEGIS Collaboration), Hyperf. Interact. 228, 121 (2014)

[9] S. Aghion et al. (AEGIS Collaboration), Nature Commun. 5, 4538 (2014)

[10] S. Aghion et al. (AEGIS Collaboration), Phys. Rev. A 94, 012507 (2016).

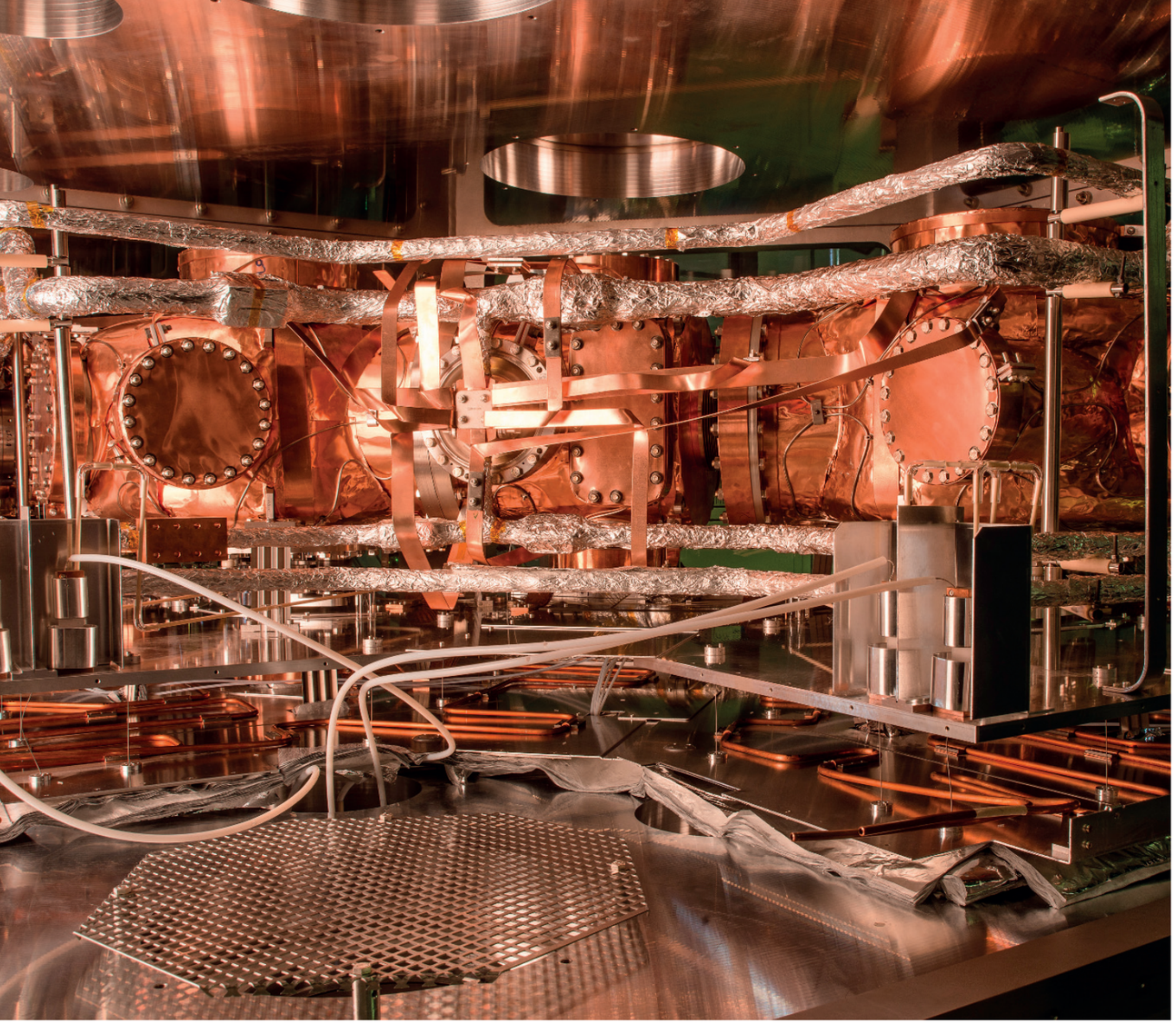

2.3 Atomic and Molecular Collisions

A corner section of the cryogenic storage ring CSR. The cryogenic beam vacuum chambers are surrounded by the large cryostat. Inside, the stored ion beam circulates on a closed orbit at ~6 K temperature and extremely low residual gas density. The corner sections house the electric field plates for the ion beam deflection. Moreover, particle detectors here observe the charged and neutral products from reactive collisions along the long straight sections of the ion orbit.

Introduction

Numerous processes in nature and technology, from astronomical and terrestrial environments to chemistry and biology, depend on the internal quantum motion of atoms and molecules. There the electrons and nuclei rarely move independently, but often in strong correlation with each other. The related many-body quantum physics challenges our understanding of matter. Collisions of atoms and molecules with charged or energetic particles intercept the internal quantum motion and create new, energetically excited states that modify the molecular properties and trigger internal dynamics. Molecules change their shape, chemical bonds are weakened and, ultimately, compounds broken up. Well-controlled particle beams as well as the counting and imaging of individual particles are cutting-edge tools to disentangle the quantum mechanisms at work. Instruments developed at the MPIK can realise atomic and molecular collisions under optimised initial conditions and then analyze the products to draw conclusions about the correlated quantum motion. They particularly focus on detecting and imaging coincidence events, with several outgoing particles from one single collision. Moreover, the initial internal states of colliding particles are carefully controlled using beams of atomic, molecular and cluster ions stored in extreme isolation from the terrestrial atmosphere and even the thermal radiation of the laboratory. Certain systems are benchmarks, studied both by experiments and by the most advanced quantum theoretical methods. In other cases, molecules and matter aggregates important in natural and technical media are targeted directly.

The Electrostatic Cryogenic Storage Ring CSR

The CSR [1] is a cryogenic electrostatic ion storage ring for collisional and laser-interaction studies over long storage times with fast atomic, molecular, and cluster ion beams. The cryogenic facility offers an ambient temperature near 6 K for the stored ion beam. The ring layout was chosen to enable experiments with crossed and merged, particle and laser beams. In-ring experiments often involve detecting fast product-particles released by reactive collisions of the stored ions. Along extended straight sections, the stored ions can also interact with collinear merging beams of electrons or atoms. For equal average velocities of the two merged beams, the effective collision velocities reach down to the thermal speeds in a low-temperature environment. The energy of the stored beams in CSR, up to 300 keV for singly charged ions, is sufficiently high that their velocity can be matched with the one of an electron beam even for large molecules (envisaging masses up to ~160 amu); this includes, e. g., small organic ring species. The merged beams areas of the CSR open the field of low-temperature ion reaction studies with electrons and atoms. Uniquely at CSR, such studies can be performed with ions that were stored for a long time in a low-pressure environment nearly free of blackbody radiation. Moreover, at the high ion beam velocity even neutral reaction fragments can be readily detected and imaged in event-by-event, multi-fragment coincidence mode.

CSR setup and performance. Ion beams in CSR are stored by a purely electrostatic arrangement of deflectors and focusing elements. The smallest bending radius of the deflectors is 1 m, corresponding to a field strength of 6 kV/cm at the maximum ion energy.

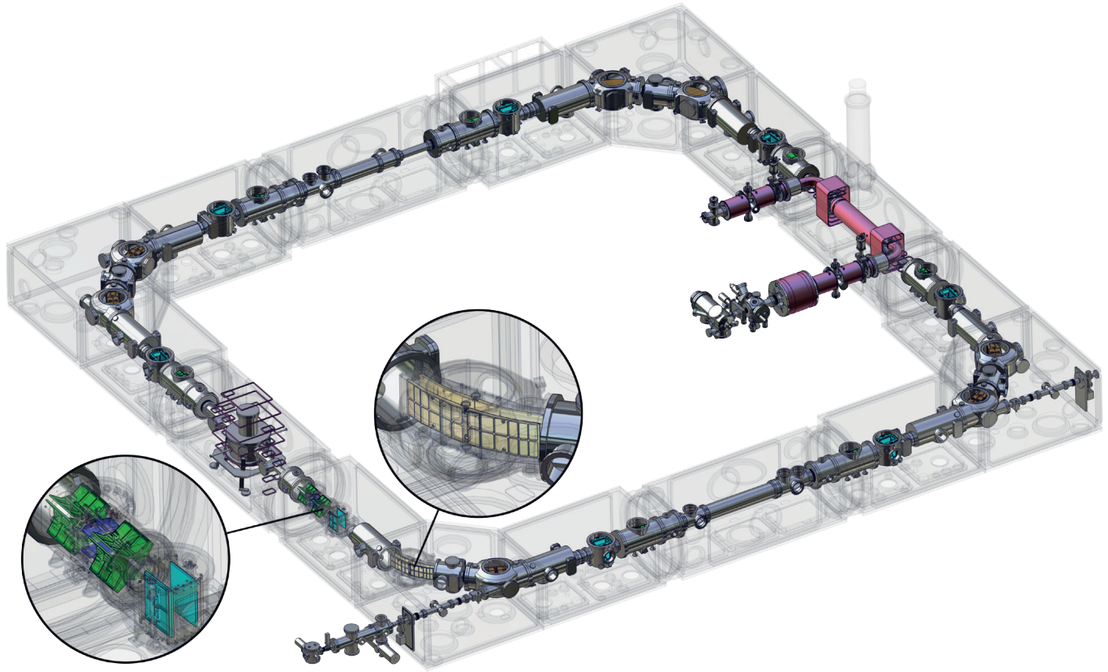

Fig. 1: Design model of the CSR. Details are shown for the electric quadrupole lenses and beam deflectors. The straight sections between the ring corners serve for ion beam injection and the neutral merged-beam experimental zone (bottom), the merged electron beam (right) and the reaction microscope (left). The upper straight section is used for ion-beam diagnostics.

With four 90°-bending corners and four field free straight sections, the CSR has a closed orbit length of 35 m. The beam pipe surrounding the ions, containing the electrostatic elements, forms the inner vacuum system. It is kept below 10 K and all gases remaining in it after pre-evacuation are frozen out on the cold walls; pumping units kept as cold as 2 K cryo-condense even hydrogen. Radiation shields at 40 and 80 K, successively, surround the experimental vacuum chambers. Like in a large cryostat, all is housed in an outer, insulation vacuum system at 10^{-6} mbar (Fig. 1). The ring successfully started operation in March 2015. The CSR inner vacuum chamber stayed below 10 K for almost 4 months. During this period, the first cryogenic beam-time of the CSR was devoted to the study of the ion-beam storage conditions and to laser interaction experiments with stored, negatively and positively charged molecules and clusters [1].

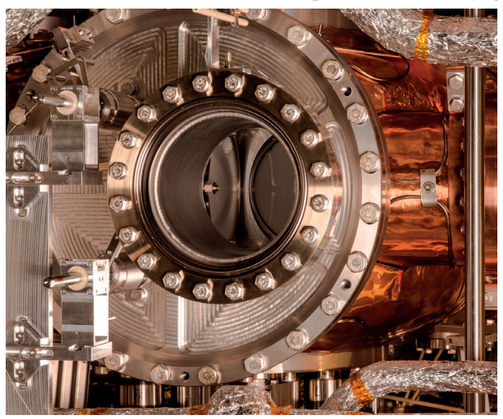

Fig. 2: Detector for molecular fragmentation events in the electron–ion merged-beams zone of the CSR. Fast counting signals from a 120 mm diameter microchannelplate detector are read out by electronic signals and a camera system, performing multiparticle coincidence imaging of neutral products from molecular fragmentation.

The beams for CSR were produced in its ion source area from discharge and sputter ion sources. Aside from its electronic diagnostic elements for stored ions, the CSR was equipped with detectors [2] for the fast particles produced when stored ions change their charge state or dissociate into fragments (Fig. 2). Such background reactions can be triggered by collisions of the stored ions with the molecules of the residual gas in the vacuum system. In conventional devices, even with ultra-high vacuum, they occur abundantly whenever an ion beam is present. Already in the first cryogenic CSR operation, however, the signal of these background reactions was hardly observable, indicating its extremely low-density vacuum.

Main studies during the first cryogenic beam time were devoted to the interaction of the stored ions with a laser beam. In a negative ion, an electron can be removed by photodetachment, leading to a neutral product triggering the particle detector. In many cases, the neutral products from photodetachment served to monitor the ion intensity. By comparing this laser-induced signal to the much lower neutral background from residual gas in the absence of the laser, the residual gas density in the CSR could be constrained, yielding

< 140 cm^{-3} [1]. This corresponds to a pressure of $< 10^{-14}$ mbar at room temperature, improving on the design value of the CSR (10^{-13} mbar) by more than a factor of 10.

Ion beam lifetime studies and Schottky noise diagnostics. Ion beam storage lifetimes in the CSR were observed (Fig. 3) to reach up to 45 min. Stored-beam signals could be observed up to three hours following a single injection. These times are largely sufficient for the envisaged experiments and almost two orders of magnitude longer than available in previous ion beam experiments at the MPIK, using the room-temperature storage ring TSR. Yet, the low residual gas densities should allow even longer storage and the mechanisms limiting the beam lifetime in these hitherto unexplored conditions are still to be understood. During the long beam lifetimes also the electronic Schottky noise of the ions could be recorded. Its spectral analysis (Fig. 4) reveals the distribution of the ion velocities in the CSR. After several minutes of storage an increase of the ion velocity spread by a diffusion of the ions in their velocity coordinates becomes visible. Further investigations on this process, potentially limiting the ion beam lifetime, are under way. Schottky-noise spectra will serve to study and optimise the phase-space cooling of the ions in the CSR using its merged electron beam.

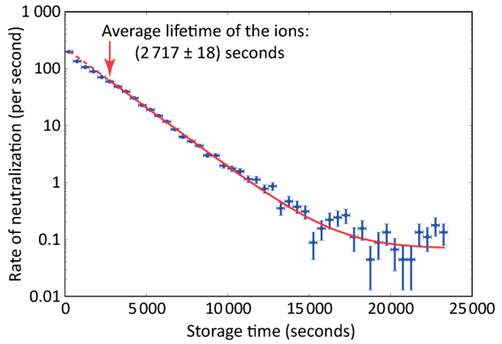

Fig. 3: Lifetime measurement of silver dimer anions (Ag_2^-) in the CSR (rate of neutral products from ion photodetachment by a 633 nm laser; ion beam energy: 60 keV). For this largest-mass ion stored so far, the achieved mean lifetime is ~45 min.

Internal cooling of stored molecular ion beams. In the first cryogenic beam-time, the radiative cooling of small hydride ions at the low level of black-body radiation inside the CSR was investigated for two cases. Resonant near-threshold photodissociation of the astrophysically important methylidyne cation, CH^+, was achieved by wavelength-tunable ultraviolet laser radiation. As described in Section 2.4, the resonances reveal the rotational levels J that are populated in the stored CH^+ ions before they are hit by the laser. The relative population in the $J = 0$ ground state, which in a 300 K black-body field would amount to ~10% only, is seen to rise continuously up to ~60% during the 240 s of storage time in the CSR. For the lowest rotational levels accessed here, this enabled a state-by-state benchmark measurement of the CH^+ resonant photodissociation cross section [3].

A second case studied was the near-threshold photodetachment of the hydroxyl anion, OH^-. A probe laser set to wavelengths close to the threshold is applied to yield photodetachment signals that represent only specific ranges of rotational levels (quantum number J) in the OH^- ions. Normalised to the J-independent photodetachment rate from a reference laser at shorter wavelength, these signals convey the relative populations of the probed rotational level ranges (Fig. 5). Through spontaneous infrared emission to lower J states, signals requiring higher rotation (such as $J \geq 2$) decay relatively fast; at longer times the decay is dominated by lowest J state of the range, which has the longest lifetime. The lowest excited rotational level ($J = 1$) needs most time to decay, reaching its equilibrium population only after ~5 min of storage. After 10 min, as much as ~90% of all ions were found in the $J = 0$ ground state. Detailed information on the rotational dependence of the photodetachment process is contained in the signals with $J \geq 0$, obtained at three different probe wavelengths. These time-resolved multi-wavelength measurements allowed the relative photodetachment cross sections of the lowest J-levels to be deduced on a purely experimental basis and also revealed precise rotational level lifetimes. This way the method of photodetachment thermometry using OH^-, increasingly applied in recent years to characterise cryogenically stored ions, for the first time became largely independent of the still uncertain theoretical predictions on state-by-state photodetachment efficiencies.

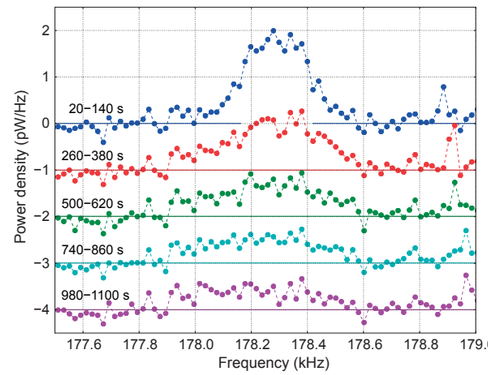

Fig. 4: Schottky-noise spectra of a 60.3 keV beam of Co^- ions stored in the CSR around the 20th harmonic of their revolution frequency. The signals were taken during the indicated time intervals after a single injection and include an offset shift of −1pW/Hz per trace.

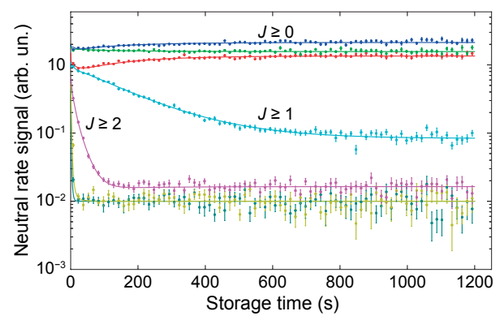

Fig. 5: Rotationally dependent near-threshold photodetachment rates of OH^- ions in the CSR. Relative signals are shown for various probe laser wavelengths, leading to the indicted ranges of the rotational quantum number J.

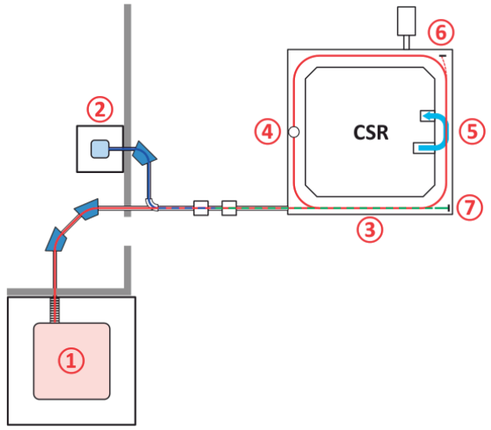

Fig. 6: Experimental areas in and around the CSR. (1) Main ion source platform, 300 kV. (2) Ion source for fast photodetached neutral beams, 60 kV. (3) Neutral merged-beam interaction zone. (4) Cryogenic reaction microscope. (5) Electron merged-beam interaction zone. (6) Detector zone for electron merged-beam interaction. (7) Neutral beam dump and detector zone for neutral merged-beam interaction.

Merged and crossed beam experimental areas. In the development of the CSR experimental areas (Fig. 6), the installation of the merged electron beam of CSR is essentially complete at the end of 2016. The implemented cryogenic system involves high-temperature superconductor magnetic coils that guide slow (down to 1 eV) electrons into overlap with the ions in a linear section of the CSR orbit. Very low energy beams from a photocathode were already realised in tests at the TSR electron target. The CSR merged electron beam device awaits first operation in 2017.

Also the neutral atomic beam setup of the CSR (positions 2, 3 and 7 in Fig. 6) is completely installed and awaits first experiments. It is fed by anion beams from a separate platform. Using a photodetachment zone with a very strong (2 kW) continuous diode laser in the injection line of CSR, fast neutral beams of hydrogen, carbon and oxygen ions can be merged with the state-controlled molecular ions circulating in the CSR. Several particle detectors were installed to analyse the products of the ion–atom interactions in the beam overlap zone.

For detecting recoil ions and electrons released in reactions of ions stored in CSR with a weak crossed gas-jet target or with a laser beam, a reaction microscope is under design (position 4 in Fig. 6). In the CSR, the combination with the fast-beam neutral fragment detection capability and the use of state-controlled molecular anions and cations, as well as low-velocity multiply charged atomic ions, the reaction microscope will offer unique opportunities of studying atomic and molecular quantum dynamics. Even ultrafast dynamics is expected to become accessible using femtosecond laser pulses.

Multipixel cryogenic microcalorimeters. By calorimetric detection, the kinetic energy of fragments from a molecular reaction can be determined. For reactions in fast beams (including the merged-beams arrangement) this kinetic energy is proportional to

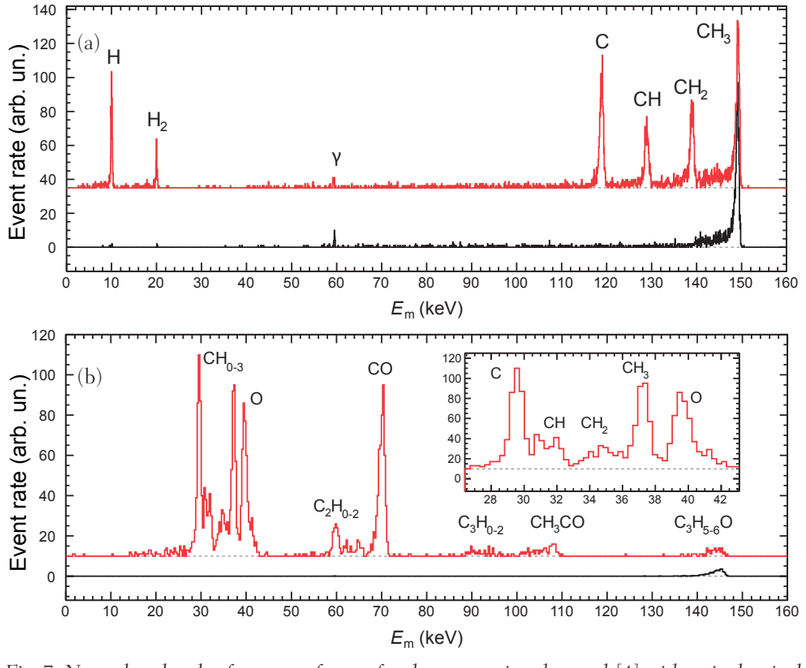

Fig. 7: Neutral molecular fragments from a fast-beam reaction detected [4] with a single-pixel MMC detector at the CSR ion platform. (a) Methyl cations CH_3^+ and (b) acetone cations $(CH_3)_2CO^+$ from the 150 keV beam are fragmented in residual-gas collisions. The kinetic energies (E_m) measured by the MMC are proportional to the fragments' mass and allow their identification.

the fragment mass. Hence, a multipixel calorimeter can identify the masses of fragments from a molecular reaction individually and independently of their charge. In the CSR with polyatomic ions up to 300 keV beam energy, such measurements can be envisaged with the highly innovative method of cryogenic microcalorimetry. Overcoming the limitations of conventional mass spectrometry, this technique is able to analyse neutral reaction fragments as well as charged ones. Moreover, by the position resolution of the multipixel calorimeter also the fragment momenta can be measured. In collaboration with Heidelberg University (Kirchhoff Institute of Physics) successful tests were performed [4] on mass-resolved molecular fragment detection with magnetic microcalorimeters (MMC) at ~20 mK temperature (Fig. 7). A 42 × 42 mm MMC chip for the CSR – the molecular camera MOCCA using strip-wise readout of 4096 pixels by 32 squid sensors – is being built by the University group while the implementation in CSR, using a dilution refrigerator, is in progress. First tests of the complete MOCCA system, preceding its installation in CSR, are expected in about a year. The experimental areas and detection systems under development at CSR will enable a wide scope of unique experiments in atomic, molecular and cluster physics.

Robert von Hahn, Andreas Wolf, Klaus Blaum

Fast Ion–Atom Collisions: Two Path Interference

The field of ion-atom collisions was strongly advanced with the advent of the reaction microscope technique which enabled kinematically complete studies and provided the most detailed insight into the collision dynamics. One of the last experiments using the van de Graaff accelerator at the MPIK studied interference effects which show up in collisions of fast molecular hydrogen ions with a helium gas target [5]. This process can be considered more clearly in the equivalent, reversed kinematics illustrated in Fig. 8: a fast helium atom being coherently scattered at the two centres of the H_2^+ ion. As result a two-path interference pattern can show up in the scattered projectile momentum distribution. In the specific reaction channel considered here the helium atom undergoes single ionisation while the H_2^+ ion becomes electronically excited and dissociates. Thus, a projectile and a target electron actively participate, implying at first glance a rather complex collision dynamics. By detecting all four free reaction products in coincidence a kinematically complete experiment was performed. The analysis allowed the alignment of the molecular axis to be fixed in space and cross sections to be studied in the molecular frame. Furthermore, particular values of the initial distances of the protons in the H_2^+ ion could be selected. For two inter-proton distances, Fig. 9 shows the cross section as function of the momentum transfer q to the molecule, determined via the inverse momentum change $-q$ of the helium atom. As expected for a two slit interference phenomenon the observed stripes lie close together in events with larger inter-proton distances (Fig. 9a) and move apart for smaller ones (Fig. 9b). In a perturbative description different first- and higher-order terms were found to contribute to the reaction. This study achieved the identification of Young-type interferences in a rather complex atomic collision, representing a correlated five-body system.

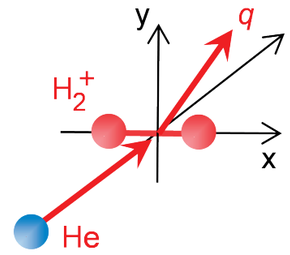

Fig. 8: Reversed kinematics for the observed collision $H_2^+ + He$ in the molecular frame. While the experiment measures the momentum transfer $-q$ to the H_2^+ ion scattered in the observed collision, the He atom in the reversed process shown here experiences a momentum transfer of q.

Alexander Dorn, Daniel Fischer

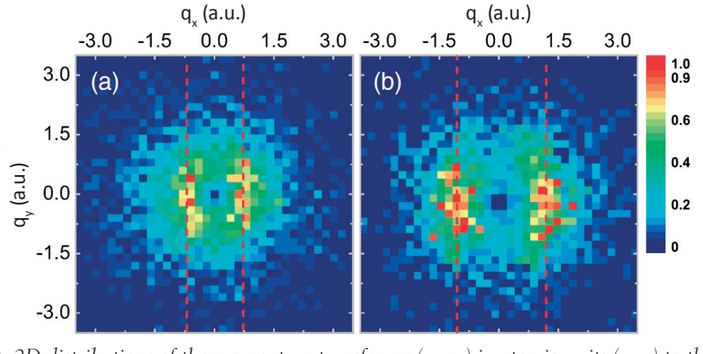

Fig. 9: 2D distributions of the momentum transfer $q = (q_x, q_y)$ in atomic units (a.u.) to the H_2^+ ion for inter-proton distances in the H_2^+ ion (a) larger than 3.1 a.u. and (b) smaller than 2 a.u.

Electron Collision Dynamics for Atoms, Molecules and Clusters

Electron collisions play an important role in natural environments as the upper atmosphere and interstellar space, but also in technical plasmas and in radiation biology. Here a large part of damage to living cells along the track of an energetic primary particle is assumed to be caused by slow secondary electrons . We have studied interatomic reactions which can multiply the number of slow electrons and produce several reactive ions. These experiments were done for atoms and for biologically relevant molecules in form of monomers and hydrated clusters. In addition, the study of slow electron collisions enables detailed insight into the correlated dynamics of fundamental few-body quantum systems and fosters the development of *ab initio* theoretical methods.

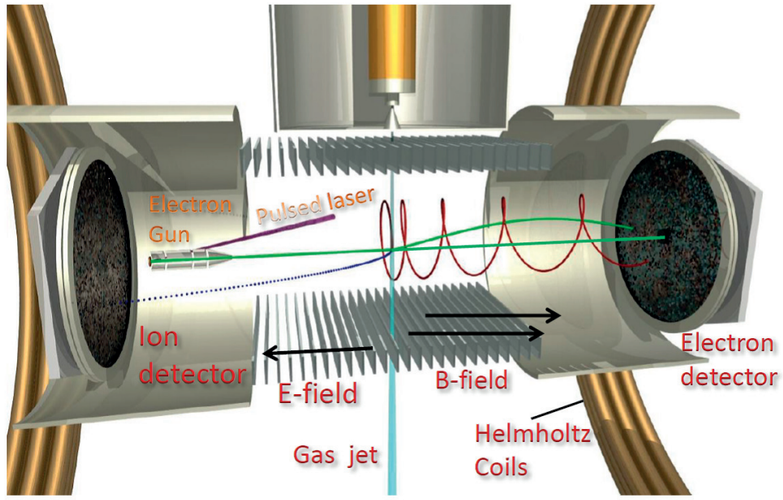

Fig. 10: Schematic view of the reaction microscope used to study electron impact ionisation.

To image the ions and electrons produced in the ionisation we use the reaction microscope developed at the MPIK specifically for electron-induced processes, which is still worldwide unique (Fig. 10). It was significantly improved concerning momentum resolution and the projectile lower energy limit. This was achieved by optimizing the electric and magnetic extraction fields and by developing a miniature electron gun with a photocathode, producing sub-nanosecond electron pulses inside the spectrometer very close to the target gas jet. The supersonic jet provides a large range of atomic, molecular and cluster targets. Detection of all free final-state electrons defines the collision kinematics and the ionised orbital's binding energy. Ion detection provides the molecular fragment masses, charge states and kinetic energy release. Coincident detection of up to three electrons and two ions was achieved.

We also built a new spectrometer that images the negative ions produced by dissociative electron attachment (DEA) to molecules [6]. This resonant process, occurring at sub-10 eV energies, is considered to significantly contribute to radiobiological damage like DNA strand breaks. Our setup achieved projectile energies down to the 1 eV region and an energy resolution in the 200 meV range.

Interatomic relaxation mechanisms in argon dimers. In weakly bound systems like liquids and clusters electronically excited states can relax in inter-particle reactions via the interplay of electronic and nuclear dynamics. Using a cold supersonic jet target of argon containing a fraction of argon clusters (dimers) we have studied two prominent examples, interatomic Coulombic decay (ICD) and radiative charge transfer (RCT), which are induced in argon dimers by electron collisions [7].

In ICD one atom is ionised and left in an excited state. Subsequently, in a transition to the ground state, energy is transferred to a neighbour atom, ionizing it. Altogether three slow electrons and two positive ions are produced (Fig. 11). The same number of charged particles is obtained in the RCT process. There, electron impact doubly ionises one atom. One of its vacancies is then filled by an electron transferred from the neighbour, any excess energy being released by photon emission.

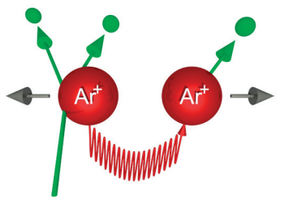

Fig. 11: Schematics of interatomic Coulombic decay in Ar_2 dimers induced by electron impact ionisation [7]. Five outgoing charged particles were detected in coincidence.

We performed full quintuple-coincidence measurements: the energies of all the charged final-state particles were detected. As result we unambiguously distinguished ICD and RCT and traced the vibrational and relaxation dynamics as function of the energies of the collisionally ionised initial states. Such interatomic processes multiply the number of electrons and shift their energies down to the critical 1–10 eV range, where they can efficiently cause chemical degradation of biomolecules. Consequently, we extended our studies to bio-relevant species.

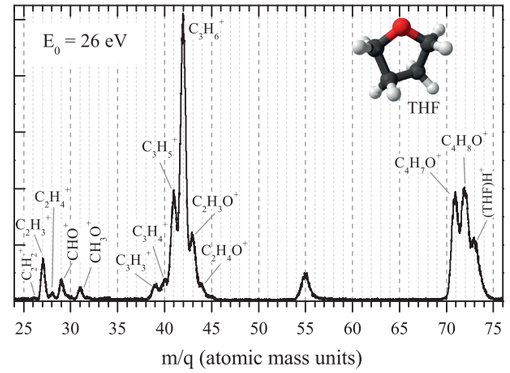

Fig. 12: Mass spectrum for ionisation and fragmentation of tetrahydrofuran by 26 eV electron impact. The parent ion mass is 72 amu.

Fragmentation of organic molecular monomers and clusters. First studies of larger molecules focused on tetrahydrofuran (THF, C_4H_8O) [8]. This compound is an analogue of deoxyribose in the backbone of DNA. Our technique provides a large amount of information on the electron-impact induced fragmentation of such targets. The ion spectrometer of our reaction microscope can resolve all fragments produced (Fig. 12). For each channel, also the binding energies of the ionised electron orbitals and the ion kinetic energies were measured [8]. Thus, a detailed understanding of the fragmentation dynamics is reached. E.g., we observe that the molecular structure stays intact for ionisation of the highest occupied molecular orbital (HOMO). Hydrogen emission is observed for ionisation of the next inner orbital and ring-breaking reactions are induced for ionisation of more strongly bound inner-valence orbitals.

An important motivation for this work is to observe modifications of the fragmentation dynamics when the molecule is embedded in an environment of water or other organic compounds. Therefore, we produced hydrated and pure THF cluster targets. Surprisingly, we found the fragmentation dynamics to be strongly modified for the clusters. E.g., ionisation of the THF HOMO orbital (leaving the structure intact for the monomer) here leads to a ring-breaking reaction. Also intermolecular energy transfer reactions, namely ICD, were found. The studies will be pursued further, also developing new target preparation techniques to obtain samples of larger biomolecular compounds.

Ionisation: fully differential electron emission patterns. With its complete solid-angle acceptance, the reaction microscope is ideally suited to record fully differential cross sections (FDCS) for single ionisation (so-called (e,2e) measurements). These critically test state-of-the-art theories. Non-perturbative models which formally solve the full many-body Schrödinger equation nowadays exactly reproduce results for the smallest systems like helium; recently even larger systems like argon came into reach. Perturbative calculations on the other hand are not exact, but give much more insight into the reaction mechanisms involved.

This was demonstrated for neon where experimental cross sections are reproduced by both the non-perturbative B-spine R-matrix model (BSR) and a perturbative distorted wave theory (3DW). In contrast, the more complex argon atom is more challenging and at the limit of both approaches (Fig. 13) [9 and references therein]. Here BSR is still doing well for the complete pattern, while 3DW is good only inside the projectile scattering plane (red frame), but fails outside this plane. This clearly demonstrates the importance of testing theory over the full solid angle of electron emission.

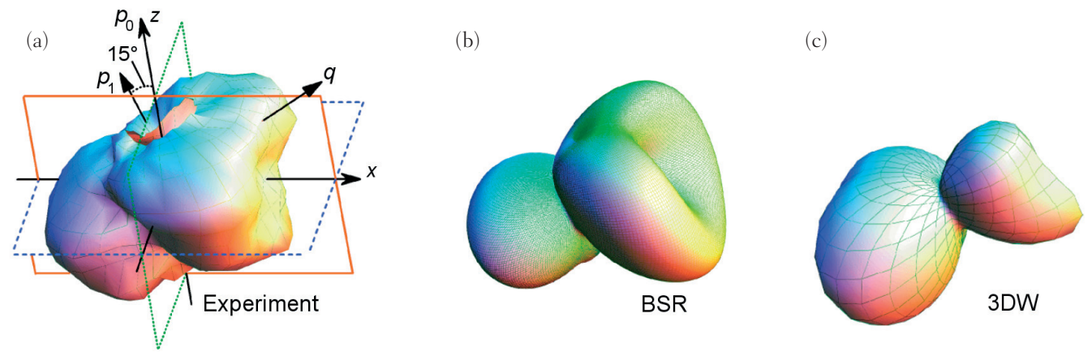

Fig. 13: Emission pattern of a 3 eV electron after 66 eV impact on argon with 15° projectile scattering angle.

(e,2e) studies were also performed for molecules of increasing complexity. For hydrogen molecules simultaneous ionisation and excitation was studied [10]. The obtained cross sections within the molecular frame show enhanced electron emission along the molecular axis due to the non-spherical potential. A second molecular (e,2e) study again concerned tetrahydrofuran (THF) where TDCS were obtained at low impact energy (26 eV) for ionisation of three different molecular orbitals.

Dissociative Electron Attachment. Low-energy electron collisions with molecules often lead to transient negative ions which subsequently dissociate into reactive negative ions and neutral fragments. With a newly setup and commissioned apparatus, we analysed the masses and momentum vectors of the negative fragments. A cold supersonic jet target offers significantly better momentum and mass resolution compared to existing setups in other groups. So far electron attachment to molecular species ranging from NH_3 to complex organic compounds was investigated. Exemplarily, for NH_3 an interesting bond angle dynamics was found [6]. Comparing a theoretical emission pattern for the NH_2^- fragment with our data it can be concluded that after electron attachment and before the dissociation, the molecular bond angle in the transient NH_3^- opens up in an umbrella-mode oscillation. We studied a range of larger molecules and clusters where the fragment kinetic energies normally are small since most of the energy release goes to internal vibration and rotation. One exception was observed for the pyridine ring molecule. Here we observed a completely symmetric dissociation reaction again yielding NH_2^- ions, but now including an internal rearrangement of hydrogen atoms.

Alexander Dorn

Cooling Dynamics of Small Anionic Metal Clusters

Radiative cooling and heating processes of small anionic metal clusters in gas phase are important observables in cluster physics. Their dynamics reveal basic characteristics about the geometrical and electronic structure of clusters. The timescales of these processes are covering many orders of magnitude. Electronically excited levels are typically depopulated within milliseconds by internal conversion. But the radiative depopulation of ro-vibrationally excited states and processes such as spontaneous electron emission are substantially slower and consequently require long observation times. The cryogenic trap for fast ion beams (CTF) – a prototype of the successful cryogenic storage ring (CSR) project [1] – is an ideal setup for the needed gas-phase spectroscopy with great time resolution.

The recent studies concentrated on anionic copper and cobalt clusters stored for several seconds in the CTF. The spontaneous electron emission process of Cu_{4-7}^- produced in highly excited ro-vibrational states was studied. The measurements reveal two-component decays in contrast to the previously excepted single power-law decay. Furthermore, laser-induced electron emission was studied to observe the radiative cooling of excited clusters in the cryogenic (~15 K) environment at the CTF [11]. While for $Cu_{4,5}^-$ no cooling could be observed even after 4 minutes of storage time, the initial equilibration process of $Cu_{6,7}^-$ stops significantly before room temperature. The measurements indicated that equilibration with the trap temperature was not reached for any of the cluster species. The underlying processes are not yet fully understood.

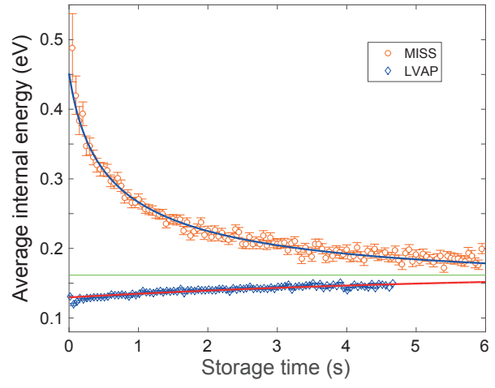

Fig. 14: Thermalisation of internal energies for Co_4^- clusters from a hot (MISS) and a cold (LVAP) ion source. At long time, similar limits are approched by both curves, suggesting equilibration of the cluster internal energy with the 300 K ambient temperature of the ion trap.

Co_4^- was used to demonstrate a novel measurement scheme continuously observing the internal energy distribution of anionic cluster systems by employing laser-induced delayed electron emission. The thermalisation of hot clusters at about 1000 K, produced in a sputter source, as well as of cold clusters at about 250 K, produced in a laser vaporisation source, with the 295 K experimental environment was followed with great time resolution (Fig. 14).

Sebastian George

Statistical Recombination: Multi-Electron Tungsten Ions

Ions in a plasma environment involving heavier elements can have very complicated electronic structures. A key process for hot plasmas governing their abundance in various charge states is the recombination with free electrons. It dominantly proceeds by resonant capture, where electrons already bound in the ion are excited and the incident electron is temporarily attached by giving up its kinetic energy. Radiative stabilisation of the resonance then leads to very high recombination cross sections.

For the realisation of a fusion reactor (like the ITER project), predicting the abundances of highly charged ions in the plasma poses a challenging problem, especially regarding heavy elements such as tungsten. Recombination rates of ions W^{q+} with intermediate charge states $q \sim 20$ are particularly difficult to predict, as the 4f atomic shell is about half-filled. The up to seven active electrons or vacancies then can lead to as many as a billion of resonant states with strong multi-electron quantum mixing.

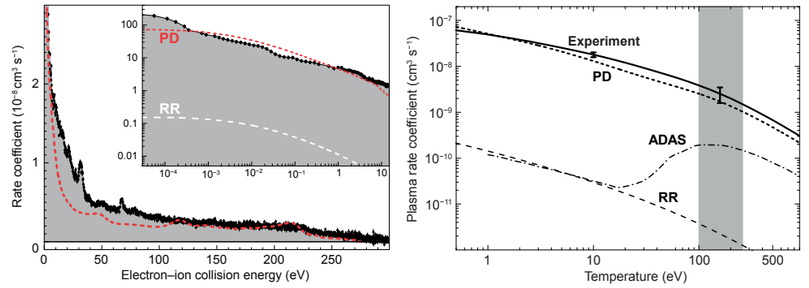

Fig. 15: Measured recombination rate for W^{19+} ions with free electrons [12]. The energy dependent reaction rate constants are measured (left) and converted into a thermal rate constant for a plasma (right).

Studies at the magnetic storage ring TSR during its last operational years showed extremely high electron recombination cross sections for W^{q+} ions, owing to this complexity. For the case of the W^{19+}, the analysis was recently completed [12] and could be successfully explained by atomic structure calculations describing the multi-electron excitation through statistical mixing of all possible quantum states (Fig. 15). Theory applies a partitioned and damped (PD) atomic structure calculation, based on a statistical description of the electron capture resonances formed by electron impact with the 9 equivalent electrons in the 4f shell of the W^{19+} ion. Calculations using radiative recombination only (RR) and presently used data-base models (ADAS) underestimate the recombination rate by an order of magnitude or more. This experimental benchmarking helped to establish the new statistical theory and now confirms its predictive power for modeling the interactions of multi-electron in hot plasma environments.

Claude Krantz, Oldřich Novotný, Andreas Wolf

References

[1] R. von Hahn, A. Becker, F. Berg et al., Rev. Sci. Instrum. 87, 063115 (2016)
[2] K. Spruck, A. Becker, F. Fellenberger et al., Rev. Sci. Instrum. 86, 023303 (2015)
[3] A.P. O'Connor, A. Becker, K. Blaum et al., Phys. Rev. Lett. 116, 113002 (2016)
[4] O. Novotný, S. Allgeier, C. Enss et al., J. Appl. Phys. 118, 104503 (2015)
[5] S. Zhang, D. Fischer, M. Schulz, et al., Phys. Rev. Lett. 112, 023201 (2014)
[6] T.N. Rescigno, C. S. Trevisan, A. E. Orel, et al., Phys. Rev. A 93, 052704 (2016)
[7] X. Ren, E. Jabbour Al Maalouf, et al., Nature Commun. 7, 11093 (2016)
[8] X. G. Ren, T. Pflüger, M. Weyland et al., J. Chem. Phys. 141, 134314 (2014)
[9] X. Ren, S. Amami, O. Zatsarinny et al., Phys. Rev. A 93, 062704 (2016)
[10] E. Ali, X. Ren, Alexander Dorn et al., J. Phys. B 48, 115201 (2015)
[11] C. Breitenfeldt, K. Blaum, M.W. Froese et al., Phys. Rev. A 94, 033407 (2016)
[12] N.R. Badnell, K. Spruck, C. Krantz et al., Phys. Rev. A 93, 052703 (2016)

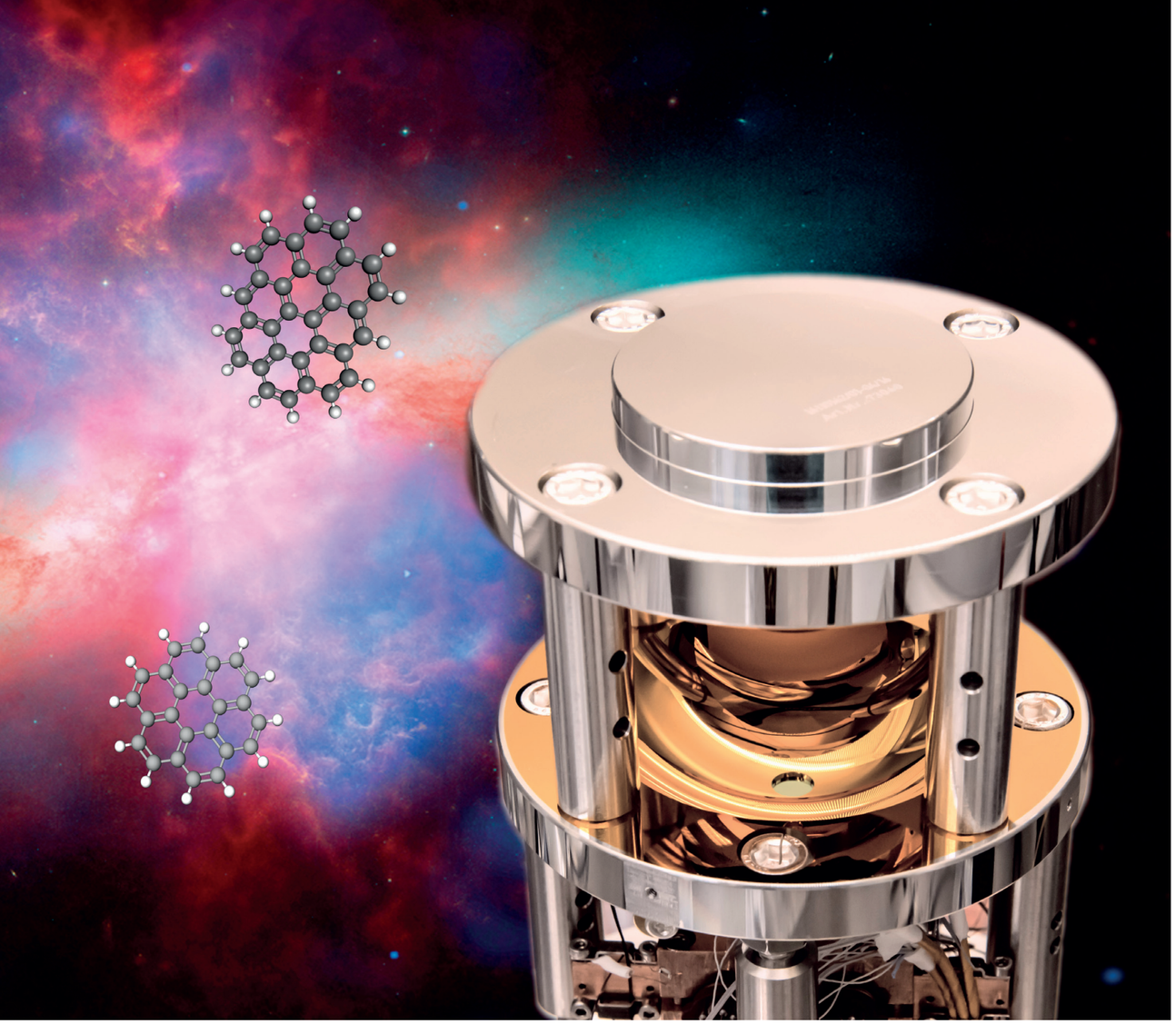

2.4 Astrophysics with Ions and Strong Light Fields

The image shows the light collector mirror assembly of a mid-infrared detector module developed to detect emission of large gas phase molecular ions in laboratory experiments. Background: Messier 82. Composite of Chandra, HST and Spitzer images (NASA/JPL-Caltech/STScI/CXC/UofA/ESA/AURA/JHU).

Introduction

The conditions in astronomical environments differ substantially from those found in most terrestrial laboratories. Simulating interstellar processes through experiment and theory thus often explores extreme regimes in both our experimental capabilities and theoretical understanding. This is reflected in the activities in our institute, which cover a wide range in temperature and density.

Astrochemical studies with stored molecular ions at the Test Storage Ring and the new Cryogenic Storage Ring aim at a detailed understanding of the formation and destruction of molecules in the cold interstellar medium, and we are currently developing a novel spectroscopic technique for complex interstellar molecules, based on the ultra-senstive detection of mid-infrared radiation. On the other hand, experiments at the various electron beam ion traps (EBIT) at MPIK study the spectral properties and photo-induced processes of highly charged ions (HCI), which are prevalent in very hot interstellar objects, covering the range from visible light to X-rays. These efforts are complemented by advanced theoretical calculations of processes in intense laser fields, which aid the interpretation of laboratory data and shed light on the origin of interstellar phenomena like ultra-relativistic jets generating positron-electron plasmas, at the far end of the temperature scale.

Photodissociation of CH^+ inside the Cryogenic Storage Ring

The methylidyne cation CH^+ was the first molecular ion detected in interstellar space and its high abundance in many interstellar environments continues to puzzle observational astronomers. No efficient formation pathway for CH^+ at low temperatures is known, and various scenarios introducing non-thermal effects, ranging from turbulent mixing to thermodynamic shocks and Alvén waves, have been proposed.

A possible pathway to create CH^+ in space relies on radiative attachment of C^+ and H. This reaction has not been studied in the laboratory yet, therefore, theory has to resort to the reverse process, the photodissociation of CH^+, to benchmark the potentials that are involved and understand the relevant resonances.

We have studied the near-threshold photodissociation spectrum of CH^+ in the new Cryogenic Storage Ring (CSR) [1], at nominal temperatures of 6 K. Unlike earlier studies, we focused on the lowest rotational quantum states $J = 0$-2, to verify the resonances originating from those states and also to monitor the rotational cooling of molecular ions inside the CSR.

To this end we have produced CH^+ ions in a caesium sputter ion source, mass-selected them, accelerated the ion beam to 60 keV kinetic energy and injected it into the CSR. The ions were stored for several minutes and then exposed to ultraviolet photons from a pulsed optical parametric oscillator (OPO) laser system. The photons excited the ions from the $^1\Sigma^+$ electronic ground state to a vibrational band inside an excited $^1\Pi$ state, just above the dissociation threshold. From here the ions pre-dissociate into C^+ and H. The neutral H atoms were detected by a single-particle detector downstream of the laser interaction zone. This two-step dissociation process leads to Feshbach resonances in a narrow energy window around the dissociation threshold. We used state-of-the-art close-coupled calculations to

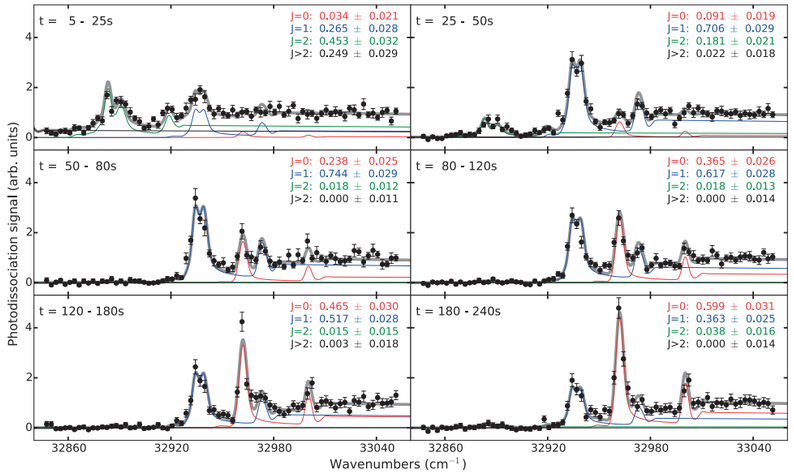

Fig. 1: Near-threshold photodissociation spectra of CH^+, recorded as a function of storage time inside the CSR. The experimental data are fitted by rotational state-specific cross sections obtained by a close-coupled calculation. From the time-dependent populations of he rotational states the cooling behavior of stored molecular ions inside the CSR can be inferred.

reproduce the experimental data and we were able to unambiguously assign all features in the spectra. This allowed us to infer the rotational population of the stored CH^+ ions inside the storage ring as a function of time.

Our results show that the rotational cooling of the stored ions is compatible with an ambient radiation field of ≈20 K [2]. The difference between this temperature and the nominal temperature of the vacuum chambers (6 K) is probably caused by stray light entering the CSR injection region or the vacuum viewports. Nevertheless, we found that after 4 min of storage, all ions are in the lowest two rotational quantum states, with ≈60% populating the $J=0$ ground state. These results demonstrate the potential of the CSR for measurements under true interstellar conditions, and they pave the way for merged beams collision studies involving interstellar ions and free electrons or neutral atoms.

Aodh P. O'Connor, Andreas Wolf, Holger Kreckel

Electron–Ion Recombination for Astrochemistry

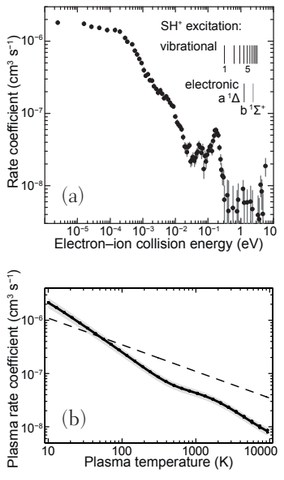

Fig. 2: Dissociative recombination rate coefficient of SH^+ ions measured with merged electron and ion beams in the TSR as a function of the electron-ion collision energy (a). Electronic and vibrational excitation thresholds of SH^+ are marked. The deduced plasma rate coefficient (b; full line) significantly deviates from previous values used in astrophysical models (dashed).

The observational capabilities of molecular spectroscopy in interstellar medium improved dramatically in recent years due to new observatories. To interpret the observations reaction networks are intensely modeled, leading to improved understanding of the composition and dynamics of these media. Dissociative recombination (DR) is an essential reaction type in the chemical networks, especially in cold interstellar clouds. Using the photocathode-produced cold electron beam of TSR we investigated dissociative recombination of several molecular ions in a collision energy range equivalent to temperatures between ≈10 K and several 10,000 K. E. g., we have measured the DR of SH^+ in order to explain the unexpectedly high observed SH^+ abundance in the cold interstellar medium. In Fig. 2a, we plot the obtained DR rate coefficient using the experimental collision energy. The DR rate decreases with the increasing collision energy, with some sharp enhancements close to 0.1 eV. This reflects the sensitive dependence of the DR cross section on the SH^+ and SH molecular structures, steering the balance between predissociation and autoionisation from the excited neutral Rydberg states. Fig. 2b shows the DR rate coefficient converted such that energy spread corresponds to a temperature in equilibrium plasma, used as a parameter on the horizontal axis here. We observe an unusually strong dependence of the DR rate coefficient on the plasma temperature. Using our results the SH^+ abundance in the astrochemical models should increase a factor up to ≈4 at high temperatures and thus better match the observations. However, it will decrease by a factor of ≈2 at low temperatures. Additionally to the rate coefficient we have determined the excitation states of the dissociation products S and H using a novel analysis method which does not rely on coincident observation of both fragments from each DR event. In the SH^+ experiment the internal ion excitation temperature amounted to 300 K because of the room-temperature experimental chamber of TSR. Besides SH^+ we have also studied electron interactions with other astrophysically relevant ions, namely NH^+ [3], Fe^{7+} [4], and Fe^{14+} [5]. We are currently finalizing the experimental setup for DR measurements in the CSR storage ring – there the cryogenic chamber will allow the molecular ions to relax down to ≈10 K. Thus we will mimic the conditions in cold interstellar clouds not only for the collisional temperature, but also for the internal ion state population.

Oldřich Novotný, Andreas Wolf

Astrophysics with Super Intense Laser Pulses

Astrophysical spectra recorded by space observatories provide the only means to determine the element composition, temperature, density, and velocity of distant celestial objects such as stars, X-ray binaries, black-hole accretion disks, or active galactic nuclei. A large body of reliable atomic data is needed, either from theory or experiment, for the extraction of the emitting objects' properties from astrophysical spectra. The X-ray lines of highly charged ions, in particular, Fe^{16+}, are among the brightest in astrophysical spectra, and were observed within the last decade with the orbiting laboratories Chandra and XMM-Newton. The X-ray spectrum of Fe^{16+} is, however, poorly reproduced by astrophysical models: the observed line-strength ratio of the X-ray lines 3C and 3D is in stark contrast with its predicted value, preventing a reliable analysis of observatory data. The sources of astrophysical discrepancy were narrowed down after the first X-ray laser spectroscopic experiment, employing a purely photonic excitation of the ions with the LCLS X-ray free-electron laser (XFEL). A disagreement of 30% between all theoretical predictions and the experimental line-strength ratio was stated, hinting to a shortcoming of atomic structure theory [S. Bernitt et al., Nature 492, 225 (2012)].

We performed a large-scale configuration-interaction calculation of line strengths including higher-order correlations, suggesting that these alone cannot explain the discrepancy [6]. In addition, quantum electrodynamic (QED) corrections were reliably estimated. We furthermore investigate the light-matter interaction of the system in a dynamic way, showing that, for high pulse intensities available at LCLS, the 3C and 3D transitions can show a complete population inversion. Thus, nonlinear dynamic effects are induced, significantly influencing the line strengths, which could not be explained by the previous weak-field modeling. Such effects possibly resolve the discrepancy, motivating the use of light-matter interaction models valid for strong fields also in the analysis of astrophysical spectra. For accurately modeling strong-field effects on line shapes, an improved experimental determination of the XFEL parameters is called for. At sufficiently high intensities, the weak-field atomic theory is also not applicable in corresponding astrophysical scenarios, e. g., in the accretion disks of stellar-mass black holes.

Under even more extreme conditions, like during gamma-ray bursts, electron-positron plasmas are emitted as ultra-relativistic jets. Thus, they represent a unique tool to test physics in unexplored regimes, also providing insights about the early stages of the Universe. In the experiment described in [7], this unique state of matter has been generated in a terrestrial laboratory, opening the possibility of scrutinizing such extreme astrophysical phenomena and regimes under controlled conditions. An ultra-relativistic electron beam, produced in an all-optical setup via laser wake-field acceleration, hit a Pb solid target. Due to the complex interaction of the electron beam with the nuclei and the electrons in the target, an ultra-relativistic electron-positron bunch was observed on the rear side of the target, with a fraction up to 50-50 of electrons and positrons depending on the target thickness. The bunch density was found to be sufficiently high that its skin-depth resulted smaller than the bunch transverse size, allowing for collective, i. e. plasma effects. In [7] we have also theoretically identified the main mechanisms responsible of the production of the electron-positron bunch and described its formation and evolution inside the solid

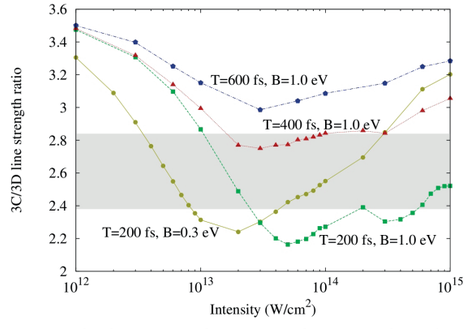

Fig. 3: The line-strength ratio for the 3C and 3D lines as a function of the intensity, duration, and bandwidth of the simulated XFEL pulse [7]. The gray shaded area shows the experimentally observed ratio together with its error bar, taken from [6].

target. As a result, only two fundamental QED processes have been found to play a substantial role: 1) bremsstrahlung of electrons and positrons, and 2) electron-positron production by photons, both occurring in the presence of the screened electromagnetic field of the target nuclei. Analytical estimations and numerical integrations of the corresponding kinetic equations agree extremely well with the experimental results on the relative population of electrons and positrons in the generated bunch.

Natalia S. Oreshkina, Zoltán Harman, Antonino Di Piazza, Christoph H. Keitel

Laser-Induced Vibrational Emission: A New Type of Spectroscopy for Complex Molecular Ions

As more and more molecules are identified in interstellar space, two spectral phenomena remain mysterious, even after decades of investigation. The first one, termed the Diffuse Interstellar Bands (DIBs), stands for more than 500 absorption features that are seen in many interstellar environments, stretching from the visible to the near-infrared. Only very recently one of those features could be attributed to the C_{60}^+ molecule. The other ubiquitous feature is the so-called Unidentified Infrared Emission (UIE) that is seen in the mid-infrared (IR) range throughout the universe. It is not clear at present whether these features have a common origin or stem from the same class of molecules, however, there are strong hints that make complex organic ions likely candidates. To shed light on the interstellar observations, spectroscopic data of complex ions in the gas phase are required. However, owing to the difficulties to achieve high enough densities, experimental data are sparse.

We are currently developing a new spectroscopic technique (in collaboration with researchers of the MPI for astronomy and the Karlsruhe Institute for Technology) based on the direct detection of emission from gas phase molecular ions using highly sensitive blocked-impurity-band (BIB) mid-IR detectors operated in a cryogenic ion beam trap. While the technique should be fairly universal, the implementation is extremely challenging, and the goal for the proof-of-principle experiment is to achieve the first true gas phase electronic spectra of C_{60}^+. To this end we will store C_{60}^+ inside the cryogenic beam trap at nominal temperatures around 10 K. The stored ions will be exposed to pulsed laser radiation in the near-infrared. As direct fluorescence is a very unlikely process in large molecules, the absorbed energy will be re-distributed among the internal degrees of freedom and – after a delay of typically several ten milliseconds – will be re-emitted at vibrational frequencies in the mid-IR. The emitted photons will be detected by the BIB detector assembly and serves as a signal that absorption took place. By monitoring the emission while scanning the frequency of the excitation laser, a gas phase absorption spectrum of the stored molecular species is recorded. After the feasibility of this approach has been demonstrated, it is foreseen to add spectral sensitivity to the mid-IR detector module and thereby get spectroscopic information on both the absorption and emission features. This would permit us to follow the heating and cooling processes that large gas phase molecules undergo in the interstellar medium in real time, and thus this technique has the potential to yield unprecedented and valuable information on the entire class of complex organic molecular ions.

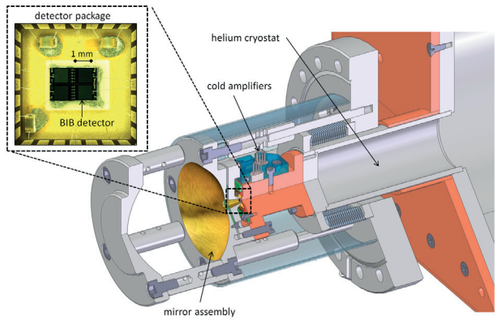

Fig. 4: Schematic of the mid-IR detection module. The drawing shows the mirror assembly and the detector mount sitting on a liquid helium cryostat. The inset shows a photograph of the four BIB detector pixels with a sensitive area of 1 mm² each.

Sunil Kumar, Sebastian George, Jürgen Göck, Holger Kreckel

Laboratory Astrophysics with Highly Charged Ions

The conditions in CryPTEx, developed at the MPIK for investigations of HCI, are close to those of interstellar clouds in terms of low radiation temperature (7 K) and residual gas density (below 10^{-14} mbar). Thus, the device is also ideally suited to study molecular ions. In commissioning experiments in collaboration with Aarhus University, we succeeded in producing molecular ions (MgH^+) at the lowest hitherto reported ro-vibrational temperature. We demonstrated another novel method for controlling at will their internal temperature in the range 7 to 60 K [8]. Our trap design has been adopted in Aarhus for future experiments. Another collaborating group at TU Munich has also chosen this design for the cooling and storage of ^{229m}Th ions for investigations of an extraordinary low-energy nuclear transition. On the high temperature sector, we have expanded our experiments with HCI in EBITs. Using highly monochromatised synchrotron radiation (~300 meV FWHM at ~6.6 keV), we have investigated the resonant photoionisation of Fe^{20+} to Fe^{23+}, key ions for the opacity of the radiative core in main sequence stars, and also the highest charge states ever accessed. We also investigated the corresponding time-reversed processes, namely photorecombination. In the polarisation of X-rays [9] emitted by these essential ion species, we unveiled hitherto neglected strong multi-electronic channels leading to clear changes in radiative and polarisation properties (see Fig. 5), and capable of modifying the average charge state of the plasma.

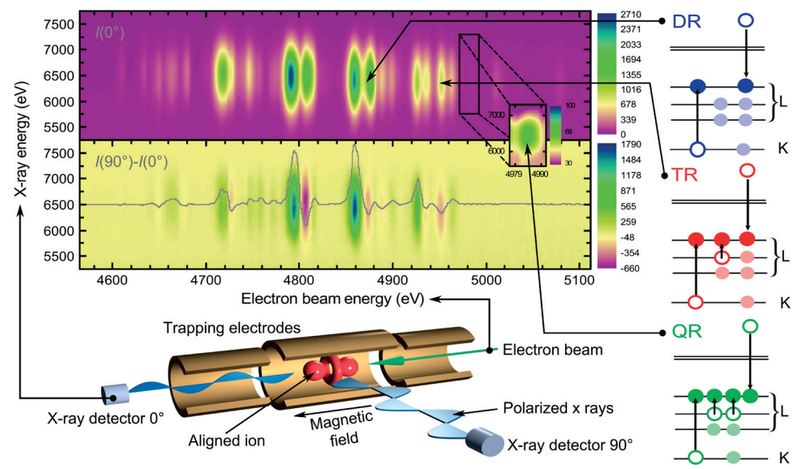

Fig. 5: Probing the X-ray emission of trapped Fe HCI recombining with electrons of variable energy. Strong resonances are observed with detectors at 0° and 90° with respect to the beam axis. Upper 2D plot: Intensity at 0°. Lower 2D plot: Difference in intensity between the two 0° and 90° detectors. Two- to four-electron resonances (DR, TR, and QR) schematically depicted on the right induce some of the strongest recombination channels and affect the polarisation.

Furthermore, we have provided experimental proof for charge-exchange-driven X-ray production at 3.5 keV [10], proving an atomic mechanism for a claimed, weak "dark-matter annihilation" signal seen in galaxy clusters, which had recently attracted enormous theoretical and observational attention. By producing S^{16+}, a naked ion, and letting it capture electrons from a neutral donor, an X-ray transition from highly excited Rydberg levels of the final ion S^{15+} to the ground state generates photons at 3.5 keV, an energy for which no atomic source was known in astrophysics. Based on the abundance of the initial HCI and hydrogen atoms as electron donors in hot galaxy clusters, a collaborating theory group in Leiden predicted that this mechanism fully explains the astrophysical signal. The calculations were then corroborated by our experiment.

José R. Crespo López-Urrutia

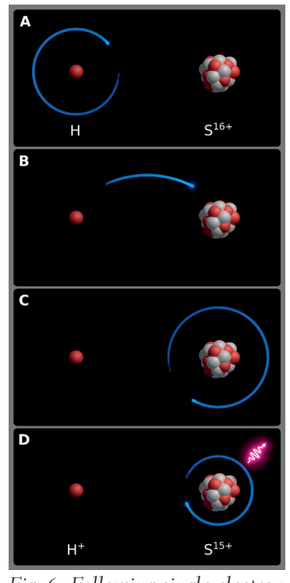

Fig. 6: Following single electron capture from an atom by naked S^{16+}, an X-ray photon is emitted at 3.5 keV. This is the likely source of the observed line in galactic spectra attributed to dark matter annihilation.

References

[1] R. von Hahn, A. Becker, F. Berg et al., Rev. Sci. Instrum. 87, 063115 (2016)
[2] A.P. O'Connor, A. Becker, K. Blaum et al., Phys. Rev. Lett. 116, 113002 (2016)
[3] O. Novotný, M. Berg, D. Bing et al., Astrophys. J. 792, 132 (2014)
[4] M. Hahn, A. Becker, D. Bernhardt et al., Astrophys. J. 813, 16 (2015)
[5] D. Bernhardt, A. Becker, M. Grieser et al., Phys. Rev. A 90, 012702 (2014)
[6] N.S. Oreshkina, S.M. Cavaletto, C.H. Keitel et al., Phys. Rev. Lett. 113, 143001 (2014)
[7] G. Sarri, K. Poder, J. M. Cole et al., Nat. Commun. 6, 6747 (2015)
[8] A.K. Hansen, O.O. Versolato, Ł. Kłosowski et al., Nature 508, 76 (2014)
[9] C. Shah, P. Amaro, R. Steinbrügge et al.,Phys. Rev. E 93, 061201 (2016)
[10] C. Shah, S. Dobrodey, S. Bernitt et al., Astrophys. J. 833, 52 (2016)

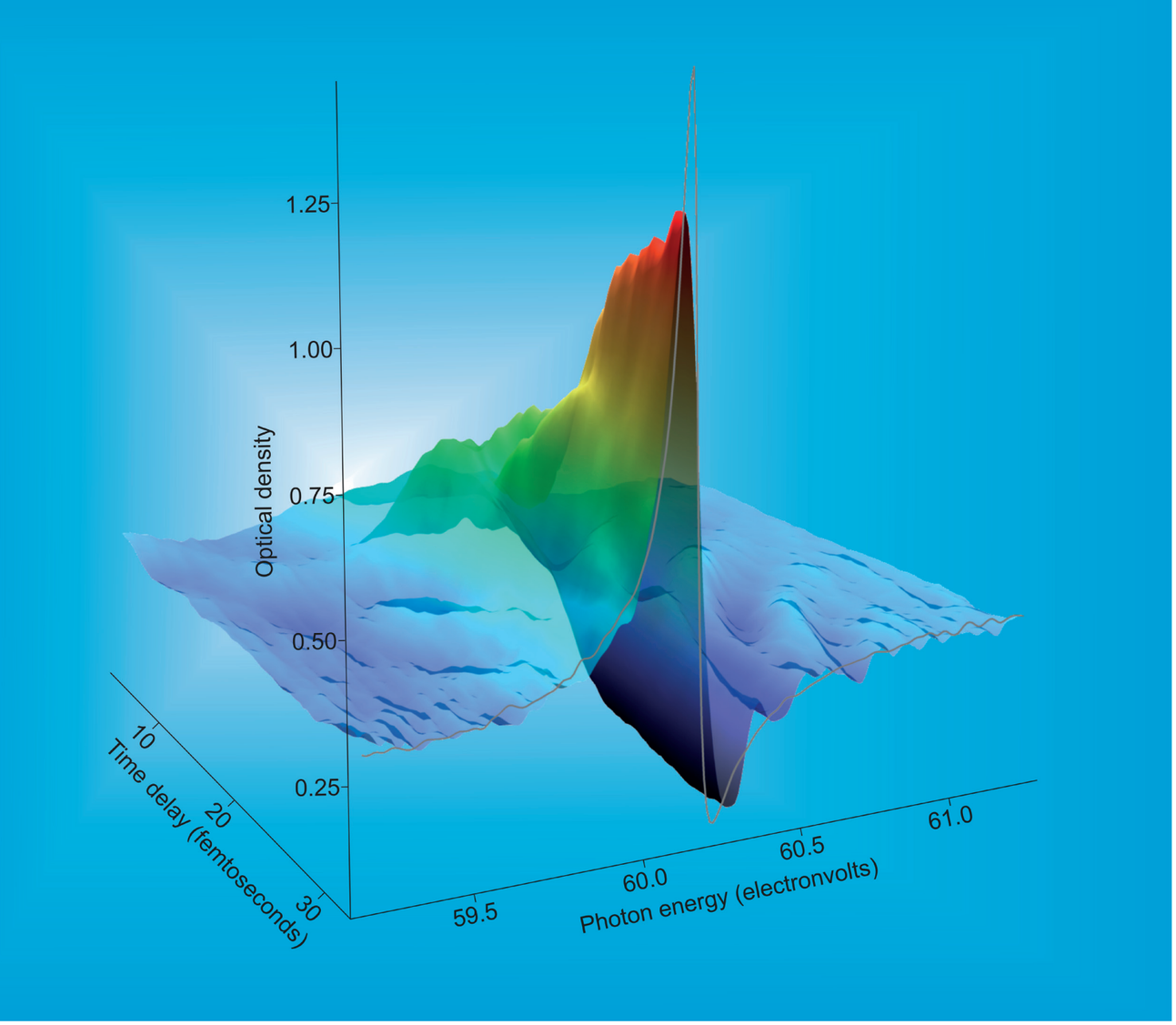

2.5 Time-Dependent Quantum Phenomena

The time-resolved formation of a Fano resonance in Helium gas, measured by observing the corresponding absorption line in the spectrum of attosecond-pulsed extreme ultraviolet light. While the latter triggered the dynamics by excitation of two electrons at time zero, a variably time-delayed strong optical laser pulse switched off the quantum phenomenon by strong-field ionisation. The grey line is a measurement of the fully developed Fano resonance, as accessible by traditional spectroscopy. The time-gating method used in this experiment is general and can thus, in principle, be applied to any fundamental physics phenomenon accessible to spectroscopy.

Introduction

Time is a fundamental dimension, and distinctly different from its space-dimensional counterparts by the opposite sign in the relativistic metric tensor. Also in the current formulation of quantum mechanics, space-time symmetry is broken: There is an operator for position, but not for time, putting the latter out of reach of a direct measurement. The quest to temporally resolve quantum dynamics is thus fundamentally limited. Nevertheless, time is the crucial parameter in quantum dynamics, manifested by the time-dependent Schrödinger equation:

$$i\hbar \frac{\partial}{\partial t}\psi(x,t) = \mathcal{H}\psi(x,t)$$

In experiments, one can change the time-dependent wavefunction by performing measurements, perturbing or interfering with, at will, the natural process of interest at specific time intervals. These time intervals can be defined by natural clocks, counting multiples or fractions of the cycle of light, whereas the "perturber events" are often (for practical reasons) short flashes of laser light. The coherent nature of the latter makes them perfectly controllable. In time-resolved experiments, these clocked intervals between two "perturber events" are achieved by splitting one pulse of light into two, and sending one of them around a spatial detour, which then translates to a characteristic delay by the constant speed of light, before the time-delay separated set of pulses interacts with the system of interest.

The measurement and interpretation of observables from such time-resolved experiments holds the key in reconstructing the time-dependent wave function. The MPIK is on a mission to explore the most complete experimental data sets of time-domain quantum dynamics in small few-body systems. This includes coincidence electron-ion detection as well as multidimensional spectroscopy and imaging with optical, XUV, and X-ray light. The following describes recent progress and breakthroughs of seeing (imaging), listening (spectroscopy) and understanding the fundamental dynamical motifs of quantum motion, and how to scale up this understanding to complex systems to eventually allow chemists to steer the course of chemical reactions even in solution phase.

Watching Bound Electrons Move in Atoms by Imaging and Spectroscopy

The imaging of bound-state electronic motion in the time domain is possible by exploiting the well-known pump-probe scheme, where a dynamically evolving electronic wavepacket is created by a very strong but ultra-short laser pulse and then, after a variable time delay, probed by a second pulse. In a recent experiment [1] such a highly non-equilibrium atomic state that essentially represents a superposition of two atomic orbitals with different angular momenta was probed as a function of time by strong-field tunneling ionisation of the excited system. The two involved electronic orbitals carry angular momenta with different orientation in space characterised by their magnetic quantum numbers $m = \pm 1$ or 0, and they exhibit slightly different binding energies. Like a typical beating between oscillating motions, this

gives rise to a periodically changing momentum distribution of the bound electrons with a period that follows from the Heisenberg uncertainty-relation between (binding) energy and time (see Fig. 1a). In the experiment the temporal evolution of this so called spin-orbit wavepacket is reflected in the velocity and the direction of emission of the electron that is removed by the probe pulse and measured with high resolution. The resulting electron distribution of velocities serves a probe for the temporally oscillating electron momentum distribution prior to the ionisation, i. e. in the atomic bound state. Electrons in the orbital with $m=0$ move preferentially along the laser field-axis, and electrons in the states with $m=\pm1$ are characterised best by a circular motion in the plane perpendicular to the laser axis. As the occupation oscillates with time between both possible states the electron velocity distribution changes its shape. The time period is about 25 fs. Even though not yet demonstrated, this method represents a promising route for the imaging and the control of electronic motion in bound systems like atoms, molecules and possibly even larger systems such as clusters.

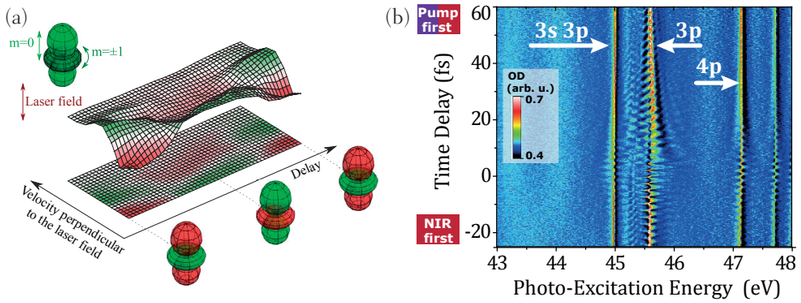

Fig. 1: Electron valence- (a) and inner-valence- (b) hole wavepackets in neon measured in a pump-probe experiment. (a) Delay-dependent velocity distribution electrons emitted by strong-field ionisation perpendicular to the laser polarisation axis. The temporally averaged distribution has been subtracted depicting enhancement (red) and decrease (green). (b) Spectroscopic measurement of a femtosecond electron wavepacket of inner-valence excited states (from [2]).

The excitation of inner electrons to outer shells within atoms defines another non-equilibrium state of matter, where electrons feel the modified attraction to the core due to a change in the screening of charges. In the case of neon, an extreme ultraviolet light pulse moves an inner electron that resides in the 2s orbital into an outer 3p state. Such excitation differs from a conventional single-electron excitation scenario since the missing inner electron causes a slight decrease in the shielding of the strong positive attraction (10 protons) to the neon core. The case gets even more interesting for outer orbitals of "s" character since they have the largest quantum mechanical overlap with the hole in the inner orbital, however a direct one-photon excitation of such states is impossible due to angular momentum conservation. We employed a spectroscopic technique termed four-wave mixing that allowed us to excite an outer 3s orbital and further visualise the thus induced coherent femtosecond wavepacket motion [2] (see Fig. 1b). The 3s state manifests itself as tilted femtosecond ripples across the $2s^{-1}$–3p resonance. In this first demonstration of the technique, only one temporal coordinate has been varied, which already enabled us to clearly identify and experimentally verify nonlinear (2-photon pump, 1-photon probe) excitation. We are currently working on a multidimensional spectroscopy scheme that would allow element-specific (molecular site-selective) pumping and probing by using intense XUV pulses from a Free-electron laser (FEL).

Robert Moshammer, Christian Ott, Thomas Pfeifer

Time-Resolved Fano Resonance

The coupling of a discrete quantum state to a continuum of states gives rise to a Fano resonance, a spectroscopic phenomenon at the heart of the quantum world. Their characteristic asymmetric shape is a direct consequence of a most fundamental physical concept: The interference of multiple pathways with the interaction of different quantum configurations. They typically arise at places were the single-particle description no longer applies and are thus also a hallmark of the onset of complexity.

In previous research we employed ultrashort femtosecond laser pulses to manipulate Fano resonances in Helium, which enabled new spectroscopic concepts to gain access to the fastest motion of few interacting quantum particles. In very recent work [3], we achieved to directly time-resolve the buildup of such Fano resonances. With an attosecond-pulsed source in the extreme ultraviolet (XUV), we populated a short-lived two-electron excited state in helium. The subsequent decay of this state, which naturally occurs within a time window of a few tens of femtoseconds, gives rise to an asymmetric spectral line shape that is imprinted on the absorption spectrum of our attosecond excitation source. Interestingly, that same resonance in helium has been the central subject of investigation when Ugo Fano formulated his original theoretical description in 1961 [Phys. Rev. 124, 1866 (1961)]. In our work, we have experimentally clocked the ultrafast buildup of this resonance with a novel time-gating approach (see Fig. 2). With a strong near-infrared (IR) femtosecond laser pulse it is possible to deplete the doubly-excited state via ultrafast strong-field ionisation. With the natural decay process, also termed autoionisation, interrupted, the resulting spectroscopic observable of an asymmetric resonance is thus also heavily modified: As a function of time delay, the absorption (quantified by its optical density) increases and the width narrows down. The theoretical predictions are confirmed by the experiment, and thus validate the time-gating method used here as a general approach to temporally resolve spectroscopically observable fundamental quantum phenomena. Our approach therefore enables a direct view into the ultrafast formation of a Fano resonance. Backed both by analytical theoretical descriptions as well as by *ab initio* numerical simulations from a collaboration team of international theory groups, this new time-domain spectroscopy approach opens new routes to temporally resolving the correlated motion of electrons from few- to many-body quantum systems.

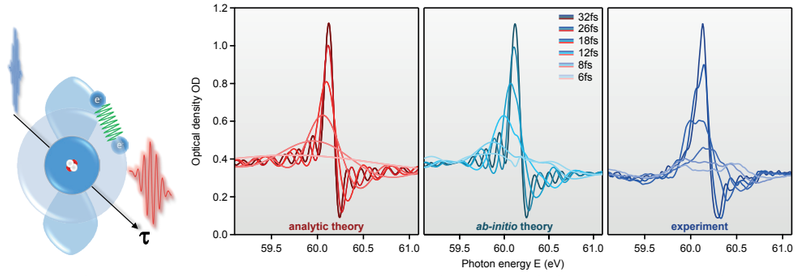

Fig. 2: Ultrafast formation of a Fano resonance observed in helium: An XUV pulse (blue) excites the two electrons. Their correlated motion (Coulomb repulsion, green) is terminated by a subsequent IR pulse (red) due to laser-induced strong-field ionisation as a function of time delay τ (left). The time-dependent buildup of the Fano absorption line shape can be measured in the XUV spectrum (right, modified from [3]) transmitted through a cloud of Helium gas.

From a very general viewpoint, these findings also hold promise to be transferable to a vast range of different research areas across disciplines such as solid state physics (e. g. the emergence of quasi-particles), physical chemistry, and quantum information technology in the future. This is evidenced by the fact that Fano resonances are a very general manifestation of fundamental interference effects in the quantum world. With the availability of appropriately short "perturber events", time-gated Fano resonances and other spectroscopic features may shed new light upon the underlying microscopic dynamics at play.

Christian Ott, Thomas Pfeifer

Electron Transfer at Short Distances

With the invention of accelerator based free-electron lasers (FELs) it is now possible to provide almost fully coherent light at XUV or even X-ray energies with femtosecond pulse durations and unprecedented intensities for wide-ranging applications from diffractive imaging of biomolecules to time-resolved atomic physics experiments. Employing an XUV-pump–XUV-probe scheme at the FEL in Hamburg (FLASH), the critical inter-nuclear distance up to which electrons can be transferred within a dissociating iodine molecule was determined. This property is critical for determining the onset of radiation damage with implications on future diffractive imaging schemes. In our experiment a very intense XUV

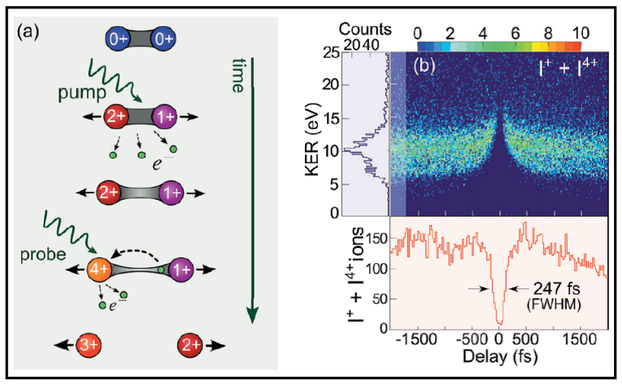

Fig. 3: (a) Pump-probe scheme for dissociative multiple ionisation of I_2. (b) 2D plot of the KER of $I^+ + I^{4+}$ ion pairs versus delay time (from [4]).

pulse creates a multiply charged iodine molecule I_2 and triggers the dissociation due to the repulsion of its positively charged constituents. A second identical probe pulse hits the molecule after a freely adjustable time-delay and removes further electrons from one of the ionic fragments. For small delays, and correspondingly small internuclear distances, any charge asymmetry induced by the probe pulse is balanced by electron transfer among the ions, as depicted in Fig. 3a.

However, at large delays the ionic fragments are already too far apart to be considered as a molecule and electron transfer is blocked. Thus, asymmetrically charged ion pairs can only be produced from certain delays on, as can be seen for the fragmentation into $I^+ + I^{4+}$ in Fig. 3b. Here, the kinetic energy release (KER) of the ion pairs is plotted as a function of the delay time. The blocking of electron transfer manifests itself as a vanishing ion yield for small delays. A projection of all events onto the time axis (red curve) allows us to extract the critical time up to which electron transfer is possible. From the projection onto the KER axis for large delays (blue curve) we are able to conclude on the intermediate charge states created by the pump pulse.

The obtained results are in good agreement with an intuitive classical model that is routinely employed in ion-atom collisions, the so-called over-the-barrier model [4]. Within this model an electron can freely propagate between the neighbouring ions as long as the binding energy of the respective electron is above the combined potential of the atomic cores. The height of the potential barrier depends on the internuclear distance and it rises above the electronic binding energy from some distance onwards. These predicted distances are in good agreement with the experimentally determined values.

Our results demonstrate that electron transfer occurs over relatively large internuclear distances of several atomic radii on time-scales much faster than the molecular dissociation. Thus, locally created charges are efficiently redistributed which leads to an accelerated explosion of the molecule. Future experiments on more complex molecules relevant for X-ray imaging are planned.

Robert Moshammer, Kirsten Schnorr, Thomas Pfeifer

Strong-Field Metrology

A key ingredient of understanding the results of strong-field time-domain experiments is the ability of exactly measuring and characterizing the employed tools, i. e., the strong laser fields at work. The experimental observables of the quantum dynamical processes at interest, and their comparison to theory, are often critically dependent on the exact laser temporal profiles, which is true especially when one aims to draw quantitative conclusions. While powerful characterisation tools of ultrashort laser pulses already exist, the highest level of characterisation can generally be gained when the pulses of interest are retrieved *in situ*, at the time and place where the actual quantum dynamics experiment is performed.

We have pursued this goal for the case of attosecond time-resolved absorption spectroscopy where both attosecond-pulse extreme ultraviolet pulses and near-infrared few-cycle femtosecond laser pulses at variable intensity, from weak to strong fields, are interacting with atoms and molecules. In a first work [5], we have developed a fully general analytical model that describes the interaction of such laser pulse geometries with quantum systems, which we termed the dipole control model (DCM). Here, a dipole is excited and manipulated in a most general way as a function of the temporal separation between these two events (see Fig. 4a): The dipole function f(t) – shown for two exemplary delay times (τ_1, τ_2) – is modified by a multiplicative complex factor "*A*". As a result, the seemingly complicated absorption line shapes (inset) can be readily understood via Fourier transform of the dipole response. Using Dirac delta functions δ(t) as perturber events in this analytical formulation enabled us to identify many characteristic features in the observed spectroscopic data, such as resonant or non-resesonant coupling of states.

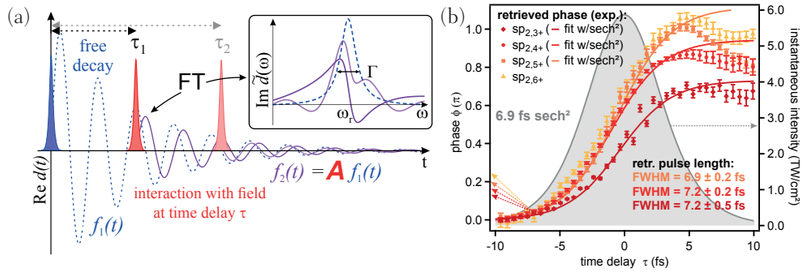

*Fig. 4: Illustration of the analytical dipole control model (a): dipole oscillation f(t) induced by a first excitation pulse (blue) and disturbed in its subsequent free decay by a second pulse at variable delay **τ** (dark & light red pulses: two exemplary cases). Absorption line shapes (inset) are analytically related to f(t) modified by a complex factor "A" via Fourier transform. Application of this concept (b) to time-resolved modification of Fano resonances $sp_{2,n+}$ in He allows to retrieve the laser pulse temporal profile (from [5] and [6]).*

The first application of this formalism then allowed us to retrieve the temporal intensity profiles of the near-infrared femtosecond laser pulses within the measured absorption data [6]. To this end, the strong-field-induced modification of the absorption profile of Fano resonances in the helium atom (doubly excited states: $sp_{2,n+}$) gives direct access to the temporal profile of the employed laser pulses *in situ* within one and the same experiment (Fig. 4b). The retrieved data can thus be used in the future to benchmark state-of-the-art quantum-dynamics theory by precision measurements of strong-field ionisation dynamics, now enabled by an enhanced knowledge of the underlying experimental laser pulse temporal profiles.

Christian Ott, Thomas Pfeifer

From Quantum to Classical Mechanisms in Molecules

One of the most prominent examples of quantum control, among others, is the ability of ultra-short laser-pulses to steer chemical reactions in small- and medium-sized molecules. Because laser light does not interact directly with the nuclei of a molecule, the control of chemical processes is exerted solely by manipulating the electrons, the 'chemical glue' of molecules. However, the complexity of the underlying physical mechanisms for even the simplest molecular systems in the presence of a strong laser field challenges our understanding. Based on experiments with diatomic molecules, H_2 [7] and O_2 [8], we succeeded in reducing the complexity of the system to the quantum mechanically most elementary case of two states that coherently evolve on time-dependent potential-energy curves. This way we were able to isolate and observe the most fundamental mechanisms of laser-controlled nuclear motion in transition states relevant for chemical reactions. As a final result we achieved a simple interpretation of our results in terms of a semi-classical model. The excellent agreement with experiment provides an unprecedented understanding of molecular reaction control. The fact that classical physics suffices to explain laser control in the lightest and fasted molecule as used in our study promises even broader applicability to larger (more classically behaving) molecules.

In the experiment a very short pump pulse first ionises neutral H_2 molecules, preparing a vibrational wave packet in the H_2^+ ground state $|g\rangle$. Then, a time-delayed intense IR laser pulse, which serves as a control pulse, couples this molecular state to the dissociative $|u\rangle$ state as illustrated in Fig. 5. The blue solid and the red dashed curves show the relevant laser-induced molecular potential curves that describe the system in the presence of the control pulse. The opening **Ω** of the resulting avoided crossing (i. e., the height of the dissociation barrier) depends on the control-pulse intensity. The blue shaded surface shows the temporal evolution of the lower potential curve. It is effectively pulled down due to the action of

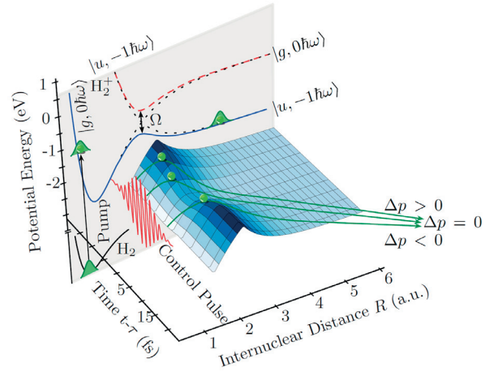

Fig. 5: Illustration of the laser-controlled dissociation kinematics of H_2^+ molecules in a time-resolved pump-probe experiment (from [7]).

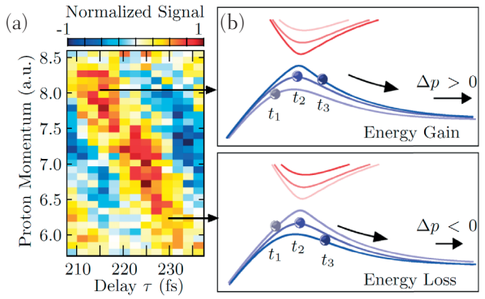

Fig. 6: The measured delay-dependent fragment momentum distribution (a) and the corresponding semi-classical motion along the laser induced molecular potential curve (b). The up- and down-shifting ("elevator mechanism") of the potential during of the passage over the barrier leads to an increase or decrease of fragment energies (from [7]).

the control pulse this way leading to a reduction of the dissociation barrier. As a consequence the molecule undergoes a fragmentation into an H^+ and a neutral H-atom along the classical trajectories sketched in the figure. The kinetic energy, or the momenta of the heavy fragments are measured as a function of the time delay τ, and a clear oscillatory behaviour reflecting the classically vibrational motion in bound state is observed. Moreover, the fragments do either gain or lose energy while traversing over the barrier (three example trajectories are shown). This leads to a delay dependent momentum of the protons as shown in the count distribution as a function of momentum and delay in Fig. 6a. It can be understood in terms of an upward and downward moving lower potential curve while the nuclear wave-packet represented by a classical ball is traversing the barrier (see illustration in Fig. 6b). It is this up-down motion like in an "elevator" that is responsible for the control of the reaction pathway through a laser-induced transition state. A semi-classical model describes and predicts this behaviour extremely well. For larger molecules, where a complete quantum-mechanical modeling is difficult if not impossible, the validity of such semi-classical mechanisms might be the key for future control applications, it provides a classical handle for tuning nuclear kinetic or vibrational energies to direct chemical reactions.

Robert Moshammer, Thomas Pfeifer

Laser-Driven Dynamics from Fundamental (Few-Body) to Complex (Many-Body) Systems

A major research theme at the MPIK is the understanding of quantum-mechanical motion. This comprises both the natural evolution of wave functions in an isolated quantum system, as well as their response to strong external fields.

In experiments in helium gas, we successfully reconstructed the quantum-mechanical wave packet of both electrons after exciting each of them into low-lying excited states by an attosecond-pulsed single-photon absorption [9]. Applying the Fano-phase formalism developed in our own earlier work, it was possible to extract the key quantity of quantum-

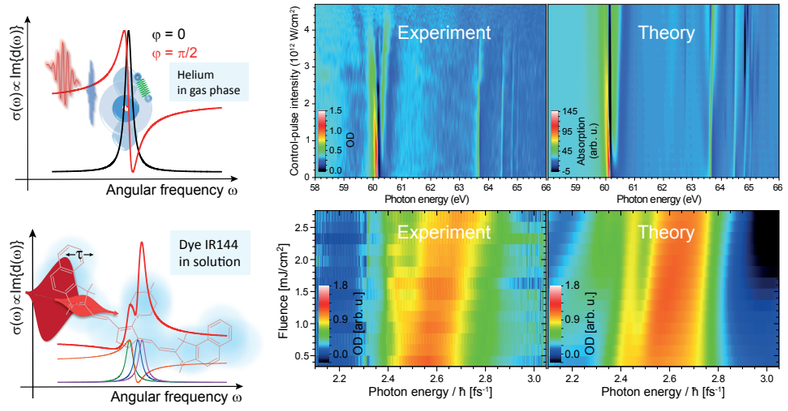

Fig. 7: Quantum control of "simple" atomic (upper row panels, helium gas) and complex molecular (lower-row panels, dye IR144 dissolved in methanol) dynamics: The intense laser field (dark red) interacts with the quantum systems after their excitation by a weaker pulse. For the case of He an attosecond pulse (blue); for the case of IR144 a weak optical pulse (light red) was used. Theoretical modeling of the intensity (and fluence-) dependent absorption spectra (OD: optical density) includes the effect of a laser-induced phase shift of the excited states. These phase shifts can vary for each specific state and lead to characteristic structures in the absorption spectrum (figure modified from [9] and [10]).

mechanical information, the wave-function phase, after the irradiation of Helium with an intense 7-femtosecond control laser pulse. Fig. 7 (upper-row panels) show the according extreme-ultraviolet (XUV) absorption spectra that get modified as the quantum-mechanical phase is tuned by the strong optical laser pulse.

As the laser-induced phase shifts of excited quantum states should be a general mechanism at work for ultrashort strong-field interactions with matter, we recently generalised our work in helium to complex large molecules in the liquid phase [10]. In the experiments, we again applied a strong control pulse following a weak probe pulse, this time both in the optical domain, covering a broadband molecular absorption band.

The experimentally measured intensity-dependent absorption spectra showed characteristic modifications that could be very well reproduced with a simple effective few-level model to approximate the molecular excited states as shown in Fig. 7 (lower-row panels). Instead of just assuming an instantaneous phase shift $\Delta\varphi = \Delta E \cdot \tau$ (ΔE, intensity-dependent energy level shift, τ strong-field pulse duration) right after the excitation of the state as for the simple atomic case, it was important to model the entire evolution of the energy-level shift $\Delta E(t)$ as a function of time during the strong pulse, as now both laser pulse and molecular coherence times acted on a similar time scale. From the model, the state-resolved coupling coefficients could be extracted, which are proportional to the state-resolved polarizability, a key quantity in strong-field light-matter interaction.

The universal applicability of this quantitative strong-field phase control concept from simple to complex molecular systems thus opens a new route for the understanding and steering of molecular quantum dynamics in strong laser fields, which may become synthetic optical catalysts and agents in future laser-directed chemistry applications.

Kristina Meyer, Thomas Pfeifer

References

[1] L. Fechner, N. Camus, J. Ullrich, T. Pfeifer and R. Moshammer, Phys. Rev. Lett. 112, 213001 (2014)

[2] T. Ding, C. Ott, A. Kaldun, A. Blättermann, K. Meyer, V. Stooß, M. Rebholz, P. Birk, M. Hartmann, A. Brown, H. Van Der Hart and T. Pfeifer, Optics Letters 41, 709 (2016)

[3] A. Kaldun, A. Blättermann, V. Stooß, S. Donsa, H. Wei, R. Pazourek, S. Nagele, C. Ott, C.D. Lin, J. Burgdörfer and T. Pfeifer, Science 354, 738 (2016)

[4] K. Schnorr, A. Senftleben, M. Kurka, A. Rudenko, G. Schmid, T. Pfeifer, K. Meyer, M. Kübel, M.F. Kling, Y.H. Jiang, R. Treusch, S. Düsterer, B. Siemer, M. Wöstmann, H. Zacharias, R. Mitzner, T.J.M. Zouros, J. Ullrich, C.D. Schröter and R. Moshammer, Phys. Rev. Lett. 113, 073001 (2014)

[5] A. Blättermann, C. Ott, A. Kaldun, T. Ding and T. Pfeifer, J Phys B 47, 124008 (2014)

[6] A. Blättermann, C. Ott, A. Kaldun, T. Ding, V. Stooß, M. Laux, M. Rebholz and T. Pfeifer., Optics Letters 40, 3464 (2015)

[7] A. Fischer, M. Gärttner, P. Cörlin, A. Sperl, M. Schönwald, T. Mizuno, G. Sansone, A. Senftleben, J. Ullrich, B. Feuerstein, T. Pfeifer and R. Moshammer, Phys. Rev. A 93, 012507 (2016)

[8] P. Cörlin, A. Fischer, M. Schönwald, A. Sperl, T. Mizuno, U. Thumm, T. Pfeifer and R. Moshammer, Phys. Rev. A 91, 043415 (2015)

[9] C. Ott, A. Kaldun, L. Argenti, P. Raith, K. Meyer, M. Laux, Y. Zhang, A. Blättermann, S. Hagstotz, T. Ding, R. Heck, J. Madroñero, F. Martín and T. Pfeifer, Nature 516, 374 (2014)

[10] K. Meyer, Z. Liua, N. Müller, J.-M. Mewes, A. Dreuw, T. Buckup, M. Motzkus and T. Pfeifer, PNAS 112, 15613 (2015)

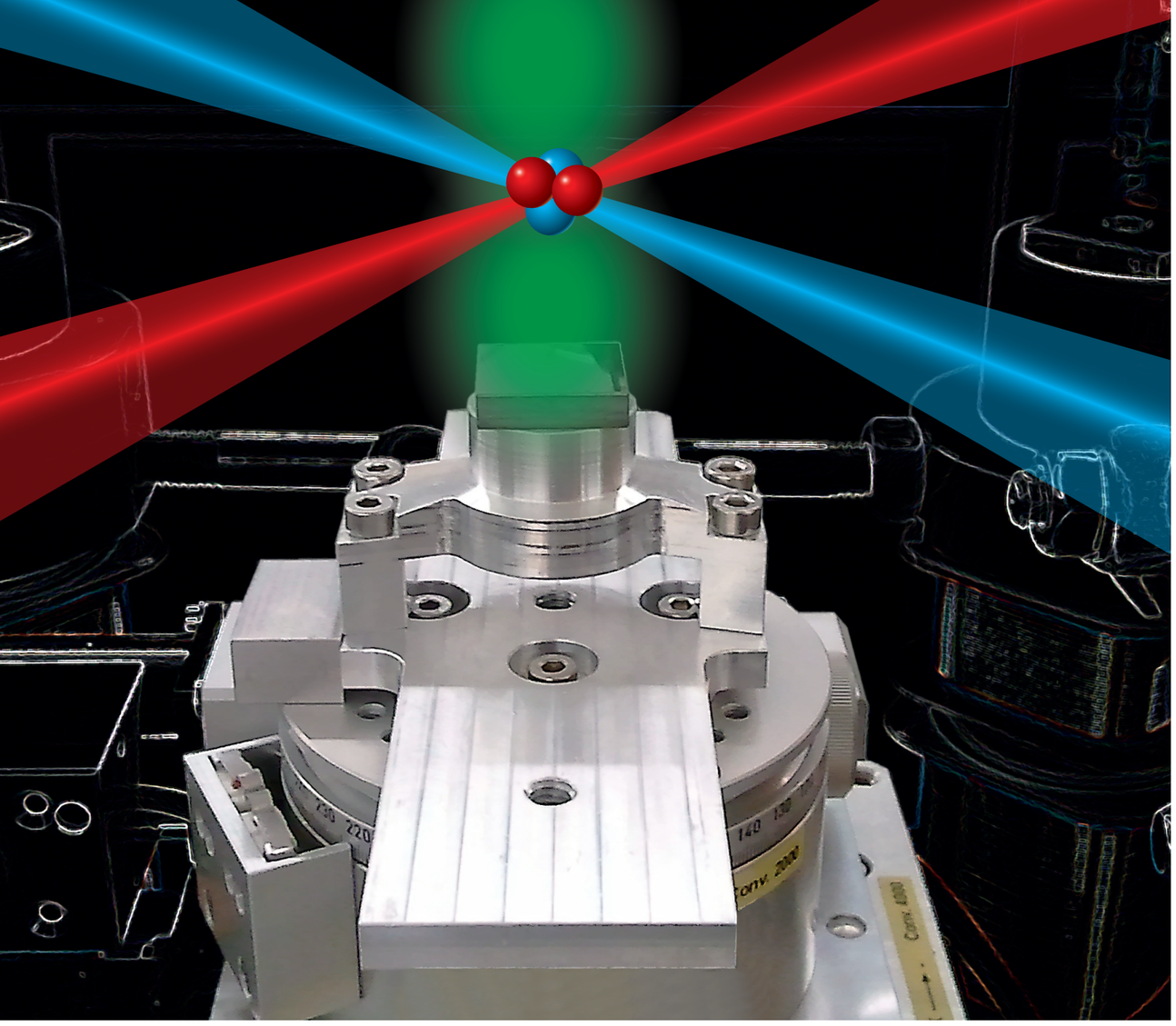

2.6 Laser Control of Atoms and Nuclei

Illustration of laser control in atoms and nuclei. The laser field shown in blue probes the state of a quantum system pictured as a nucleus surrounded by electrons (green orbitals) . The red light field symbolises various methods to control the system. The photo in the background shows a thin-film waveguide cavity containing ^{57}Fe nuclei (gray cuboid) used for quantum control experiments in the hard X-ray domain.

Introduction

The possibility to control the quantum state of a given system provides access to a multitude of fascinating applications. It also serves as a stringent test of the theoretical understanding of the underlying quantum dynamics and fundamental principles – in particular, if more complex systems, interactions with strong fields, or far-from-equilibrium dynamics are considered. General quantum states are superpositions of various eigenstates of the system, weighted by an amplitude and shifted in phase with respect to each other. It is therefore crucial for any control scheme to offer handles for both these quantities and, in the best case, find a direct experimental signature for the induced amplitude and phase modifications. But in particular the phase information is notoriously hard to measure, since conventional detectors are sensitive only to the intensity.

In the following, we outline some of our recent theoretical and experimental results towards quantum state control and its applications. A common theme is to identify fundamental principles of laser control, which apply to atoms, ions and nuclei alike, with characteristic energy scales ranging from the infrared up to hard X-rays.

Fano Resonance Control in Atoms and Nuclei

A key method to access phase information is interferometry. In spectroscopy, Fano line shapes are an archetype signature of different interfering quantum pathways. Over the last years, we have established Fano resonances and in particular the interplay of its energy- and time-domain interpretation as a powerful tool to investigate and also control quantum dynamics. Recently, we have continued this effort in a series of experiments.

In a first experiment, we prepared a nuclear two-level system into a tunable superposition of its states, and subsequently reconstructed the relative phase of this superposition from the emitted X-rays [1]. The two-level system was realised using an ensemble of ^{57}Fe nuclei embedded in a nanoscale planar cavity. We operated the system in such a way that the incident X-rays couple the nuclear ground state to a single collectively excited state of the large ensemble of nuclei, effectively forming a two-level system. The incident X-ray pulses were nearly instantaneous on the nuclear life time scale and prepared the two-level system in a superposition state with variable relative phase. On the much slower time scale of the nuclear life time, the two-level system then emitted its excitation as X-ray light, which enabled us to characterise the initial state prepared by the X-ray pulse. We achieved phase sensitive measurements by interpreting our cavity as an X-ray interferometer, see Fig. 1. The first arm of the interferometer is formed by all possible X-ray pathways through the cavity which do not involve interactions with the nuclei. The second arm comprises all other contributions with one or more interactions with the nuclei. Interference between the two pathways converts the Lorentzian spectral response of the nuclei into Fano lineshapes. The phase of the light emitted by the nuclei then becomes accessible via the variation of these lineshapes as function of phase shifts Δ in the first interferometer arm. The experiment was performed in a joint collaboration between theoretical and experimental groups at the institute, together with the team of Ralf Röhlsberger (DESY, Hamburg) at the Dynamics Beamline P01 of the synchrotron source PETRA III at DESY. It forms a first step towards

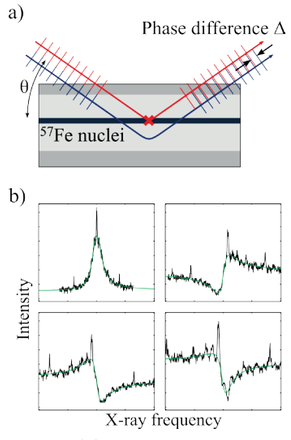

Fig. 1: (a) X-ray cavity as an interferometer. The dependence of the observed Fano spectra (see b) on the phase difference enables to reconstruct the original nuclear quantum state.

X-ray quantum state tomography. Moreover, the capability to detect tiny phase changes with high precision, assisted by a precise theoretical model for the different observed line shapes, invites for applications in precision spectroscopy and metrology. Our phase recovery does not make use of the theoretically known line shape of the two-level system. Thus, we expect the method to apply also to more complex systems.

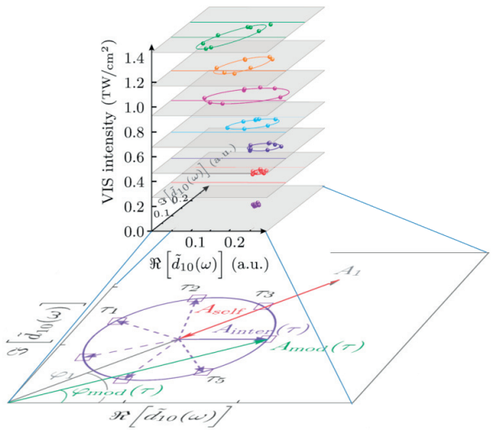

Fig. 2: Extracting complex-valued amplitude and phase information from strong-field laser interaction (adapted from [2]). In the experimental results, various coupling pathways with their individual components can be identified and observed as a function of intensity, shedding light on a thus-far hidden coupling pathway via an excited-state continuum.

In another recent work [2], we experimentally induced and extracted amplitude and phase modifications in strong-field laser interactions with doubly excited states in helium atoms. A high-harmonic attosecond-pulsed extreme-ultraviolet (XUV) field is used to excite both electrons by absorbing a single photon. An ultrashort near-visible (VIS) laser with variable time delay and intensity relative to the XUV field then is used to couple different doubly excited states, inducing near-resonant single and two-photon transitions. This enables us to steer the phase via quantum interference and laser-induced energy shifts, while population transfer among the doubly-excited states manipulates the amplitudes. To finally characterise the prepared state, the induced amplitude and phase changes are "holographically" mapped into the spectroscopic line shapes recorded via time-resolved XUV spectroscopy. As a result, quantum-state coefficients can directly be read out as a function of the time delay between the XUV and the VIS pulse, and be represented in an intuitive phasor diagram (see Fig. 2). The latter representation not only helped us to pin down the intensity-dependent physical interaction pathways, but also to uncover a thus-far neglected coupling pathway through an excited-state continuum. From a broader perspective, the two-electron excited helium serves as an archetypical system exhibiting physics beyond the single-active electron approximation. The understanding gained in this few-electron system also opened the door to induce and understand strong-field effects in much more complex systems, as discussed for the case of solution-phase molecules in chapter 2.5.

The latter experiment crucially relies on a strong control field. However, at X-ray energies with nuclei, such strong control fields are generally not available, which severely restricts current experimental capabilities. To overcome this problem, we have developed methods to simulate the effect of strong control fields for nuclear quantum optics without actually applying external light fields, which is a promising approach to realise more complex control schemes with nuclei. Very recently, again in a collaboration between theory and experimental groups at the institute, we could verify the general concept in two proof-of-principle experiments involving nuclei at PETRA III and the European Synchrotron Radiation Source (ESRF). This paves the way for significant manipulations of the optical properties of the nuclei, which are unfeasible using established control methods.

Jörg Evers, Kilian P. Heeg, Christoph H. Keitel, Thomas Pfeifer

Cooperative Quantum Dynamics

In contrast to the broad capabilities available in labs operating at lower frequencies, the implementation of advanced laser-coupled quantum systems in the X-ray domain remains a challenge due to basic experimental limitations. We develop methods to overcome these limitations, and to establish X-ray quantum optics with nuclei. One of our long-term goals is to demonstrate nonlinear light-matter interactions with nuclei, which is a key requirement for fundamental and applied quantum optical technologies alike. For this, we enhance the usually weak non-linearities via cooperative and coherence effects. An archetype example is electromagnetically induced transparency (EIT), which enables one to enhance non-linearities while simultaneously suppressing the linear absorption. Recently, we demonstrated EIT-based group velocity control of spectrally narrow X-ray pulses (SNXP) [3]. In the experiment, subluminal light propagation was achieved by inducing a steep positive linear material dispersion, and verified by direct measurements of the temporal delay imposed on the SNXP, see Fig. 3. As a result, the experiment demonstrated coherent control, as well as cooperative and cavity enhancements of light-matter interaction in a single setup.

It was performed at the nuclear resonance beam line (ID18) of the European Synchrotron Radiation Source (ESRF, Grenoble) in collaboration with an experimental team around Ralf Röhlsberger (DESY, Hamburg). To realise the required material dispersion, a large ensemble of ^{57}Fe nuclei embedded in a thin film planar X-ray cavity was manipulated in such a way that the required multi-level setup was achieved. To enable the direct detection of the temporal pulse delay, we further proposed and implemented a flexible scheme to generate frequency-tunable SNXP from broadband synchrotron radiation, which will also find other applications in X-ray quantum optics. This method crucially relies on a high-purity X-ray polarimetry setup developed in the group around Gerhard G. Paulus (University and Helmholtz Institute Jena). The experimental results obtained are in good agreement with our quantum optical theory (see Fig. 3), and form an important step towards the exploitation of nonlinear effects with nuclei.

The EIT experiment required the implementation of a suitable three-level setup with nuclei. More complex nuclear level schemes could not only further enhance the nonlinear response, but also are a key requirement for many other quantum optical applications. However, such schemes are currently not available with nuclei in the lab, mostly due to technical limitations. To overcome these, we have recently proposed a systematic approach to design artificial quantum optical systems in the X-ray regime with limited resources [4]. Our basic idea is to tailor cooperative effects in large ensembles of nuclei in such a way that, effectively, a single artificial quantum system is simulated with collective properties going beyond those of the basic two-level constituents. In particular, we have shown how the transition frequency and the spontaneous decay rate of the artificial quantum system can be controlled over a considerable range. This way, a single nuclear species can be employed to engineer different quantum optical systems, by controlling cooperative effects, e. g., via the ensemble density or geometry. Combining several of such tailored ensembles could enable the realisation of tunable multi-level setups. The key step for our results was the development of a comprehensive theoretical framework for single-photon superradiance, which enables us to "reverse engineer" cooperative effects in the sense that we can determine the necessary ensemble properties to achieve a desired artificial quantum system. From a broader perspective, this framework also provides a bridge between the various theoretical and experimental approaches currently pursued to explore cooperative effects in extended media.

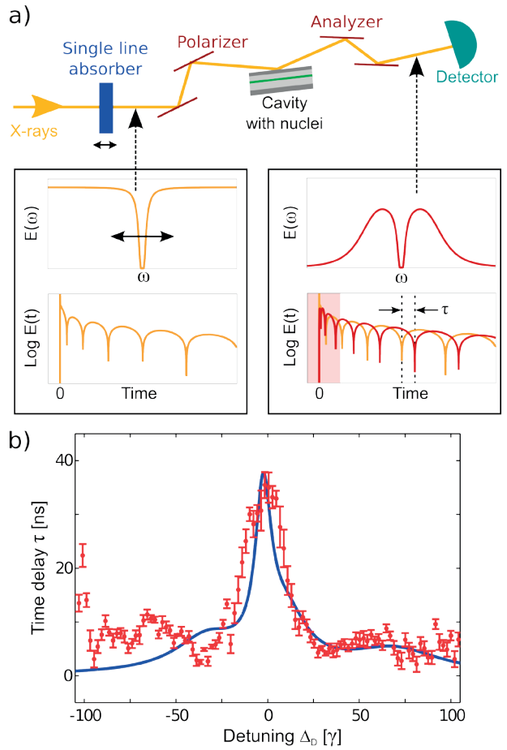

Fig. 3: (a) Schematic setup of the experiment. A single line absorber imprints echo-like signatures onto the incoming short X-ray light. The nuclei delay the X-ray pulse which can easily be seen in the shift of these echos. (b) This delay can be controlled by changing the detuning of the nuclei with the narrow-band x-ray pulse, and reaches up to 35 ns.

Jörg Evers

Strong-Field Quantum Phase Control

Quantum phases carry key information on the dynamics of microscopic systems. Quantifying the phase response of atomic and molecular systems to strong femto- and attosecond laser pulses is therefore crucial for applications aiming at their ultrafast preparation and control. Nevertheless, the extraction of quantum phases is a very demanding task. Traditional spectroscopy enables access to the amplitudes, i. e. the probability that a quantum system is in different states. Only recently its time-resolved analog – transient-absorption spectroscopy – has provided full access to the dynamics of quantum systems both in terms of amplitude and phase. In a pump-probe geometry, a short pump pulse of tunable intensity excites a quantum system, whose ensuing dynamical evolution is measured by a weak probe pulse. The state of the atomic system encountered by the probe pulse determines the absorption line shapes, enabling direct access to the bound-state dynamics triggered by the pump pulse. Even more interestingly, absorption line shapes can also be controlled in a more counter-intuitive probe-pump setup, with a subsequently arriving, intense pump pulse used to nonlinearly modify the excited state generated by the weak probe pulse.

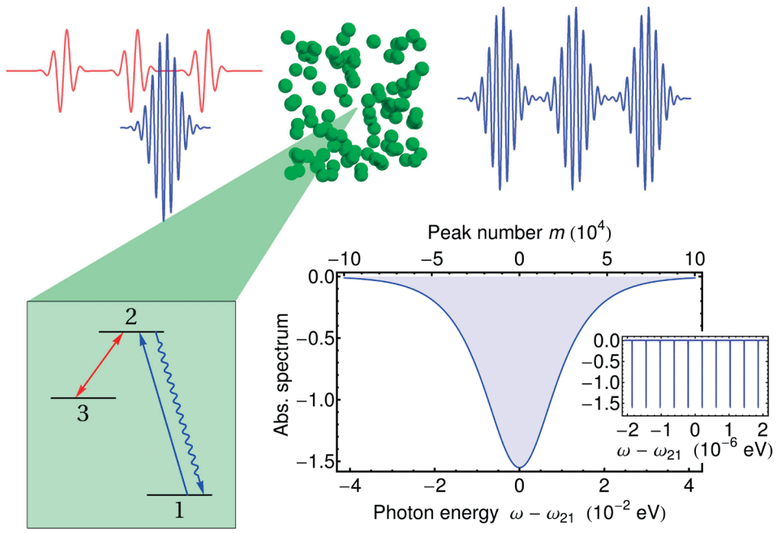

Fig. 4: Generation of an X-ray frequency comb with a laser-controlled gas (green): the ionic energy levels and the associated transitions are shown in the center (X-ray in blue, optical in red), with the driving X-ray pulse and optical frequency comb on the left, and the X-ray comb on the right. Broadband X-ray frequency comb absorption spectrum, with the comb structure highlighted in the inset.

In a joint collaboration between experimental and theoretical groups at the institute [6], we have shown how the atomic phases generated by an ultrashort pump pulse are encoded in the line shape of transient-absorption spectra, thereby providing the thus far missing link for their quantification and control. This was demonstrated experimentally, by using intense femtosecond pulses to excite optical transitions in rubidium atoms, and confirmed by comparison with quantum-theory predictions. With the help of time- and intensity-resolved absorption spectra, we provided interpretation for both above-mentioned scenarios, i. e. for a pump pulse either triggering or modifying the atomic dynamics, and explained which different, complementary information is thereby accessed. This represents an essential step towards the use of deterministic control techniques in the strong-field regime and the application of transient-absorption spectroscopy to fully reconstruct quantum states and dynamics in amplitude and phase (quantum holography).

Such line-shape-manipulation techniques are promising also at higher, e. g., X-ray, frequencies, where X-ray free-electron lasers provide intense ultrashort pulses for the coherent manipulation and control of atoms, ions, and nuclei. In a work involving theoretical and experimental groups at the institute [7], a method was proposed to imprint an X-ray frequency comb into the absorption spectrum of an ultrashort high-frequency pulse. The method can be described in analogy to the probe-pump schemes introduced previously: a transition with a high photon energy is excited by a short X-ray pulse, and a train of coherent pulses from an optical-frequency-comb laser is subsequently employed to manipulate the system's dipole response and shape the X-ray absorption spectrum into a comb (see Fig. 4). Specifically, the scheme provides higher comb frequencies and requires lower optical-comb peak intensities than previously explored methods, preserves the overall width of the optical comb, and may be implemented with currently available X-ray technology. Used to bridge a reference transition and an unknown X-ray frequency, it promises to enable precision spectroscopy in the thus far unexplored X-ray domain, with wide-ranging applications such as stringent tests of quantum electrodynamics, a more sensitive search for the variability of fundamental constants, and precision studies of nuclear structure.

Stefano M. Cavaletto, Zoltán Harman, Christoph H. Keitel, Thomas Pfeifer

Mutual Control of X-Rays and Nuclear Transitions

The recent interest in X-ray quantum optics in nuclear systems is motivated by attractive applications that rely specifically on the interaction between high-frequency fields and nuclei, for instance a nuclear energy storage solution or a gamma-ray laser. Such applications are based on the driving and control of nuclear transitions by strong X-ray fields. Switching the roles, nuclear excitations can also be used to store and control single X-ray photons, which are appealing for quantum information applications in the X-ray regime. In our theoretical investigations, we have addressed both aspects of this mutual control between X-rays and nuclear transitions.

The new X-ray free electron laser (XFEL) facilities promise both the high photon energy and the brilliance necessary for driving nuclear transitions and for controlling the population of nuclear states. Of special interest are metastable nuclear states or isomers, since their controlled population and depletion could offer a clean and reliable energy storage solution. To this end we have investigated the interaction of an XFEL pulse with a solid-state target containing the ^{93m}Mo isomer which stores 2.4 MeV energy and can be depleted by 4.8 keV photons. Our results have shown that, surprisingly, an attempt to deplete the isomeric state of ^{93}Mo by photoexcitation at the XFEL will be dominated by as much as six orders of magnitude by secondary electronic processes taking place in the XFEL-produced plasma [8]. The coupling between nuclear excitation and plasma electrons recombining in atomic shells thus dominates by far the direct impact of the XFEL for the controlled release of the nuclear isomer energy. These ground-breaking and unexpected results are not only restricted to isomers but have a general character for the nucleus-XFEL interaction.

Equally exciting are the perspectives of controlling single X-ray quanta with the help of nuclear transitions. Compared to optical photons, X-rays have the advantage of much tighter focusing, thus allowing for potential applications for photonic circuits on a very compact scale. We have investigated theoretically how spectrally narrow X-ray pulses typically containing at most one photon can be mapped and stored as nuclear coherence in thin-film planar X-ray cavities [9]. The latter are special layered structures that contain ^{57}Fe with its 14.4 keV Mößbauer transition from the ground to the first excited nuclear state. This novel storage mechanism relies on interference effects possible due to the occurrence of spontaneously generated coherences specific to the nuclear system. The role of the control field is played here by a hyperfine magnetic field which induces interference effects reminiscent of electromagnetically induced transparency. By switching off the control magnetic field, a narrow-band X-ray pulse resonant to the nuclear transition can be completely stored in the cavity for approximately 100 ns. These are exciting prospects for future processing and control of X-ray qubits and quantum information applications in the X-ray regime. In a related work, we could further show that the scattering channels of single X-ray quanta can be manipulated in such a way that two excitation waves counterpropagating through nuclei can become entangled [10]. This gives rise to a subangstrom-wavelength standing wave excitation pattern that can be used as a flexible tool to probe matter dynamically on the subatomic scale.

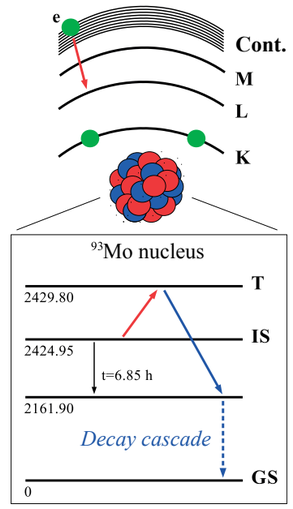

Fig. 5: ^{93m}Mo excitation induced by electron recombination from the plasma into the atomic L shell with subsequent decay to the nuclear ground state (long blue solid and dashed arrows).

Adriana Pálffy, Christoph H. Keitel

References

[1] K.P. Heeg et al., Phys. Rev. Lett. 114, 207401 (2015)
[2] A. Kaldun et al., Phys. Rev. Lett. 112, 103001 (2014)
[3] K.P. Heeg et al., Phys. Rev. Lett. 114, 203601 (2015)
[4] P. Longo, C.H. Keitel, and J. Evers, Sci. Rep. 6, 23628 (2016)
[5] M. Gärttner et al., Phys. Rev. Lett. 113, 233002 (2014)
[6] Z. Liu et al., Phys. Rev. Lett. 115, 033003 (2015)
[7] S. M. Cavaletto et al., Nature Photonics 8, 520 (2014)
[8] J. Gunst et al., Phys. Rev. Lett. 112, 082501 (2014)
[9] X. Kong and A. Pálffy, Phys. Rev. Lett. 112, 197402 (2016)
[10] W.-T. Liao and A. Pálffy, Phys. Rev. Lett. 112, 057401 (2014)

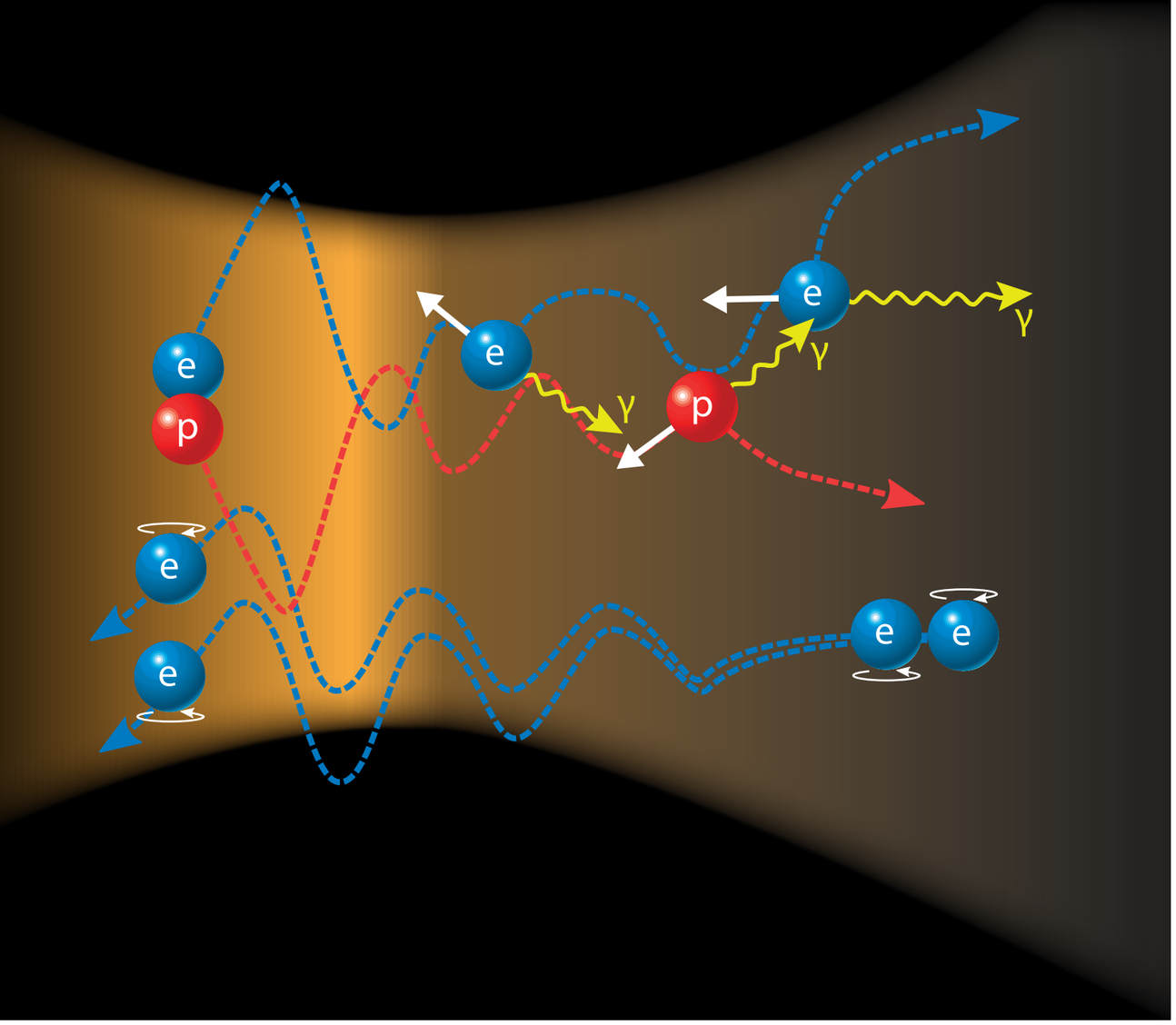

2.7 Matter in Extremely Intense Laser Pulses

Schematic representation of typical scenarios considered in this section: Electron-positron pairs may be created from the vacuum in the focus of an extremely strong laser field (upper half) where the subsequent acceleration causes the emission of highly energetic photons. In the nonlinear quantum regime, this emission is accompanied by a substantial recoil which discontinuously changes the classical trajectory (indicated by dashed lines). In addition, the trajectories of electrons traveling in strong electromagnetic fields depend on the particle's initial spin orientation (lower half).

Introduction

The continuous development of novel laser sources with ever increasing intensities and frequencies has established the meanwhile mature scientific area of extreme-field laser science. The so-called “Extreme Light Infrastructure” currently under construction in Prag, Bucharest and Szeged constitutes one of Europe's largest and most expensive research facilities in this area and will deliver light sources sufficient to carry out competitive nuclear and high-energy physics with laser fields. The use of free-electron lasers will strongly enrich the field of nuclear physics and in combination with traditional accelerators the vacuum can be rendered instable and quantum electrodynamics as well as weak interactions may be tested in unexplored regimes. The precise control of lasers is also likely to allow for applications including laser-based laboratory astrophysics, laser colliders and laser-triggered nuclear batteries. In this section, we begin with an introduction into the dynamics of free as well as "ion and vacuum bound” electrons in strong laser pulses and focus on the intrinsic quantum features of relevance in such situations. The radiation in ultra-strong laser pulses and their back action on the dynamics in the quantum regime of hard photons will be the key topic of the second part. Then, we address the important question how the spatial extent of vacuum fluctuations can be enhanced with the aim to establish a laser-based collider and how weak interactions could be tested with extreme photon background fields. In the two final contributions the role and the technical handling of ultra-short pulse shapes and the virtues of laser-based nuclear excitations are investigated.

Relativistic Quantum Dynamics in Extremely Intense Laser Pulses: Spin Effects, Pair Creation and Tunneling Times

The fundamental interaction of light and matter is governed by the laws of quantum mechanics. This is even of relevance for electrons and positrons in ultra-strong laser pulses being composed of a very large number of photons. Furthermore, quantum mechanics often challenges our intuition when confronting us with phenomena that are beyond our daily experience, for example, wave-particle duality, nonlocality, spin effects, tunneling or pair creation. For this reason, (semi) classical models are commonly applied to describe phenomena of the quantum world. Such models are valuable for obtaining an intuitive understanding of quantum effects. Furthermore, models of (semi) classical physics are mathematically and computationally often much more easy to solve. In particular, many-particle quantum systems cannot be simulated efficiently on a classical computer and are often also hard to treat analytically.

According to classical electrodynamics the motion of an electron is determined by the Lorentz force. This force is induced via an interaction of the electron’s charge with the electromagnetic fields. The Lorentz force (in its standard form) does not account for the electron’s spin degree of freedom, which naturally emerges within the framework of relativistic quantum mechanics and the Dirac equation. Therefore, different classical theories have been put forward and are commonly applied in various branches of physics to describe the relativistic dynamics of electrons by coupled equations for the orbital motion and spin precession. Little, however, is known how well these classical models agree with the more fun-

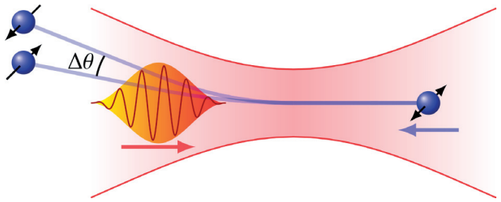

Fig. 1: A relativistic electron is scattered at a counterpropagating tightly focused laser pulse due to ponderomotive forces. The scattering angle depends also on the electron's initial spin orientation. Final momenta of spin-up and and spin-down electrons differ by the angle Δθ, which depends on the applied classical model. Adapted from [1].

damental Dirac theory. In [1], the Frenkel model and the classical Foldy-Wouthuysen model with spin-dependent (Stern-Gerlach) forces are exemplarily benchmarked to the Dirac equation. Both classical theories can lead to different or even contradicting predictions how the Stern-Gerlach forces modify the electron's orbital motion, when the electron moves in strong electromagnetic field configurations of emerging high-intensity laser facilities. In this way, one may evaluate the validity and identify the limits of these classical theories via a comparison with possible experiments to provide a proper description of spin-induced dynamics. Our results, as testable in the scenario of Fig. 1, indicate that the Foldy-Wouthuysen model is in better agreement with the Dirac theory than the widely used Frenkel model and that deviations become significant in the feasible ultra-relativistic regime.

One of the most intriguing predictions of quantum electrodynamics is certainly the possible breakdown of the vacuum in the presence of ultra-strong electromagnetic fields into pairs of electrons and positrons. This is expected to set in at the Schwinger critical field strength of $E_c = 1.3 \times 10^{18}$ V/m which may be approached in the rest frame of laser-accelerated electrons. At field strengths below the Schwinger limit, pair creation via electric fields is commonly interpreted as a tunneling effect similar to tunnel ionisation from bound states via strong electric fields. Electromagnetic fields created by ultra-intense lasers are the most promising means for realizing strong-field pair creation. The standard tunneling picture of pair creation, however, becomes inapplicable in the presence of magnetic fields (in addition to the electric field). For this reason, the tunneling picture was generalised to this situation in order to account also for magnetic fields in [2] (see Fig. 2). The new tunneling picture comprises the electron's (positron's) kinetic energy (dashed line in Fig. 2) and a pseudo energy (solid lines in Fig. 2), which depends on the magnetic field and a possible external photon. Various features of pair creation can be inferred qualitatively from the enhanced picture. For example, an additional photon lowers the potential barrier due to the photon's energy but also increases the particle's relativistic mass due to the photon's additional momentum. Due to this increased relativistic mass, the electron and the positron stay "longer" under the barrier until they gain enough energy to become real. An additional magnetic field, however, will also change the momentum under the barrier and, in this way, the relativistic mass. Depending on the magnetic field's direction and magnitude it may counteract the increase of the relativistic mass due to the photon's momentum and, therefore, increase the pair production probability.

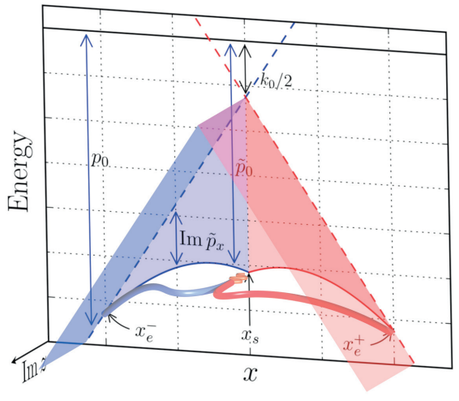

Fig. 2: The new tunneling picture of pair creation. The electron and the positron start their (imaginary) trajectory at x_s and travel to their respective exits x_e^- and x_e^+, where the trajectories become real. The tunneling dynamics is along the real x axis and the presence of a magnetic field may cause a nontrivial motion along the imaginary z axis. The degree of suppression of pair creation can be inferred qualitatively by the shaded areas, enclosed by the thin solid and dashed red and blue lines; figure taken from [2].

When electrons tunnel through classically forbidden regions of space, naturally the question arises how much time an electron needs to cross the tunneling barrier. This old problem of quantum mechanics has attracted renewed interest in recent years after several experiments have been performed aiming to determine the tunneling time in strong-field ionisation from the spectrum of ionised electrons. Following our earlier relativistic approach, it has recently been shown by solving numerically the time-dependent Schrödinger equation and employing a virtual detector at the tunnel exit that there is a non-vanishing positive time delay between the electric field maximum and the instant of ionisation [3]. Moreover, a nonzero exit momentum in the direction of the electric field was found. Thus, it is essential to incorporate the electron's initial momentum in the direction of the external electric field to extract proper tunneling times from asymptotic momentum distributions of ionised electrons.

Heiko Bauke, Christoph H. Keitel

Quantum Radiation Reaction

The advent of petawatt-class lasers enables GeV electron beams in strong electromagnetic fields to be studied experimentally using all-optical systems. Motivated by this, we have studied several

promising configurations that explore previously untested regimes, where the radiation emitted incoherently by the beam plays a major role in shaping its dynamics. In classical physics, the radiation emitted by an accelerated charge gives rise to the radiation reaction force and, therefore, to a modification of the trajectory. However, this picture loses its validity when the energy of a single incoherently emitted photon is comparable to the energy of the charged particle itself. Instead, in this regime of quantum radiation reaction it is possible to adopt a semi-classical picture in which the particle follows an unperturbed non-radiating trajectory that is stochastically punctuated by discrete instantaneous emission events. This regime can be probed by the experimental setup sketched in Fig. 3 [4].

An effect characteristic of the quantum regime is that of "straggling" in which particles with the same initial trajectory undergo different energy losses. If, for example, a GeV electron, propagating along the optical axis to the left in Fig. 3 and entering into the counterpropagating laser pulse, waits an unusually long time before radiating a photon, it can find itself in the strong fields in the centre of the pulse with an energy larger than that of its companions. As a result, it is much more likely to emit an energetic photon. In contrast, the classical picture predicts the same emissivity for all particles with the same initial conditions, since these uniquely define the trajectory. Quantum effects can, therefore, be detected by measuring either the electron distribution after propagation through the laser pulse, or the spectrum and angular distribution of the gamma-ray photons emitted whilst inside the pulse. In [4] we developed a Monte-Carlo simulation technique to quantify these effects as they appear in the configuration shown in Fig. 3, allowing for the finite transverse extent of the laser pulse as well as its finite duration. As expected, we find that the electron distribution that emerges from the pulse has a much larger spread in energy than it would be expected in the classical case. However, the relatively large number of electrons that fail to pass through the regions with the strongest field significantly dilutes this signal. Consequently, we find that the most sensitive indicator of quantum effects is the yield of very high energy photons: when electrons of 1 GeV pass through a laser pulse of peak intensity 10^{22} W cm^{-2} in the experimental configuration of Fig. 3, the number of photons emitted with energy greater than 600 MeV exceeds the classical prediction by more than one order of magnitude.

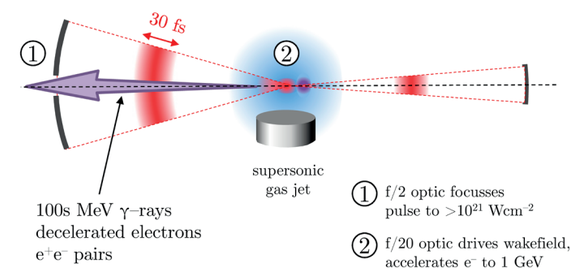

Fig. 3: Diagram of an experiment that could demonstrate quantum radiation reaction. GeV electrons are produced at 2 where an intense laser beam is incident from the right onto a supersonic gas jet. These electrons then pass through the tight focus of a 30 fs laser pulse incident from the left, which decelerates them by causing them to emit 100 MeV gamma-rays; figure taken from [4].

Generally, the detection of various modifications of the radiation spectrum due to quantum radiation reaction requires accurate quantitative measurements. However, in [5] we have identified signatures of quantum radiation reaction for Compton radiation spectra which are easily detectable in an experiment due to distinct qualitative characteristics. We have investigated features of the angle-resolved spectra of Compton radiation when an ultrarelativistic electron beam counterpropagates with a strong focused ultrashort laser pulse of variable duration. With increasing laser-pulse duration the angular spread of radiation is shown to initially rise in a narrow range due to laser focusing and then continuously decrease because of quantum radiation reaction. This unique behaviour does

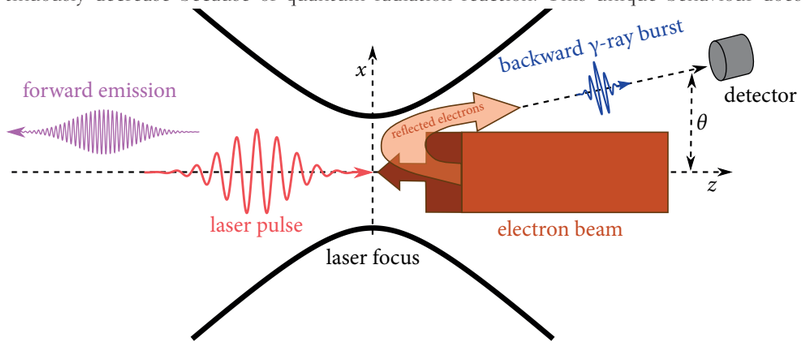

Fig. 4: Schematic representation for our scenario of the generation of ultrashort gamma-ray bursts; figure taken from [6].

not exist in the classical radiation reaction regime. The spectral bandwidth of the radiation in the quantum regime is by orders of magnitude larger than in the classical regime. The qualitative behaviours mentioned are robust and observable in a broad range of electron and laser-beam parameters.

The quantum radiation reaction can also be harnessed for the generation of ultrashort gamma-ray pulses, which are aspired for time resolved nuclear spectroscopy. In [6], we demonstrated the feasibility of multi-MeV gamma rays of several hundreds of attoseconds duration via nonlinear Compton scattering of an intense laser pulse by a counterpropagating electron beam of much longer duration. We found an interaction regime when only a small fraction of the electron beam loses sufficient energy due to radiation reaction to be reflected and emits gamma rays close to the laser propagation direction during a short time while leaving the laser focal region, see Fig. 4. The length of the gamma-ray pulse is much shorter because the front of the gamma pulse and the tail of the electron beam counterpropagate.

The scheme relies on the nonlinear effects of the regime of interaction, the tightly focused driving laser pulse, and the crucial effect of radiation reaction. All of these three ingredients are necessary to realise the ultrashort duration of the emitted gamma rays determined solely by the intrinsic interaction mechanism and yielding brilliant attosecond gamma-ray bursts.

Karen Z. Hatsagortsyan, John Kirk, Christoph H. Keitel

High-Energy Processes in Ultra-Intense Laser Fields

The Heisenberg uncertainty principle represents one of the most profound conceptual novelties in quantum mechanics. In the realm of quantum field theory it implies the existence of "vacuum fluctuations", i. e. the temporary appearance of pairs of virtual particles-antiparticles. As electrons and positrons have a finite mass, the conversion of a photon into a real electron-positron pair violates energy-momentum conservation and is forbidden in vacuum. According to the Heisenberg uncertainty principle, however, this transformation is transiently allowed and such a "virtual electron-positron pair" can cover a distance of the order of the Compton wavelength $\lambda_C = 3.9 \times 10^{-11}$ cm (see Fig. 5a). As to be anticipated, the presence of vacuum fluctuations leads to qualitatively altered theoretical predictions. One of the most appealing examples is the feasibility of light-by-light scattering. Classically, the superposition principle holds in vacuum and implies that in vacuum two light waves do not experience mutual interactions. Due to the presence of virtual charged particles in the quantum vacuum, however, a feeble light-by-light scattering cross section is obtained. While the influence of vacuum fluctuations is well studied in the perturbative regime of quantum electrodynamics (QED), considerably less is known about their behaviour in the presence of strong electromagnetic fields. Here, strong means comparable with the critical fields of QED $E_{cr} = 1.3 \times 10^{16}$ V/cm and $B_{cr} = 4.4 \times 10^{13}$ G. Notably, a virtual electron-positron pair can absorb energy of the order of its rest energy from a pure electric field of critical strength. Accordingly, its lifetime is no longer limited by the Heisenberg uncertainty principle in the presence of strong background fields. Pictorially speaking, a critical field is capable of separating two charges bound within the quantum vacuum by converting virtual into real particles. This process is also called spontaneous or Schwinger pair production from the vacuum. Evidently, the distinction between real and virtual particles becomes difficult in the realm of strong-field QED and we have to revisit our intuition and notation which stems from the perturbative sector of QED.

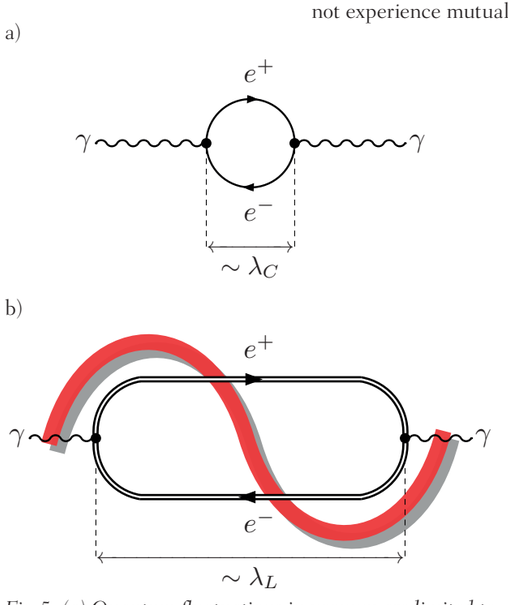

Fig. 5: (a) Quantum fluctuations in vacuum are limited to the Compton scale λ_C. (b) Recollision processes in ultra-intense laser beams extend over a macroscopic length.

Owing to the impressive development of laser technology within the past decade, the critical field of QED becomes nowadays accessible experimentally by colliding strong optical laser pulses with highly energetic particles. In particular, the interaction of light with light could be probed if GeV gamma photons propagate through petawatt-class laser pulses. So far two types of qualitatively different effects have been considered for this experimental setup. On the one hand, the presence of vacuum fluctuations on

microscopic length scales changes the polarisation of the gamma photon, a phenomenon known as vacuum birefringence. This process is described theoretically by the polarisation operator, represented in the leading order by an electron-positron loop which mediates the coupling between background field and gamma photon. On the other hand, the decay of the gamma photon into a real electron-positron pair is feasible via the nonlinear generalisation of the so-called Breit-Wheeler process. Notably, these two types of processes differ in the number of laser photons which can be absorbed. An electron-positron pair, which represents a genuine quantum fluctuation, annihilates on a microscopic scale (see Fig. 5a), implying that only a few laser photons are efficiently exchanged with the background field. Conversely, a large amount of energy is transferable classically to a real electron-positron pair. In [7] we discovered a third type of fundamental phenomenon – previously not associated with electron-positron loops – which combines both aspects. It was demonstrated for the first time that the polarisation operator also describes recollision processes which happen on macroscopic length scales of the order of the laser wavelength λ_L compared to the microscopic Compton scale λ_C (see Fig. 5b). Pictorially speaking, the laser produces initially a real electron-positron pair, which is then accelerated over at least one laser half cycle, and finally annihilates again at the intersection point of the classical trajectories. In essence, the laser acts as a microscopic "vacuum" collider. This semiclassical three-step model reveals ample similarities with phenomena like high-harmonic generation in atomic physics even though the involved energy scales are here much higher than in the atomic case. The large amount of energy, which is transferred during a recollision event, facilitates high-energy reactions like the production of heavy particles and thus predicts qualitatively new experimental signatures.

The Standard Model is the most complete available theoretical framework in elementary-particle physics. While traditional accelerators are employed to test the Standard Model at higher-and-higher energies, i. e. lower-and-lower distances, modern petawatt- and multipetawatt-class optical lasers can be utilized to test the theory in the complementary high-intensity, nonlinear regime. Moreover, as optical photons have energies in the eV regime, existing and upcoming laser facilities are particularly well suited to investigate the properties of light particles. Among them, since the discovery of the Higgs boson, neutrinos represent the least understood constituents of the Standard Model. Even though the existence of flavour oscillations proves the finiteness of the neutrino masses, their theoretical origin is still opaque (see Fig. 6a). Due to the absence of protecting quantum numbers only the lightest neutrino should be absolutely stable and the other mass eigenstates can decay radiatively, i. e. by emitting a photon (see Fig. 6b). However, the Standard Model predicts a lifetime much larger than the age of the universe, which renders the experimental investigation of this process extremely challenging. The presence of strong electromagnetic background fields, however, catalyses the radiative decay and enhances the photon-neutrino coupling by several orders of magnitude (see Fig. 6c). In the light of this observation, we have investigated how the interactions between photons and neutrinos could be tested with modern ultra-intense laser systems. To shed light on this question, we have studied the coupling between photons and the W and Z bosons (which mediate the weak force) in the presence of a strong laser field which is approximated as a plane wave [8]. We have found that the nonlinear interactions with the background field enhance the coupling substantially. Besides its importance to understand the coupling between neutrinos and photons, the investigated interplay among the different electro-weak gauge bosons via charged leptons is also interesting from a fundamental point of view. For example, we have shown how the presence of axial vector currents implies that the coupling tensor exhibits the so-called Adler-Bell-Jackiw anomaly. Finally, as an important application of our results, the electromagnetic catalysis of the neutrino decay probability can be calculated in the presence of a plane wave of arbitrary temporal shape and polarisation.

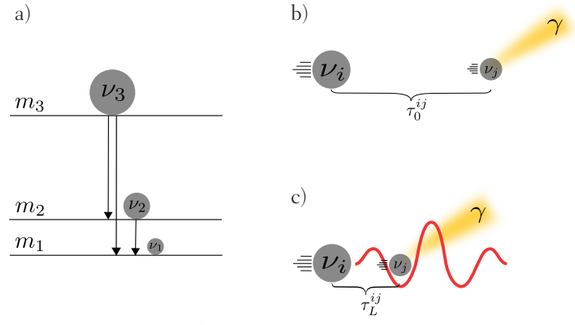

Fig. 6: (a) The existence of neutrino oscillations proves that neutrinos have a finite mass m_i. (b) As a consequence, only the lightest neutrino is absolutely stable. In vacuum, however, the radiative lifetime τ_0^{ij} for the transition $\nu_i \rightarrow \nu_j + \gamma$, with $m_i > m_j$, is much larger than the age of the universe. (c) Inside a strong background electromagnetic field the decay probability is enhanced by several orders of magnitude and therefore $\tau_L^{ij} \ll \tau_0^{ij}$ (electromagnetic catalysis).

Sebastian Meuren, Karen Z. Hatsagortsyan, Christoph H. Keitel, Antonino Di Piazza

Ultrarelativistic Electron States in a Tightly Focused Laser Beam

Due to their ever increasing power, strong optical laser fields are becoming a unique tool to test quantum electrodynamics (QED) in yet unexplored regimes where quantum nonlinear effects dominate the particles' dynamics. The electric field strength where such nonlinear effects become sizable identifies the "strong-field QED" regime and is given by the so-called Schwinger field or critical field of QED: $E_{cr} = 1.3 \times 10^{16}$ V/cm. Due to the extremely large value of E_{cr}, present and upcoming lasers have to be tightly focused in space and in time in order to approach E_{cr}. Nonetheless, the value of E_{cr} exceeds by about four orders of magnitudes presently available laser-field amplitudes. However, the effective field at which a QED process occurs is that experienced by participating charged particles in their rest frame. Thus, by employing, for example, ultrarelativistic electron beams, the strong-field QED regime can be in principle already effectively probed. In fact, electron beams with energies of about 5 GeV (approximately corresponding to a relativistic Lorentz factor of 10^4) are already available also by employing modern laser-wake-field acceleration techniques. Now, all systematic approaches to investigate analytically strong-field QED processes rely on approximating the laser beam as a plane wave, which allows for solving the Dirac equation exactly but which cannot account for laser spatial focusing effects. In [9] we have realised that in order to enter the strong-field QED regime at present and upcoming laser facilities, the electrons have to be so highly relativistic that the Wentzel-Kramers-Brillouin (WKB) approximation can be employed (at the next-to-the-leading order) to solve analytically the Dirac equation in the presence of a background laser field practically of arbitrary space-time shape. The physical reason is that, by requiring that the electric field of an optical laser (laser photon energy of the order of 1 eV) in the rest frame of an electron beam is of the order of the E_{cr} automatically implies that the Lorentz factor of the electron bunch is so large that the electrons are barely deflected by the laser field itself. The electron wave functions obtained in this way open the possibility of investigating analytically and in a systematic way strong-field QED processes in the presence of a tightly focused laser beam of complex and realistic space-time shape by employing the so-called Furry picture. Indeed, we have already determined analytically the energy spectrum and the angular distribution of the electron-positron pairs produced in the collision of a photon bunch with an intense and tightly-focused laser beam (nonlinear Breit-Wheeler pair production) [9]. As a by-product, by means of a numerical implementation of the analytical results, we have proven that the inclusion of the laser tight focusing is essential for a correct quantitative estimate of the number of created pairs. In fact, as also expected, approximating a tightly focused laser field as a plane wave would largely overestimate the number of produced pairs especially in those regions close to but not exactly at the laser peak (see Fig. 7).

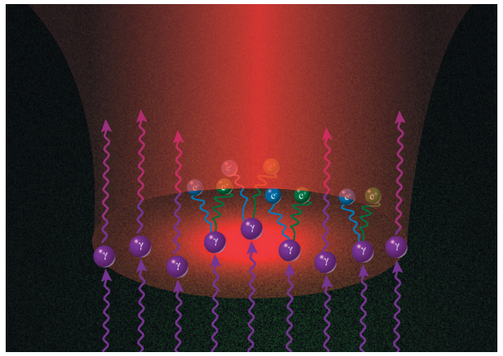

Fig. 7: In the collision of a photon bunch with a tightly focused laser beam electron-positron pairs are more likely to be produced at the central peak of the laser beam than in the neighbor regions where the field is less intense.

Antonino Di Piazza

Nuclear Processes in Ultra-Intense Laser Fields

Recent experimental developments in laser physics promise to open the new field of laser-induced nuclear reactions in a so-far unexplored domain. Efforts are under way to generate a multi-MeV laser beam at the Nuclear Physics Pillar of the Extreme Light Infrastructure (ELI) and at the International Center on Zetta-Exawatt Science and Technology (IZEST). The prospect of a laser beam with photon energies comparable to typical nuclear excitation energies raises important questions. How will an intense laser pulse interact with a medium-weight or heavy nucleus? To answer this question, we first have to consider that the nucleus is bound by the strong force. As a consequence, the laser-nucleus interaction is much weaker than its more studied counterpart, the laser-atom interaction. Furthermore, processes which differ significantly from the standard photon-induced nuclear reactions are expected to occur only if the gamma-ray photons in the laser pulse are coherent. It is only via coherence that the dipole absorption rate may attain values in the MeV range, rendering it comparable to the other characteristic nuclear energy scales.

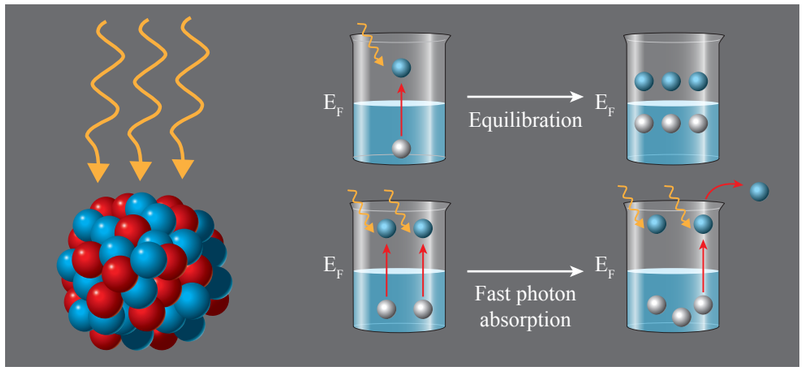

Fig. 8: A coherent MeV-photon laser pulse excites single nucleons (neutrons or protons) above the Fermi energy E_F and creates so-called particle-hole pairs. Equilibration distributes the excitation over many such pairs. A strong pulse can however overcome the equilibration rate and remove several up to all nucleons from a medium weight or heavy nucleus.

Gamma photon absorption leads to the excitation of single nucleons, creating so-called particle-hole pairs. This process is in competition with the nuclear residual interaction, which has no counterpart in atoms and has the tendency to drive the system towards statistical equilibrium, see Fig. 8. The laser energy absorbed by single nucleons is thereby distributed among all nucleons on a time scale governed by the so-called nuclear spreading width. The ratio between the effective dipole and the nuclear spreading width determines the regime of interaction. New nuclear physics insights arise when one considers the case that the effective dipole and the nuclear spreading width are of equal magnitude. This defines the quasi-adiabatic regime, in which after each absorption, the nucleus has time to equilibrate. This in turn supports the absorption of the next photon leading to multiphoton excitation and to the formation of a compound nucleus, i. e. a nucleus with many excited nucleons, which has just modest angular momentum. Our theoretical studies have shown that multiple photon absorption may produce compound nuclei in the so-far unexplored regime of several hundred MeV excitation energies [10]. Here, further photon absorption is limited by neutron decay and induced nucleon emission. We have investigated semiquantitatively the competition between photon absorption, photon-induced nucleon emission, fission and neutron evaporation. With neutron evaporation becoming dominant before the excitation is saturated, proton-rich nuclei far off the line of stability are produced. Stronger excitation in the sudden regime where equilibration cannot compensate photon absorption may offer for the first time the possibility to study the transition from a bound system of strongly correlated nucleons to single independent particles. These are exciting perspectives which open further unexplored nuclear physics avenues.

Adriana Pálffy

References

[1] M. Wen, H. Bauke, C.H. Keitel, Sci. Rep. 6, 31624 (2016)
[2] A. Wöllert, M. Klaiber, H. Bauke, C.H. Keitel, Phys. Rev. D 91, 065022 (2015)
[3] N. Teeny, E. Yakaboylu, H. Bauke, C.H. Keitel, Phys. Rev. Lett. 116, 063003 (2016)
[4] T.G. Blackburn, C.P. Ridgers, J.G. Kirk, A.R. Bell, Phys. Rev. Lett. 112, 015001 (2014)
[5] J.X. Li, K.Z. Hatsagortsyan, and C.H. Keitel, Phys. Rev. Lett. 113, 044801 (2014)
[6] J.X. Li, K.Z. Hatsagortsyan, B. Gallow, C.H. Keitel, Phys. Rev. Lett. 115, 204801 (2015)
[7] S. Meuren, K.Z. Hatsagortsyan, C.H. Keitel, and A. Di Piazza, Phys. Rev. Lett. 114, 143201 (2015)
[8] S. Meuren, C.H. Keitel, and A. Di Piazza, J. High Energy Phys. 2015, 127 (2015)
[9] A. Di Piazza, Phys. Rev. Lett. 113, 040402 (2014); ibid. 117, 213201 (2016)
[10] A. Pálffy and H.A. Weidenmüller, Phys. Rev. Lett. 112, 192502 (2014)